Experimental and Modeling Study on the Absorption of CO_2 in Novel Activated Amine Solvents

TELLAGORLA RAMESH

Experimental and Modeling Study on the Absorption of CO_2 in Novel Activated Amine Solvents

Thesis

Submitted in partial fulfilment of the
Requirements for the degree of

DOCTOR OF PHILOSOPHY

By

Tellagorla Ramesh

(Roll No. 136107043)

Department of Chemical Engineering

Indian Institute of Technology Guwahati

Guwahati- 781039, Assam, India

April, 2022

Dedicated

to

My Parents and my lovely brother Suresh

Department of Chemical Engineering
Indian Institute of Technology Guwahati
Guwahati 781039, Assam, India

CERTIFICATE

It is certified that the work in this thesis entitled "Experimental and Modeling Study on the Absorption of CO_2 in Novel Activated Amine Solvents" submitted by T Ramesh has been carried out under our supervision. This work has not been submitted elsewhere for a degree.

Prof. Sasidhar Gumma
Professor
Department of Chemical Engineering
Indian Institute of Technology Tirupati
Tirupati 517506

Prof. Bishnupada Mandal
Professor
Department of Chemical Engineering
Indian Institute of Technology Guwahati
Guwahati 781039

ACKNOWLEDGMENTS

I would love to express my sincere respect towards my thesis supervisors **Prof. Sasidhar Gumma** and **Prof. Bishnupada Mandal,** for their extreme guidance and patience throughout this research program. I want to thank both the supervisors for contributing their valuable time and providing good suggestions for the entire duration of this research to approach different issues.

I must also thank my doctoral committee members **Prof. Prabirkumar Saha**, **Prof. Amit Kumar**, and **Prof. Chivukula V Sastri** for their valuable and constructive suggestions for my research work.

I would like to express my love towards **Prof. A.K Ghoshal** for his contribution and kind cooperation during my early stage and encouragement towards my research work.

I must also thank all the **Faculty members** of the Department of Chemical Engineering for their support and help during my stay.

I'm also grateful to our department's **Technical staff** for their unwavering assistance and support throughout this project. I want to express my gratitude to all of the employees at IITG, particularly **Mr. Deep Jyothi Sinha, Mr. Jayanth Kumar Mout, Mr. Sailen Das,** and **Mr. Harsaraj Biswanath,** for their help in many ways.

I'd also like to express my gratitude to **Ms. Sweta C. Balchandani** for her invaluable assistance and cooperation throughout my Ph.D. program. Various research-based discussions with Ms. Sweta, a member of my research group, and her strong analytical skills greatly aided me in modeling the current research topic.

I'd also like to express my gratitude to **Dr. Babul Prasad, Dr. Satyanarayana Edubilli, Dr. Abhik Bhattacharjee, Dr. Rajashree borgohain, Dr. Mridusmitha, Dr. Pradip Das, Mr. Prudhvi Raj Medikonda, Ms. Geetanjali Bhati**, members of my Research Group at IIT Guwahati, for their support and contributions.

My sincere thanks to all my friend's cricket mates of IITG **Dr. Sudarshan, Dr. Malli, Dr. Narasimha, Dr. Santhosh, Dr. Bharath, Dr. Srinu, Dr. Manish, Dr. Mirza, Mr. Durga, Mr. Pilli, Mr. Rambabu, Mr. Hanumanthu, Mr. Sunku, Mr. Mukesh, Mr. Vishnu, Mr. Prasad, Mr. Anudeep, Ms. Mounika** were all outstanding colleagues and friends during my Ph.D. research term. I want to express my gratitude to every one of them. And sincere thanks to my attender Mr. Brigu for his cooperation during experiments.

My humble regards and respect are sent to my **parents, brother and mama (Srinivasa Reddy)**. Their love, concern, sacrifices, and support have enabled me to progress so far. I shall be eternally grateful to **God** for providing me with everything I have.

Ramesh

Research output

Journal Publications:

- **Tellagorla Ramesh,** Swetha C. Balchandani, Sasidhar Gumma, Bishnupada Mandal, Equilibrium CO_2 solubility of novel tris(2-aminoethyl) amine as a promoter to N-methyldiethanolamine and 2-amino-2-methyl-1-propanol. **Separation and Purification Technology (Elsevier)** 279, 119705 (2021).
- **Tellagorla Ramesh,** Swetha C.. Balchandani, Pradip Das, Sasidhar Gumma, Bishnupada Mandal, Measurement and correlations of physicochemical properties of the novel solvent tris(2-aminoethyl) amine and its blend with N-methyldiethanolamine and 2-amino 2-methyl-1-propanol**. Revision submitted to Journal of Chemical & Engineering Data (ACS),** 2021**.**

Conference Presentations:

- **Tellagorla Ramesh**, Bishnupada Mandal, Sasidhar Gumma, 'Pilot plant study on amine-based absorption process for CO_2 capture', **CHEMCON 2015** organized by Indian Institute of Technology Guwahati (**IITG**).
- **Tellagorla Ramesh**, Bishnupada Mandal, Sasidhar Gumma, 'Physicochemical properties of aqueous single and blended amines using a novel activator for CO_2 capture', 1st Euro-Asia Conference on CO_2 capture and utilisation ($EACCO_2CU$) August 6-7th 2019, organised by Research center for carbon dioxide capture and utilisation school of science and technology, **Sunway University, Malaysia.**

Workshops attended:

- *Workshop on Hydrogen storage materials*: "Attended a workshop on Hydrogen storage materials" organized by **Indian Oil R&D center**, Faridabad, Haryana on Friday, December 7, 2018.
- *State of the art in refinery operations*: Participated one-day workshop titled "State of the art in refinery operations" organised by department of chemical engineering **IIT Guwahati and Guwahati refinery** on 4th April 2018.
- *Indo*-German workshop: Attended an Indo-German workshop on "Advances in materials, Reaction & separation process" **IIT Guwahati**, February 23-26, 2016 (IIT Guwahati, India and the **Max Planck Institute for Dynamics of Complex Technical Systems, Magdeburg, Germany**).

Abstract

Experimental and Modeling Study on the Absorption of CO_2 in Novel Activated Amine Solvents

The increasing concentration of carbon dioxide (CO_2) in the atmosphere has had a negative impact on the environment over the previous few decades and has been a focus of global attention. CO_2 capture, one of the most important greenhouse gases (GHG), is now a critical stage in the functioning of electric power plants, petroleum refineries, chemical fertiliser plants, coal gasifiers, cement plants, and steel mills. Gas scrubbing with activated aqueous alkanolamine solutions has recently emerged as the most reliable post-combustion CO_2 collection retrofit option.

The current study looks into a new activator called tris (2-aminoethyl) amine (TAEA), which could be an excellent way to remove CO_2 from flue gas. The thesis presents novel experimental CO_2 solubility data of absorption in various aqueous (TAEA+MDEA+H_2O) and (TAEA+AMP+H_2O) systems compositions over wide temperatures and pressure ranges of (293.15-323.15) K and (2-500) kPa, respectively. The modified Kent-Eisenberg (KE) equilibrium model is used to model the experimental solubility data. To fit the equilibrium CO_2 solubility data, the equilibrium constants related to amine deprotonation and carbamate production reactions are regressed as a function of essential operating parameters such as CO_2 partial pressure, amine concentration, and temperature. The results of the KE model's projected solubility are in good accord with the experimental data. The modified KE model established in this study may also be used to estimate the concentrations of various ionic species in the solvent phase at equilibrium conditions. With the variation of α_{CO2}, the distribution of different

reaction products arising from the CO_2 –amine reaction has been estimated. The pH of CO_2-loaded amine solvents can also be predicted using the KE model. From the standpoint of CO_2 capture process design, understanding the pH of the loaded solvent is essential.

Feed forward Artificial Neural Network (ANN) model is used to correlate the solubility data. The Levenberg-Marquardt back propagation technique is utilised as the training function in this ANN architecture. Hyperbolic tangent sigmoid and linear functions are used as transfer functions for the hidden and output layers. The experimental data and the anticipated value from the feed-forward neural network model agree pretty well. FTIR and qualitative ^{13}C NMR were also used to evaluate the many major reaction products and appraise the CO_2- amine reaction scheme. To assess the performance of the researched solvents in this study, a detailed comparison of CO_2 loading with other standard solvents was presented.

Over a temperature range of (293.15-333.15) K, important thermophysical parameters of the solvents, such as density and viscosity, are measured and reported. Diffusivity is also calculated using the measured viscosity values through the modified Stokes-Einstein relation. Along with physical solubility (Henry's law constant) of (TAEA+H_2O), (TAEA+MDEA+H_2O) and (TAEA+AMP+H_2O) are also investigated at different temperatures (293.15-323.15) K and other compositions. These features are essential in determining flow behavior, intermolecular interactions, the design of the absorber or regenerator column, solvent pumping costs, mass transfer, and CO_2 kinetic rates in solvents. The earliest principal models, Redlich-Kister and Grunberg-Nissan, were used to model density and viscosity. For the correlation, Henry's law constant an Arrhenius type equation is used. As a function of temperature and composition, all attributes were connected. The results showed a reduced variance between the experimental and predicted data, indicating that the models were accurate.

LIST OF CONTENTS

LIST OF FIGURES

LIST OF TABLES

This page is intentionally left blank

Chapter 1

Introduction, Literature Review, and Objectives

The present movements in universal greenhouse gas emissions and their influence on the environment are presented in this chapter. The need to implement efficient carbon capture storage systems (CCS) has been discussed, and a quick overview of various carbon capture technologies. A detailed literature review on chemical absorption via aqueous single and blended amine systems is also presented in this chapter. It goes into detail on the background of the research project and the significance and goals of the project.

1.1 Introduction

Global warming and climate change difficulties caused by significant emissions of greenhouse gases and other ozone-depleting compounds, mainly CO_2, have been a global concern in recent years. Due to increased global energy consumption, CO_2 discharges from energy-related sources rose 1.7 percent to a notable high of 33.1 Gt of CO_2 in 2018 [1]. This was the fastest rate of increase since 2013, and it was also 70% greater than the yearly average pace since 2010. Higher energy demand and a robust global economy have resulted in higher emissions. Extreme weather conditions in some regions have also increased the need for additional energy for extra cooling and heating. While several factors contributed to the increased emissions, the power sector accounted for roughly two-thirds of the entire increase in worldwide greenhouse gas emissions. Coal-fired power stations are the primary source of CO_2 emissions from fossil-fueled power plants, accounting for almost 40% of total CO_2 emissions [2]. According to data compiled by the International Energy Agency (IEA), the four largest CO_2 emitters globally are (i) China (9839 Mt CO_2), (ii) the United States (5270 Mt CO_2), (iii) the European Union (3544 Mt CO_2), and (iv) India (2467 Mt CO_2), with total global emissions totaling 36153 metric tons

in 2017 [3]. The general trends of total greenhouse gas emissions by significant emitter countries and the European Union are depicted in Fig 1.1. These top emitters account for almost 70% of world emissions [4].

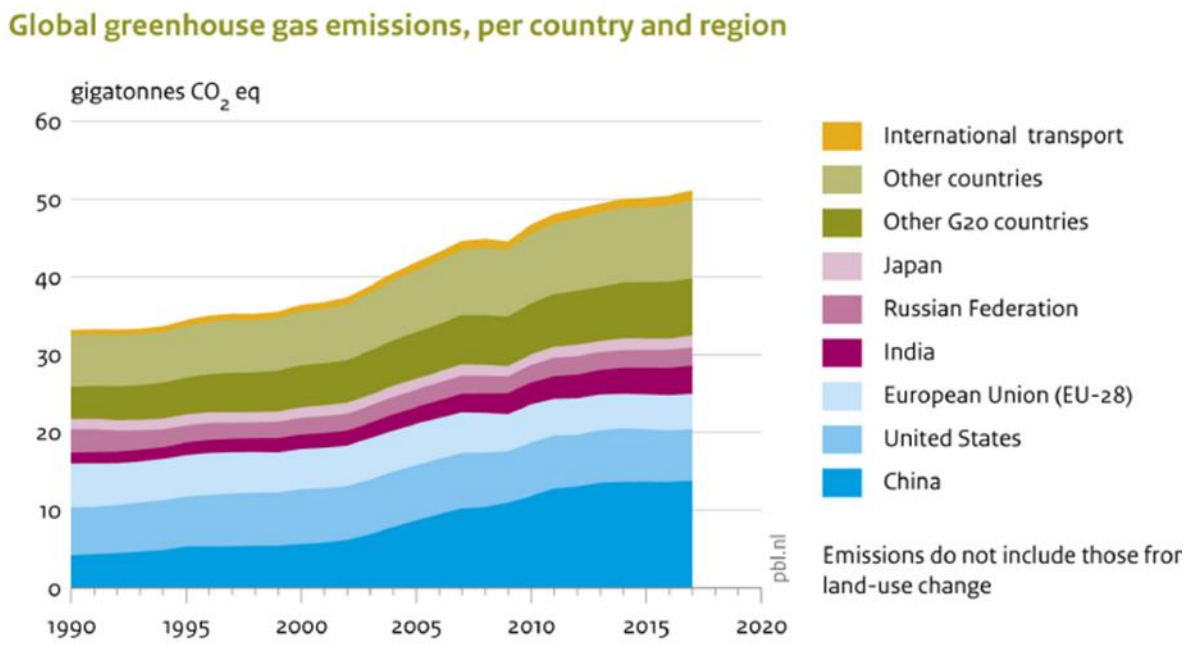

Figure 1.1 Emissions of greenhouse gases around the world [4].

However, there are significant inequalities observed globally in the yearly per capita emission of CO_2. The world's largest per capita CO_2 emitters are the major oil-producing nations. In 2017, Qatar recorded the highest emissions at 49 tonnes (t) per person, followed by Trinidad and Tobago (30 t), Kuwait (25 t), United Arab Emirates (25 t), Brunei (24 t), Bahrain (23 t) and Saudi Arabia (19 t) [5].

In the category of more populous countries, Australia (17 t), the United States (16.2 t), and Canada (17 t) have some of the largest per capita emitters (15.6 t). This statistic is more than three times greater than the global average, 4.8 t in 2017. These patterns clearly show that countries with better living standards have more giant carbon footprints. On the other hand, some industrialised European countries have per capita emissions close to the global average. In 2017, emissions in Portugal, France, and the United Kingdom were 5.3 t, 5.5 t, and 5.8 t, respectively [5]. The energy source used is important since a large portion of energy generation

in many European countries comes from nuclear and renewable sources, resulting in a lower carbon footprint. With 1.7 t/yr of total per capita emissions, India ranks 61st globally [3]. Continuous emissions, on the other hand, have resulted in a massive increase in carbon dioxide concentration in the atmosphere, which in 2018 passed the 411 ppm milestone [4]. As a result, there is a pressing need to address the issue of CO_2 emissions into the atmosphere while preserving quicker economic growth. In this context, effective CO_2 collection technologies and subsequent abatement, such as carbon capture and storage (CCS), play a critical role [4]. In its yearly report, the IPCC stated that a modern conventional power plant coupled with efficient CCS technology might reduce atmospheric CO_2 emissions by 80-90 percent.

1.2 A quick overview of various carbon capture technologies

When selecting a CO_2 collection technique, keep in mind the application, the upfront and ongoing costs of technology deployment, and whether or not the present system requires any modification to connect to current technology. CO_2 capture from industrial exhaust gas streams can be accomplished in three ways. (Figs. 1.2 - 1.4).

1.2.1 Pre-combustion

It is the process of capturing CO_2 before it is burned. For this situation, the fossil fuel (coal) is partially oxidised in a gasifier to yield syngas. The syngas (combined CO and H_2) are then steam reformed to produce CO_2 and H_2 [6]. The CO_2 was then concentrated and injected into the scrubber column, where it came into contact with the appropriate solvents to begin the absorption process. In the regenerator column, CO_2-rich solvent is passed, where it is stripped of CO_2, and the separated H_2 stream can be employed as a source of energy. Chemical or physical solvents can split CO_2 depending on the working conditions of pressure, temperature, and CO_2 concentration. This technology is primarily practical for newer facilities because it requires significant changes in the architecture of power plants.

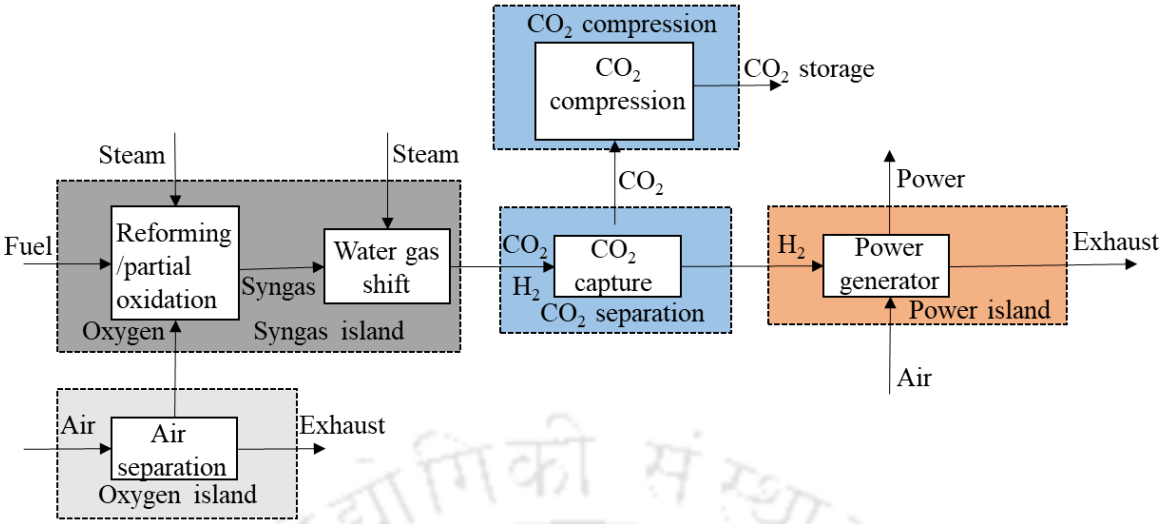

Figure 1.2 The pre-combustion capturing procedure is depicted schematically

1.2.2 Oxy-fuel combustion

One of the most striking features of oxy-fuel combustion is that it takes place with pure oxygen rather than air. As a result, pure CO_2 is produced as the primary combustion product. This technology necessitates using a separate air separation unit that purifies the air by removing nitrogen and other contaminants. This stream is then introduced into the boiler, where it undergoes combustion, resulting in steam creation to power the turbine and generate electricity [7].

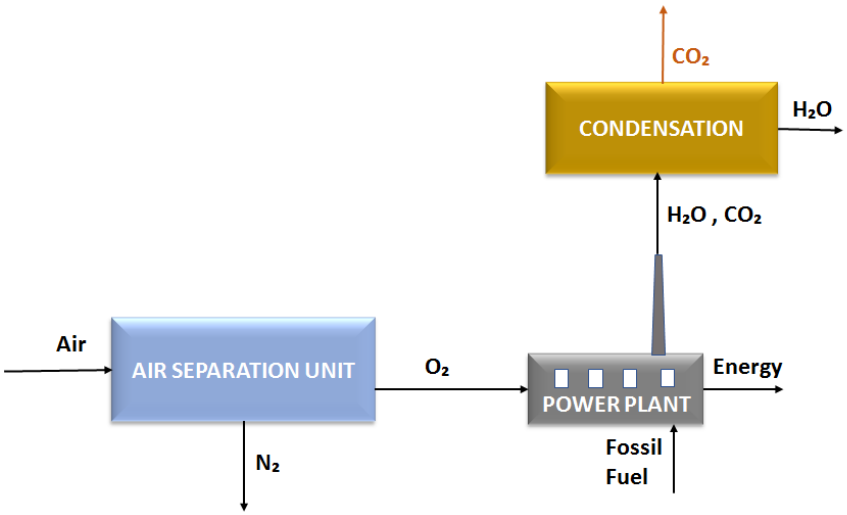

Figure 1.3 The oxy-fuel combustion process is depicted in a diagram

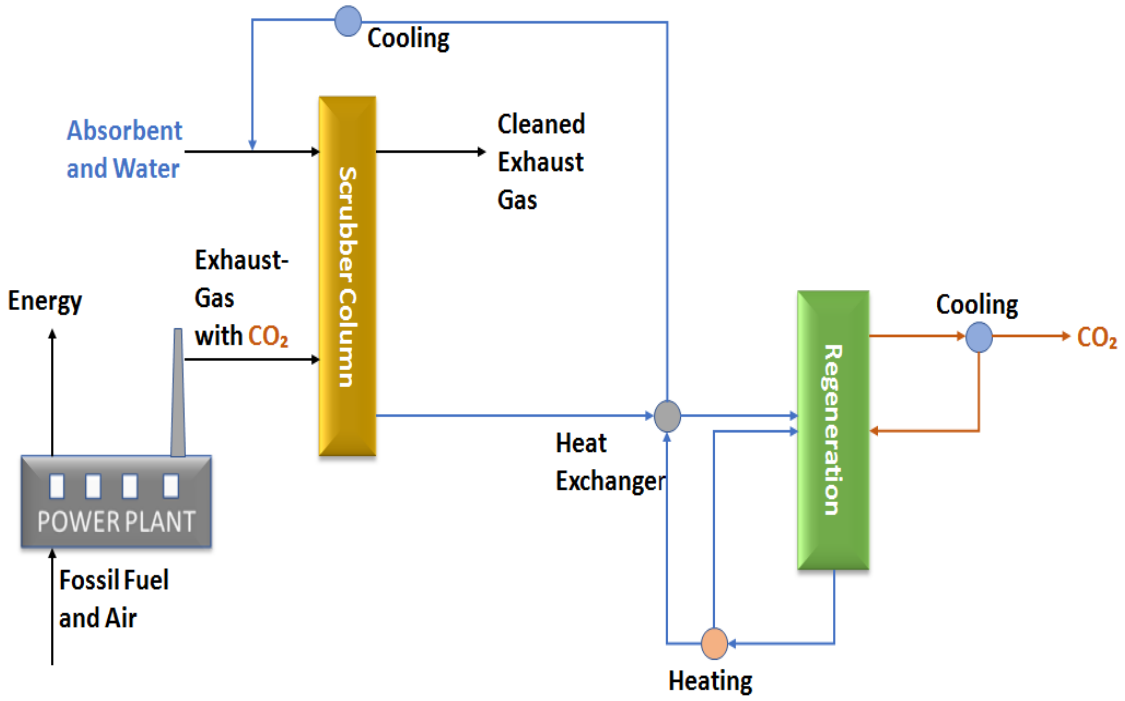

Figure 1.4 Graphic design of post-combustion capture process

1.2.3 Post-combustion

CO_2 is caught after combustion in post-combustion capture technology and deployed as a distinct separation unit in thermal power plants or other significant point sources. Because CO_2 in the exhaust stream is diluted by nitrogen in the combustion air, many gases must be handled. Membrane separation, adsorption, physical absorption, and chemical absorption are some of the separation processes used. [8].

1.3 Carbon dioxide capture technologies for the post-combustion process

Various CO_2 separation processes, such as absorption, adsorption, cryogenic distillation, and membrane separation, can be used within the post-combustion capture (PCC) technology [8]. The leading technologies used in PCC applications are summarized in Fig 1.5.

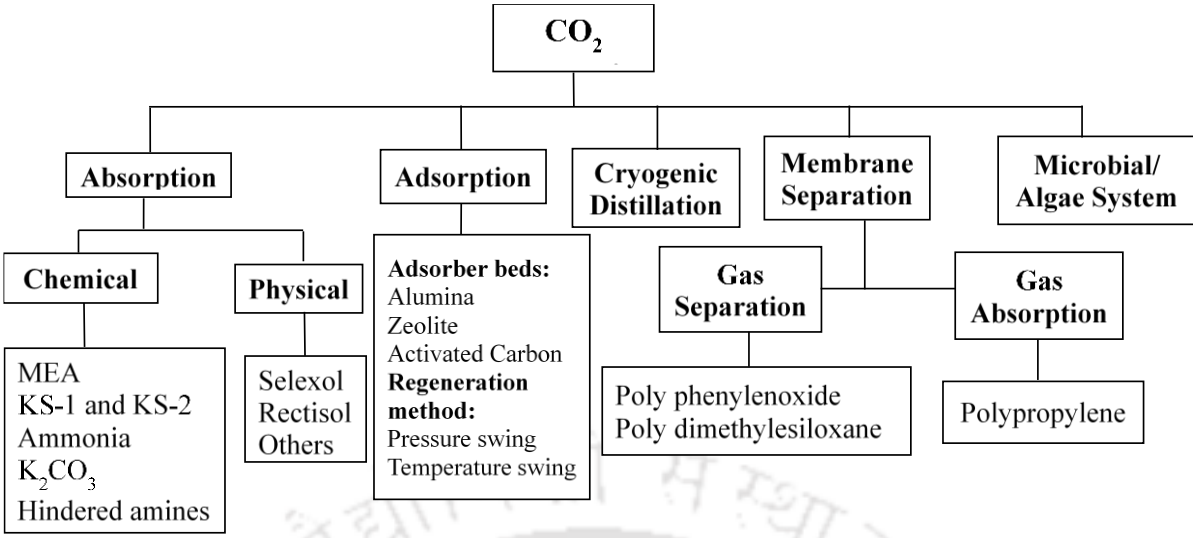

Figure 1.5 Post-combustion CO_2 capture process technologies [10]

Various CO_2 separation technologies are now available, and they are all explained in detail [8]. According to [9], chemical solvent absorption (reactive absorption) is the most practical method in most circumstances. The most common absorbents utilised in the gas processing sector are aqueous alkanolamine solutions. Amines, alkaline amino acid salts, and carbonate-bicarbonate buffers are also used in bulk CO_2 removal.

1.3.1 Chemical absorption process

Chemical absorption's central premise is based on the varying reactivities of solute gases with solvents. The process in the system is mainly reversible, allowing the CO_2-rich solvent to be regenerated at the same time. Basic absorbents such as aqueous ammonia, alkali carbonates, and alkanolamines are utilised as solvents in the absorption process. The chemical solvents significantly interact with CO_2, resulting in faster CO_2 removal in a single stage of the absorption process.

The primary amines, monoethanolamine (MEA) and diglycolamine (DGA), the secondary amines, diethanolamine (DEA) and diisopropanolamine (DIPA), and the tertiary amines,

methyldiethanolamine (MDEA), and triethanolamine (TEA) are all industrially important alkanolamines for CO_2 removal, according to Kohl and Nielsen [10]. MEA is extensively used for gas purification due to its high reactivity with CO_2.

A closed-loop absorption-desorption cycle comprising CO_2 absorption in an MEA scrubber, regeneration of the CO_2-rich solution by desorption, and recycling of the lean regenerated MEA solution to the scrubber represents a standard process configuration. MEA, on the other hand, has several drawbacks, including a low CO_2 loading capacity, a high solvent regeneration cost, the formation of toxic products due to degradation in an oxygen-rich environment (for example, flue gas), reduced scrubbing efficiency due to amine decomposition, and equipment and piping corrosion [10-11]. Besides, MEA has a high vapour pressure, and hence, it is not suitable for low-pressure operations due to possible vaporisation losses. As a result, finding other candidate amines is desirable. MEA requires more steam regeneration than DGA and DIPA. Although MDEA is less reactive than MEA, it has a larger CO_2 loading capacity. Another potential solvent is 2-amino-2-methyl-l-propanol (AMP), a sterically hindered primary amine that mimics the hindered form of MEA. The CO_2 loading capacity and reaction rates of AMP are more significant than those of MEA, according to reference [12]. AMP and DEA are more resistant to solvent degradation and corrosion than MEA; additionally, according to [13], no degradation or erosion occurs when MDEA is used.

MEA and DEA are primary and secondary alkanolamines that react quickly with CO_2 to generate carbamates. The heat of absorption associated with carbamate production, on the other hand, is quite considerable. As a result, the expense of solvent regeneration is significant. Furthermore, the capacity of such alkanolamines to load CO_2 is restricted to 0.5 mol CO_2 per mol of amine. Tertiary alkanolamines, which have a low reactivity toward CO_2, lack a hydrogen atom linked to the nitrogen atom, as do MEA and DEA, and hence cannot undergo

the carbamation reaction. On the other hand, Tertiary amines stimulate the CO_2 hydrolysis reaction, which produces bicarbonates. Because the reaction heat emitted in bicarbonate creation is smaller than that released in carbamate synthesis, solvent regeneration costs are lower.

Furthermore, tertiary amines have a sizeable CO_2 loading capacity of l mol CO_2/mol amine, as evident from the activated methyldiethanolamine (MDEA) technology suggested by BASF SE, the addition of promoters to tertiary amines accelerates the reactive absorption process. Thus, the cyclic diamine piperazine (PZ) enhances the CO_2 absorption rates in aqueous MDEA solutions. Conventional primary and secondary amines (e.g., MEA and DEA) and other polyamines (e.g., hexamethylene diamine or HMDA) also are efficient activators in aqueous solutions of tertiary amines [14]. Conventional alkanolamine used in the PCC process includes monoethanolamine (MEA), diethanolamine (DEA), N-methyldiethanoalmine (MDEA), 2-amino-2-methyl-1-propanol (AMP), piperazine (PZ), etc. [6, 15-16]. The molecular structures of some crucial amines are shown in Fig. 1.6.

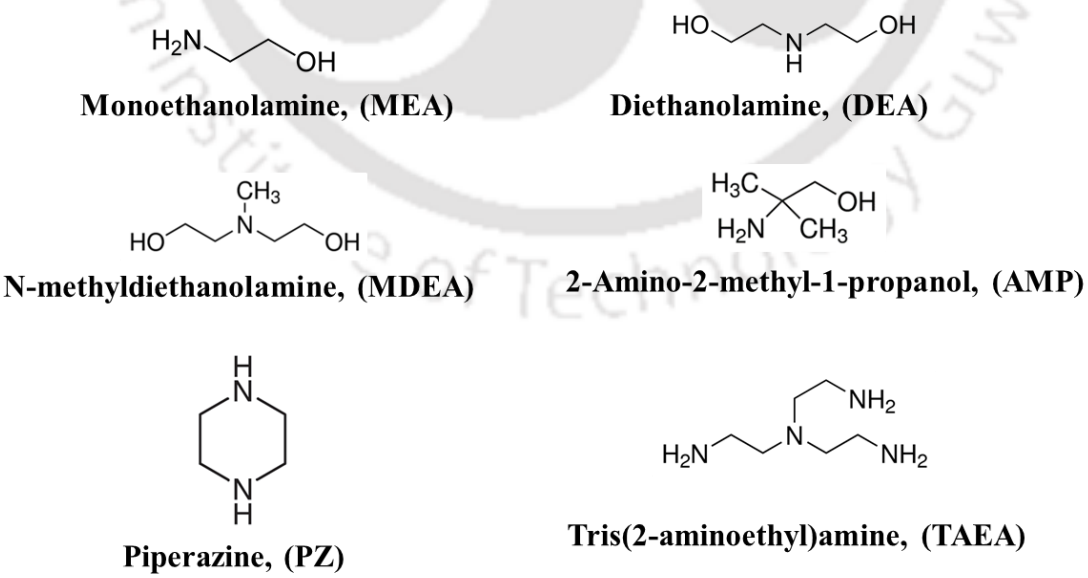

Figure 1.6 Chemical structure of amines used in CO_2 capture application.

Blended amine solvents, which blend primary and secondary amines with tertiary or sterically hindered amines that have superior CO_2 loading with faster reaction kinetics, are also viable for CO_2 capture for the post-combustion process. Piperazine (PZ), a rate activator, has been combined with slow reacting alkanolamines with promising results [16]. PZ is more resistant to heat and oxidative degradation than typical amines, allowing lower amine concentrations to be used.

An absorption column and a regenerator column make up an amine-based chemical absorption system (Fig 1.7). As part of the post-combustion CO_2 separation method, flue gas from power plants enters a packed tower from the bottom, making counter-current contact with the CO_2-lean amine solvent.

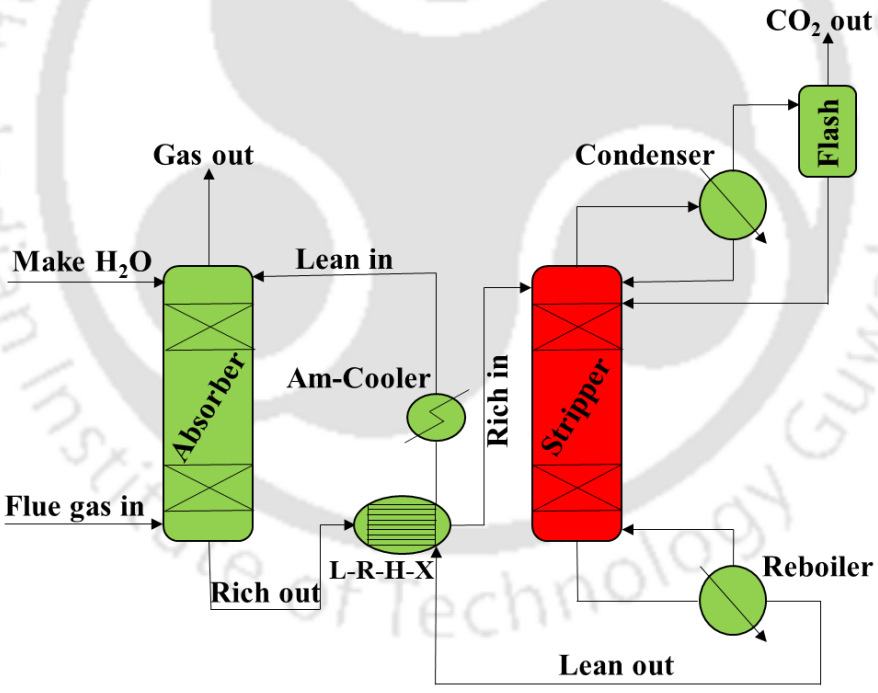

Figure 1.7 Schematic of CO_2-amine absorption technology

After the chemical reaction-aided absorption phase, the CO_2-rich solvent enters the stripper column via a heat exchanger for solvent regeneration. Steam is used in the regenerator column to extract CO_2 from the solvent at temperatures of 393.15-403.15 K. The pure CO_2 stream from the regenerator column can be compressed even further for storage or other downstream

applications, while the lean amine solvent is cooled to 313.15-333.15 K and returned to the absorption column via a lean, rich heat exchanger [17]. There are, however, certain energy costs associated with this technique. The first is the reboiler's heat duty, which includes steam generation and desorption heat to remove CO_2 from the solvent. The second energy source is utilised to compress CO_2 to the requisite storage conditions and power the numerous intermediary metering devices.

1.3.2 Physical absorption process

According to Henry's law, CO_2 gas molecules are absorbed in a liquid solvent during the physical absorption process. As a result, the entire absorption process is controlled by temperature and pressure. Instead of reacting chemically, the technique uses organic solvents to absorb the solute component physically. The weak van der Waals or electrostatic force is responsible for the essential connection between the solvent molecules and the solute CO_2 gas. In comparison to chemical solvents, these linkages are weaker. The partial pressure of the gas can be proportionately connected to the volume of solute gas absorbed in the system. When the partial pressure of CO_2 is higher and the temperature is lower, this reaction is more favorable. Reducing the system pressure or heating can help in the regeneration process. Commercially accessible physical solvents include cold methanol (Rectisol), N-methyl-2-pyrollidone (Purisol), polyethylene, dimethyl ether of polyethylene glycol (Selexol), propylene carbonate (Fluor Process), and sulfolane. [6]. The employment of a physical solvent as the only post-combustion capture approach is limited, however, due to the low partial pressure of CO_2 in the flue gas. As a result, some CO_2 capture units looked into using mixed solvents, which combine physical and chemical solvents. The sulfinol procedure, which used a mixture of physical solvents like sulfolane and chemically reactive amines like DIPA or MDEA, is the most prevalent example given here.

1.3.3 Physical adsorption process

The adsorption technique relies on a solute molecule's inherent thermodynamic characteristics to shift from the gas phase to preferentially adsorb on the adsorbent's surface. Physisorption and chemisorption are two types of adsorption. After adsorption, either pressure swing or temperature swing adsorption can regenerate or desorb the material. The active molecular sieves with amine coatings, metal-organic frameworks (MOF), and grafted zeolites are the subjects of considerable research [18-19]. Polyethyleneimine or Na_2CO_3 based adsorbents are often utilised grafting agents for this sorbent to adsorb CO_2 from exhaust gas [20]. However, this approach will need a lot of R&D before it can be used to treat high-volume flue emissions in the industry.

1.3.4 Cryogenic separation process

Cryogenic separation is based on the idea that CO_2 may be separated from other gases by chilling and condensation. Cryogenic separation effectively treats gas streams with high CO_2 concentrations (> 90%), but it is less effective in treating dilute CO_2 streams. Cooling gases to shallow temperatures (below -346.45 K) allows CO_2 to be frozen out or liquefied and separated [21]. CO_2 is recovered/extracted as a liquid, making it easy to transport to storage facilities or pump to injection locations for enhanced oil recovery (EOR) applications. The high expense of refrigeration and removing water traces from streams to avoid condensate traps are the procedure's key drawbacks.

1.3.5 Membrane technology process

CO_2 may be removed from flue gas streams using gas separation membranes. Gas separation membranes and gas absorption membranes are two types of membrane technologies that can separate CO_2 from other gases. Gas separation membranes for PCC are available in various grades, including porous or non-porous organic polymeric or inorganic membranes (carbon,

zeolite, ceramic, or metallic) [22]. Another type of membrane is imbued with reactive agents like amine, which selectively reacts with CO_2 [19]. Even though membranes have some advantages over traditional absorption technology, such as minimal regeneration energy demand and a simple modular system, they cannot consistently achieve a higher degree of separation, necessitating the use of multiple recycling stages [23]. Other drawbacks of membranes include their increased sensitivity to Sulphur compounds and other trace elements. Researchers have recently combined membrane separation methods with other methodologies such as chemical absorption processes to reap the benefits of the procedures.

The high expense of solvent regeneration is the key source of worry for amine-based chemical absorption techniques. Furthermore, the solvent's oxidative and thermal breakdown need a more significant amount of solvent to make–up. On the other hand, chemical absorption has the advantage of being the most well-established method for CO_2 capture and is suitable for retrofitting existing plants. Chemical absorption is recognised as a reliable and somewhat cost-effective technique to reduce CO_2 emissions compared to other known technologies for CO_2 capture from industrial flue gas streams [8]. Using an energy-efficient aqueous amine solvent, chemical absorption is also the most practical technique for industrial mass scale acid gas separation. The alternatives are either in development or are too expensive. As a result, novel amine solvents, such as sterically hindered amines or tertiary amines, are currently the focus of global R&D, aided by amine activators with improved CO_2 selectivity, degradation resistance, and lower reboiler heat duty.

1.4 Literature review

Amine-based absorption-regeneration has been routinely utilised to remove acid gases from flue gas and natural gas streams for many years. Li et al. [24] observed that boosting CO_2 loading capacity can increase the hindrance placed on the amino-functional groups found in

distinct amine categories. Trends include primary amines, secondary amines, tertiary amines, and diamines. The thorough characterization of a solvent for usage in the PCC unit requires a fundamental understanding of acid gas solubility and thermophysical properties.

1.4.1 CO_2 absorption in a single amine solvent

For the rational design and optimization of acid gas removal units, data on CO_2 solubility in aqueous amine solutions under various experimental parameters, such as temperature, pressure, and solvent concentration, is critical. Carbon dioxide solubility in single aqueous amines has been thoroughly examined by several researchers throughout the world, as shown in Table 1.1. Because of their stochiometric restrictions with CO_2, primary and secondary amines have a lower CO_2 loading capacity than tertiary and sterically hindered amines. On the other hand, the increased loading could be due to carbamate species hydrolysis at higher CO_2 partial pressures. Many studies on the solubility of aqueous monoethanolamine solution have been published [25-30]. It is frequently employed as a base case solvent in comparison investigations of new solvents for CO_2 absorption, in addition to its use as a low-cost conventional solvent in acid gas treatment technologies. The use of highly concentrated MEA, according to Bouillon et al. [31], can improve CO_2 absorption performance.

Table 1.1 CO_2 solubility measurement in several single amine solvents: a summary of the literature

Amine	Concentration, wt%	Temperature, K	CO_2 Partial Pressure, kPa	Reference
Monoethanolamine	30	0-348.15	1.387 – 100.2	Mason et al. [25]
(MEA)	15.3	313.15-413.15	0.56 – 4862	Jones et al. [26]
	30	0 – 333.15	0.0012-19954	Jou et al. [27]
	(15-30)	313.15-373.15	0.288 – 842.7	Lee et al. [28]
	30	393.15	7.3 – 191.9	Mamun et al. [29]
	(15-60)	313.15-393.15	0.001 - 20	Aronu et al. [30]

Diethanolamine (DEA)	(10-30)	373.15-473.15	105 - 2451	Kennard et al. [32]
	(20-30)	303.15-323.15	0.1-100.9	Benamor et al. [33]
	(25-35)	303.15 –323.15	0.098 - 100	Sulaiman et al. [34]
Diisopropanolamine (DIPA)	30	313.15-373.15	2.7 - 5888	Isaacs et al. [35]
N-Methyldiethanoalmine (MDEA)	30	313.15-373.15	1.2 - 1890	Shen et al. [36]
	50	328.15-85358.15	65 - 754	Mamun et al. [29]
	50	298.15-373.15	8.27 – 140	Park et al. [37]
	50	373.15-473.15	138-4930	Chakma et al. [38]
	(5-75)	323.15-373.15	1-235	Rho et al. [39]
Triethanolamine (TEA)	(20-30)	303.15-323.15	1.62- 98	Chung et al. [40]
2-(diethylamino)-ethanol	(30-40)	333.15 – 353.15	3.7 - 192	Xu et al. [41]
2-amino-2-methyl-1-propanol (AMP)	(20-30)	303.15-323.15	4.05 -91	Kundu et al. [42]
	30	323.15	4.3 - 5645	Teng et al. [43]
	(30-40)	298.15-328.15	0.601-1450	Dash et al. [44]
1-dimethylamino-2-propanol (DMAP)	30	298.15-333.15	8.2- 100	Liang et al. [45]

In their study, Aronu et al. [30] looked at CO_2 solubility in an aqueous MEA system over a wide range of experimental temperatures and CO_2 partial pressures. Their findings reveal that at more significant loadings, the CO_2 solubility is strongly influenced by the solvent content. With increasing amine content and CO_2 loading, the equilibrium CO_2 partial was discovered to increase. To correlate the solubility data, the extended Uniquac model was used. The model was used to great success to forecast the ionic speciation profile, heat of absorption, and amine volatility. MEA has a high heat of absorption, which directly impacts the heat duty. For a 2 M and 4 M aqueous diethanolamine (DEA) solution, Benamor et al. [33] achieved CO_2 loadings of 0.786 and 0.671 at a CO_2 partial pressure of roughly 100 kPa. They used titration analysis

to determine the carbamate ion concentration and compared the model's predictions. The solubility data were fitted simultaneously to estimate the numerous binary interaction factors needed to compute the Deshmukh Mather Model's activity coefficients [33].

Even though tertiary amines, such as N-methyldiethanolamine (MDEA), have slower kinetics, they have several essential characteristics with primary amines, such as lower vapour pressure and superior thermal and chemical durability. MDEA can also be used at a high concentration in gas sweetening technology since it has a lesser corrosion behavior. Using a highly concentrated solvent reduces the rate of solvent circulation in the absorption process, resulting in better plant economics. Because MDEA does not react with CO_2 in the absence of water, water plays a crucial role in the tertiary amine – CO_2 reaction system [39]. Furthermore, as suggested by Barth et al. [47], the aqueous media enhances the dissolution of MDEA by hydrogen bonding, and this interaction promotes the hydration process of CO_2. Rho et al. [39] evaluated and expressed CO_2 solubility in the variable concentration range of (5 to 75) wt percent to investigate the effect of solvent concentration. According to their findings, the CO_2 loading reduces as the mass concentration of MDEA increases at a given operating temperature and CO_2 partial pressure. The absorption capacity plot was used to express the solubility data (mol of CO_2 per volume of solution). The plot shows that using a 20.5 wt percent MDEA solution at pressures below 10 kPa is preferable. However, using 50 mass percent MDEA at higher pressures yields superior results. In addition, the Gibbs-Helmholtz equation was used to calculate the enthalpy of CO_2 absorption, which was determined to be 54.6 $kJ.mol^{-1}$ for 50 mass percent MDEA. Furthermore, research into substitute tertiary amines with faster kinetics than MDEA leads to the discovery of 1-dimethylamino-2-propanol (1DMA2P), a novel tertiary amine category. The findings of Liang et al. [45] show that 1DMAP has a more excellent equilibrium CO_2 solubility than other standard amines like MEA and MDEA. According to the mass transfer study, the overall mass transfer coefficient (KGav) in a packed column is MEA

> 1DMA2P > MDEA. The CO_2 absorption heat calculated using the Gibbs-Helmholtz equation was -30.5 kJ.mol^{-1}, which is significantly lower than MEA and the commonly used tertiary amine MDEA.

Sartori and Savage [12] indicated that sterically hindered amines could be investigated as a potential CO_2 capture solvent. Among the sterically hindered amines, AMP is the most common due to attractive characteristics, including a theoretical capacity that is double that of MEA. According to Chakraborty et al. [48], 13C NMR analysis, the AMP carbamate generated in a relatively small amount compared to its fast-reacting unsubstituted equivalent, MEA. Xu et al. [49] measured the intermediate carbamate species and discovered that it was only 10^{-4} of the total amine concentration. This observation suggests that the unstable carbamates generated during the process may undergo fast hydrolysis, resulting in the formation of bicarbonate ions and free amine species. Dash et al. [44] report a theoretical and experimental investigation of CO_2 solubility in an aqueous AMP solution at various concentrations. According to their findings, when the aqueous AMP solution's concentration increases at a constant operating temperature and CO_2 loading, the CO_2 partial pressure rises. Kundu et al. [42] reported similar trends. The thermodynamic model created based on the electrolyte non-random two-liquid (ENRTL) theory describes the experimental solubility data. The model's projected activity coefficients were used to forecast the liquid phase ionic speciation profile concerning changes in CO_2 loading. According to the speciation plot, the AMP disappears as CO_2 loading increases, and protonated species and bicarbonate ions dominate the system. The thermodynamic model was also used to predict the volatility of AMP, which was found to be 0.001 kPa for a 40 wt percent aqueous amine solution at 338 K using the thermodynamic model. In addition, between T = (313 - 373) K, the average heat of absorption was determined to be 70 kJ.mol^{-1} CO_2.

1.4.2 Absorption of CO_2 in the blended amine solvent

In acid gas separation technology by chemical absorption, the notion of acceptable amine blending is gaining prominence to overcome the constraints of a single amine solvent. The blended amines are formulated using the synergetic effect of primary or secondary amines' improved reaction kinetics and tertiary or sterically hindered amines' higher CO_2 loading and lower regeneration energy. Table 1.2 briefly summarizes the literature review of CO_2 solubility in blended amine systems.

Table 1.2 CO_2 solubility measurement in several blended amine solvents: a summary of the literature

Amine blends	Concentration, wt%	Temperature, K	CO_2 Partial Pressure, kPa	References
Monoethanolamine + *N*-Methyldiethanoalmine	MEA : (6 – 18) MDEA : (12 – 24)	313.15 – 373.15	1.12 - 2080	Li et al. [50]
	MEA : (12 – 24) MDEA : (6 – 18)	313.15 – 373.15	1- 2016	Shen et al. [36]
Monoethanolamine + 2-amino-2-methyl-1-	MEA : (6 – 24) AMP : (6 - 24)	313.15 – 373.15	0.86 - 199	Li et al. [51]
Diethanolamine + 2-Amino-2-methyl-1-	DEA : (6 – 15) AMP : (15 - 24)	303.15 – 323.15	1.021 - 354	Kundu et al. [52]
Diethanolamine + *N*-Methyldiethanolamine	DEA : (1.5 – 4.5) MDEA : (25.5 – 28.5)	303.15 – 323.15	2.4 - 90	Kundu et al. [53]
2-amino-2-methyl-1-propnaol + N-Methyldiethanolamine	AMP : (8.9 – 17.7) MDEA : (11.8 – 23.4)	303.15 – 343.15	106.25 - 4110	Suleman et al. [34]
N-Methyl-2-ethanolamine + N-Methyldiethanolamine	MAE : (3 - 24) MDEA : (6 - 27)	303.15 – 323.15	0.503 – 545.6	Kumar et al. [54]
2-amino-2-methyl-1-propnaol + N-Methyl-2-	MAE : (1.5 - 21) AMP : (9 – 28.5)	303.15 – 323.15	0.511 – 515.7	Kumar et al. [54]

As a preliminary amine blend for CO_2 absorption, mixtures of primary and tertiary amines (MEA + MDEA) have been extensively explored. Li et al. [50] investigated the solubility of CO_2 in aqueous (MEA + MDEA) over a wide range of temperature and pressure working conditions. According to their research, CO_2 solubility decreases steadily as temperature rises from 313.15-353.15 K. At a position when the partial pressure of CO_2 is 45 kPa, the solubility curves also intersect. Another study by Li et al. [51] looked at the CO_2 absorption properties of a mixture of MEA and sterically hindered AMP solvent. CO_2 solubilities are higher in solutions with a higher AMP mass fraction than those with a high MEA mass fraction. The Kent-Eisenberg model is used to correlate the solubilities. As a function of reaction temperature, amine concentration, and CO_2 loading, the equilibrium constants of amine-based reactions are calculated. The solubility of CO_2 in (DEA + AMP) and (DEA + MDEA) blends was examined by Kundu et al. [52-53]. They saw a cross-over in the solubility curves of various blended compositions. The explanation for this can be linked to the fact that DEA can react with CO_2 faster than MDEA at low to moderate loadings due to its quicker kinetics. However, as CO_2 loading rises, the free DEA species decreases, resulting in a higher MDEA to DEA ratio in the aqueous system. The equilibrium is closer to MDEA than DEA with more significant loadings, causing the curves to cross. The modified Clegg-Pitzer equations are used to correlate the solubility data. A simulated annealing approach was used to calculate interaction parameters and determine the equilibrium composition of various ionic species present in the liquid phase.

More recently, there has been increased interest in using enhanced and activated alkanolamine solvents for CO_2 removals, such as piperazine (PZ) activated MDEA or AMP [55-56]. These activated blended solvents have the desirable characteristics of considerably greater reaction speeds and higher activating agent solubility. These activating agents are frequently used with

non-carbamate forming amines, with higher loading capacity and lower regeneration heat duty. Table 1.3 provides a quick summary of the CO_2 solubility measurement in the activated amine system. The CO_2 loading increases with the increase in PZ content in the mixed amine solvents of (PZ + MDEA) up to a loading of 1.0, according to Dash et al. [56]. A crossover has been recorded at a steady CO_2 partial pressure beyond this threshold value, where the loading decreases with increasing PZ concentration. This phenomenon is linked to the creation of intermediate reaction products such as PZ- carbamate, PZ-dicarabamte, and protonated PZ carbamate, according to Bishnoi and Richelle [57]. As a result of synthesizing all of these intermediates, the total carbamate stability improves, and more amine molecules are attached to each incoming CO_2 molecule in the absorber column.

Table 1.3 CO_2 solubility measurement in several activated amine solvents: a summary of the literature

Amine Blends	Concentration, wt%	Temperature, K	CO_2 Partial Pressure, kPa	Researchers
Piperazine + 2-amino-2-methyl-1-propanol	PZ: (2 - 8) AMP: (22 - 28)	313.15– 393.15	5.7 – 463.5	Tong et al. [55]
Piperazine + N-Methyldietahanolamine	PZ: (2 - 8) MDEA : (22 - 28)	303.15 – 323.15	1.85 - 1246	Dash et al. [56]
	PZ: (8.5 – 16.8) MDEA : (11.8 – 23.4)	303.15 – 343.15	102.5 - 4490	Suleman et al. [34]
Piperazine + Diethylenetetramine	PZ: (5 - 15) DETA : (15 - 25)	313.15- 353.15	0.8 - 923	Chang et al. [58]
Hexamethylenediamine + N-Methyldiethanolamine	HMDA: (5 - 20) MDEA : (10 - 25)	303.15 – 333.15	0.5 - 111	Mondal et al. [59]
Hexamethylenediamine + 2-amino-2-methyl-1-propanol	HMDA: (5 - 20) AMP : (10 - 25)	303.15 – 333.15	1.04 -110.57	Mondal et al. [60]
Ethylenediamine + N-Methyldiethanolamine	EDA: (5 - 15) MDEA : (85 - 95)	293.15 – 313.15	40 - 180	Hafizi et al. [61]
Diethylenetetramine + N-Methyldiethanolamine	DETA: (5 - 15) MDEA : (85 - 95)	293.15 – 313.15	40 -180	Hafizi et al. [61]

Triethylenetetramine + N-Methyldiethanolamine	TETA: (5 - 15) MDEA : (85 - 95)	293.15 – 313.15	30 - 180	Hafizi et al. [61]
Tetraethylenepentamine + N-Methyldiethanolamine	TEPA: (5 - 15) MDEA : (85 - 95)	293.15 – 313.15	30 -190	Hafizi et al. [61]
1,3-diaminopropane + Monoethanolamine	DAP: (2.5 - 5) MEA : (10 – 12.5)	313.15 – 333.15	3 - 215	Khodadi et al. [62]
Piperazine + Potassium carbonate	PZ: (7.5 - 10) K_2CO_3 : (15 - 20)	313.15 – 363.15	1.8 - 675	Kim et al. [63]
2-methylpiperazine + Potassium carbonate	2-MPZ: (7.5 - 10) K_2CO_3 : (15 - 20)	313.15 – 363.15	1.8 - 675	Kim et al. [63]
2-((2-aminoethyl)amino)ethanol + N-Methyldiethanolamine	AEEA: 5 MDEA: 30	308.15 – 368.15	103 - 4445	Zoghi et al. [64]

Dash et al. [65] used the ENRTL model to explain the thermodynamics of CO_2 absorption in the (AMP + PZ) mixed amine system. Within the AAD value of 12%, the model was employed to describe the solubility data adequately. The predicted speciation plot differs significantly from the single AMP or PZ system. Compared to 30 and 40 wt percent systems, the mixed blend concentration of 50 wt percent has the maximum cycle capacity. Among the examined systems, the mixed system with the composition (42 wt percent AMP + 8 wt percent PZ) had a maximum capacity of 1.8. The thermodynamic model was also used to evaluate amine volatility, which was lower than that of single amines. The findings of Tong et al. [55], who investigated CO_2 solubility for two different mixed amine compositions, back up the above essential results. The solubility data are well correlated with a modified Kent-Eisenberg model based on non–rigorous equilibrium, yielding an average absolute relative deviance. Compared to the usual 30 wt percent MEA solvent, the investigated amine system has double the CO_2 loading capacity. Despite its excellent characteristics, the applicability of PZ in concentrated form is limited due to solid precipitation under both lean and rich CO_2 loading circumstances. Concentrated PZ solution (8 $mol.kg^{-1}$) requires a net CO_2 input of 0.25 mol of CO_2 per mol of

alkalinity to remain prevalent in the aqueous solution at room temperature (295 K) without precipitation. Solids can form at greater CO_2 concentrations as well [66].

Another intriguing class of activators, derivatives of piperazine, has been investigated for their potential use in CO_2 absorption from acid gas streams. Kim et al. [63] reported the CO_2 absorption rate and capacity after mixing K_2CO_3, an inorganic solvent, with 2-methylpiperazine (2-MPZ) and piperazine (PZ). Because 2-MPZ has a methyl group attached to PZ's cyclic diamine structure, it has a steric hindrance effect. Compared to piperazine, this results in the creation of unsatable carabamte and a substantial amount of bicarbonate and carbonate species, potentially lowering the total regeneration cost (PZ). They discovered that the aqueous blend of (20 wt% K_2CO_3 + 10 wt% 2-MPZ) and (20 wt% K_2CO_3 + 10 wt% PZ) had the lowest equilibrium CO_2 partial pressure for any corresponding CO_2 loading at the same temperature. These solutions, however, saw a considerable number of $KHCO_3$ crystals at temperatures lower than 313 K. Before starting the reaction with CO_2, the aqueous system separated into two liquid phases.

Another possible piperazine derivative, 1-(2-aminoethyl) piperazine (AEP), has recently been discovered to have more great absorption properties to PZ. At 303, 313, and 323K, Paul et al. [67] examined the kinetics of dilute aqueous AEP solution and found that the second-order rate constants k_2 were 31867.6, 56354.2, and 100946 $m^3.kmol^{-1}.s^{-1}$. The second-order reaction rate constant measured is somewhat higher than the aqueous PZ solution. Du et al. [66] combined a less concentrated PZ solution with AEP to solve the precipitation problem while preserving all of the desirable properties of PZ solutions for PCC applications. The ENRTL model correctly analysed the thermodynamics of the mixed solvent system, and the CO_2 solubility, speciation, and amine volatility were accurately reproduced. The mixed system is predicted to

have a cyclic capacity of 0.86 mol.kg^{-1}, compared to 0.50 mol.kg^{-1} for the 7 mol.kg^{-1} MEA system. Ramazani et al. [68] reported the promoting impact of 1-(2-aminoethyl) piperazine on the equilibrium CO_2 solubility of monoethanolamine. As the concentration of AEP in the blend increases, the loading capacity of the blended solution increases, with maximum loading attained at a molar ratio of 0.8, equivalent to a (0.5 M AEP + 2.5 M MEA) system. The link between the numerous independent factors on the CO_2 loading capacity was assessed using the response surface methodology based on central composite design.

Hexamethylenediamine is another possible activator recently studied in the literature (HMDA). The CO_2 loading capacity of different amines with numerous amine groups was compared by Singh et al. [69]. They looked at the CO_2 loading capacity of several straight-chain diamines and concluded that HMDA has superior absorption to other straight-chain diamines. Mondal et al. [59-60] widened the scope of the inquiry. With AMP and MDEA as primary amines, their research spans binary and mixed systems. When HMDA is added to a mixed amine system, the CO_2 loading increases dramatically. The CO_2 loading for the (15 wt. percent HMDA + 15 wt. percent AMP) system was increased by 30% compared to the 30 wt. percent AMP system. The authors also assessed the heat of absorption in the aqueous HMDA and (HMDA + MDEA) systems in addition to the solubility investigation [70]. The heat of absorption is the most critical factor to consider when choosing a solvent because it directly affects the energy penalty in the regeneration process. Because highly reactive amines have a greater enthalpy of CO_2 absorption, the increase in reaction rate due to blending is also linked to the increased absorption heat. As a result, the blending ratio should be tuned using kinetic, solubility, and enthalpy data. The aqueous mix of (15 wt. percent HMDA + 15 wt. percent MDEA) translates to H_{abs} = 79 kJ.mol^{-1} at a CO_2 partial pressure of 15 kPa and a temperature of 313 K, compared to 84 kJ.mol^{-1} for a 30 wt. percent MEA solution.

Their chain length also influences the CO_2 absorption capacity of alkylamines. The initial absorption rate decreases as the chain length increases and CO_2 loading increases. The impact was studied by Hafizi et al. [61], who combined MDEA with several Polyamines containing varied numbers of alkyl and amine groups, such as EDA, DETA, TETA, and TEPA. The CO_2 loading is enhanced from 0.91 for pure MDEA to 0.94, 0.99, 1.01, and 1.05 for 15 wt% EDA, DETA, TETA, and TEPA boosted solvent systems their findings. Continuous absorption-desorption operations were used to investigate the solvents' cyclic capacity. Primary carbamate > primary - primary dicarbamate > primary secondary dicarbamate, in that order, is the most stable of the produced ions. The desorption investigation further reveals that amine blends with a larger ratio of secondary to primary amine groups result in more secondary carbamate and dicarabamate species, resulting in better or complete regeneration of these species.

1.5 Importance and objectives of present work

The complete literature research shows the vast industrial significance of acid gas (such as CO_2) absorption utilising activated alkanolamine solutions. As a result, a novel amine activator with faster reaction kinetics and high equilibrium loading capacity was required to reduce solvent circulation rate, improve degradation resistance, and minimise corrosivity, all of which would result in cheaper capital costs. The absorber column will be substantially smaller due to the quick reaction, and hence the price will be lower.

Above all conditions, we introduced a novel activator Tris(2-aminoethyl)amine (TAEA), with three primary amine groups and one tertiary amine group. And it is expected to have a larger equilibrium loading capacity than PZ. TAEA also has a lower evaporation rate than PZ due to its greater molecular weight. Furthermore, no such amine activator has been found in the

literature to our knowledge. TAEA was chosen as an unique CO_2 absorption activator for several amine mixtures in this investigation. In addition, because of the potential of AMP and MDEA, two novel aqueous blends were chosen in this study: (TAEA+MDEA+H_2O) and (TAEA+AMP+H_2O). Any new solvent system's physicochemical characteristics and absorption of CO_2 are critical for its commercial application. As a result, the following are the goals of this research project:

- To measure thermophysical characteristics (density, viscosity, and diffusivity) of aqueous single (TAEA+H_2O) and blended amine solutions (TAEA+MDEA+H_2O), (TAEA+AMP+H_2O) solutions were measured over a wide temperature range (293.15-333.15) K and at various amine concentrations.
- To model the measured thermophysical properties using well-established empirical models like Redlich-Kister and Grunberg-Nissan.
- To measurement the physical solubility (Henry's law constant of N_2O) in the aqueous single (TAEA+H_2O) and blended amine solutions (TAEA+MDEA+H_2O), (TAEA+AMP+H_2O) over a wide range of temperature (293.15-323.15) K and different amine concentrations.
- To model the physical solubility with an Arrhenius type equation.
- To generate equilibrium solubility data of CO_2 in blended aqueous solutions of N-methyldiethanolamine (MDEA) and 2-amino2-methyl-1-propanol (AMP) with the novel activator tris(2-aminoethyl)amine (TAEA) at various amine compositions over the temperature range of (293.15 -323.15) K and between the CO_2 partial pressure of 2-500 kPa.
- To model the equilibrium solubility data over blended solvent systems (Kent – Eisenberg equilibrium-based equation).

- To implement a Feed-forward Neural Network model utilising the Levenberg-Marquardt (LM) back propagation algorithm and correlation of the results of CO_2 solubility.

1.6 Thesis organization

The thesis is organized according to the given below.

Chapter 1: This chapter covers the background of the work related to CO_2 capture and the complete literature review, the thesis objectives, and the thesis outline.

Chapter 2: The reaction mechanisms of various categories of amines with CO_2, as well as the solubility modeling methodologies used in this study, are described.

Chapter 3: The measurement of critical thermo-physical properties such as density, viscosity, diffusivity, and Henry's law constant of (TAEA+H_2O), (TAEA + MDEA + H_2O), (TAEA + AMP + H_2O), and their correlation using Redlich Kister, Grunberg Nissan type equation, and Arrhenius type equation is the focus of this chapter.

Chapter 4: The solubility of CO_2 in blended aqueous solutions of N-methyldiethanolamine (MDEA) and 2-amino2-methyl-1-propanol (AMP) with the novel activator tris(2-aminoethyl) amine (TAEA) was measured experimentally throughout a wide range of composition, temperature, and CO_2 partial pressure in this chapter. The modified Kent-Eisenberg model is used to correlate the solubility data further. The equilibrium constants associated with amine deprotonation and carbamate hydrolysis reaction are regressed to link the solubility data. The CO_2-loaded solvent's pH and liquid phase speciation were also calculated using the thermodynamic equilibrium model. To evaluate the reaction scheme, FTIR-ATR and ^{13}C NMR studies are used. An optimal Feed forward neural network model using the Levenberg-Marquardt algorithm was built to correlate the solubility data.

Chapter 5: In a final remark, the overall results of this work, as well as future research directions, have been mentioned in this chapter.

References

[1] V.M. Delmotte, P. Zhai, H.O. Pörtner, D. Roberts, J. Skea, P.R. Shukla, A. Pirani, W. Moufouma-Okia, C. Péan, R. Pidcock, S. Connors, J.B.R. Matthews, Y. Chen, X. Zhou, M.I. Gomis, E. Lonnoy, T. Maycock, M. Tignor, T. Waterfield. IPCC, (Inter Governmental panel for climate change) 2018. World Meteorological Organization, Geneva, Switzerland, 32 pp.

[2] International Energy outlook 2018 Highlights, US Energy information administration, https://www.eia.gov/outlooks/ieo/.

[3] http://www.globalcarbonatlas.org/en/CO_2-emissions

[4] J.G. Oliver, A.H.W. Peters, Trends in global CO_2 and total greenhouse gas emissions, 2018, PBL Netherlands Environmental assessment agency.

[5] https://ourworldindata.org/per-capita-CO_2

[6] A.A. Olajire, CO_2 capture and separation technologies for end-of-pipe applications-A review, Energy 35 (2010) 2610-2628.

[7] Sreedhar, T. Nahar, A. Venugopal, B. Srinivas, Carbon capture by absorption – Path covered and ahead, Renew. Sustain. Energy Rev. 76 (2017) 1080–1107.

[8] A.B. Rao, E.S. Rubin, A technical, economic, and environmental assessment of amine-based CO_2 capture technology for power plant greenhouse gas control, Env. Sci. Tech. 36 (2002) 4467-4475.

[9] Meisen, X. Shuai, Research and development issues in CO_2 capture, Energy convers. Manage, 1997, 38, S37-S42.

[10] Kohl, R. Nielson, Gas purification, 5th ed, Gulf publishing company, Houston, 1997.

[11] R.J Hook, An investigation of some sterically hindered amines as potential carbon dioxide scrubbing compounds, Ind. Eng. Res, 1997, 36, 1779-1790.

[12] G. Sartori, D.W. Savage, sterically hindered amines for carbon dioxide removal from gases, Ind. Eng. Chem. Fundamen. 22 (1983) 239 – 249.

[13] Aroonwilas, A. Veawab, Characterization and comparision of the CO_2 absorption performance into single and blended alkanolamines in a packed column, Ind. Eng. Chem. Res, 2004, 43, 2228-2237.

[14] P.N. Sutar, P.D. Vaidya, E.Y. Kenig, Activated Deea solutions for CO_2 capture-A study of equilibrium and kinetic characteristics, Chem. Eng. Sci, 2013, 100, 234-241.

[15] S.K. Dash, A.N. Samanta, S.S. Bandyopadhyay, Simulation and parametric study of the post combustion CO_2 capture using aqueous 2-amino-2-methyl-1propanol and piperazine, Int. J. Greenh. Gas Control 21(2014) 130-139.

[16] J.T. Cullinane, G.T. Rochelle, Thermodynamics of aqueous potassium carbonate, piperazine, and carbondioxide, Fluid Phase Equilib. 227 (2005) 197-213.

[17] Stewart, M. Hessami, A study of methods of carbon dioxide capture and sequestration -the sustainability of a photosynthetic bioreactor approach, Energ. Convers. Manage. 46 (2005) 403-420.

[18] X.C. Xu, C.S. Song, J.M. Andresan, B.G. Miller, A.W. Scaroni, Novel Polyethyleneimine-modified mesoporous molecular sieve of MCM-41 Type as high-capacity adsorbent for CO_2 capture, Energ. Fuel 16 (2002) 1463-1469.

[19] S. Ullah, M.A. Bustam, M.A. Assiri, A.G. Al-Sehemi, M. Sagir, F.A. Abdul Kareem, A.E.I. Elkhalifah, A. Mukhtar, G. Gonfa, Synthesis, and characterization of metal-organic frameworks -177 for static and dynamic adsorption behavior of CO_2 and CH_4, Micropor. Mesopor. Mat. (2019) 109844.

[20] M.G. Plaza, C.Pevida, A. Arenillas, F. Rubiera, J.J. Pis, CO_2 capture by adsorption with nitrogen enriched carbons, Fuel 86 (2007) 2204-2212.

[21] Hart, N. Gnanendran, Cryogenic CO_2 capture in natural gas, Energy Procedia (2009), 697-706.

[22] Y. Han, W.S. W. Ho, Recent advances in polymeric membranes for CO_2 capture, Chi. J. Chem. Eng. 26 (2018) 2238 – 2254.

[23] V. Sluis, C.A. Hendriks, K. Blok, Feasibility of polymer membranes for carbon dioxide recovery from flue gas, Energ. Convers. Manage. 33(1992) 429-436.

[24] J. Li, A. Henni, P. Tontiwachwuthikal, Reaction kinetics of CO_2 in aqueous ethylenediamine, ethyl ethanolamine, and diethyl monoethanolamine solutions in the temperature range of 298-313 K, using the stopped-flow technique, Ind. Eng. Chem. Res. 46 (2207) 4426 – 4434.

[25] J.W. Mason, B.F. Dodge, Equilibrium absorption of carbon dioxide by solutions of the ethanolamines, Trans. Amer. Inst. Chem. Eng. 32 (1936) 27- 48.

[26] J.H. Jones, H.R. Froning, E.E. Claytor, Solubility of acidic gases in aqueous monoethanolamine, J. Chem. Eng. Data 4 (1959) 85-92.

[27] F. Jou, A.E. Mather, F.D. Otto, The solubility of CO_2 in a 30 mass percent monoethanolamine solution, Can. J. Chem. Eng. 73 (1995) 140 – 147.

[28] J.I. Lee, F.D. Otto, A.E. Mather, The solubility of H_2S and CO_2 in aqueous monoethanolamine solutions, Can. J. Chem. Eng. 52 (1974) 803 – 805.

[29] S. Mamun, R. Nilsen, H.F. Svendsen, Solubility of carbon dioxide in 30 mass % monoethanolamine and 50 mass % methyldiethanolamine solutions, J. Chem. Eng. Data 50 (2005) 630-634.

[30] U.E. Aronu S. Gondal , E.T. Hessen , T.H. Warberg , A. Hartono, K.A. Hoff , H.F. Svendsen, Solubility of CO_2 in 15,30,45 and 60 mass % MEA from 40 to120^oC and model representation using the extended UNIQUAC framework. Chem. Eng. Sci. 66 (2011) 6393 – 6406.

[31] P.A. Bouillon, E. Lemaire, A. Mangiaracina, C. Tabasso, First results of the 2.25 t/h post-combustion CO_2 capture pilot plant of ENEL at the Brindisi coal power plant with MEA from 20 to 40% wt. In: Proceedings of the first post-combustion capture conference (PCCC1), 2011, 17–19May, Abu Dhabi.

[32] M.L. Kennard, A. Melsen, Solubility of carbon dioxide in aqueous diethanolamine solutions at elevated temperatures and pressures, J. Chem. Eng. Data 29 (1984) 309-312.

[33] Benamor, M.K. Aroua, Modeling of CO_2 solubility and carbamate concentration in DEA, MDEA and their mixtures using the Deshmukh-Mather model, Fluid Phase Equilib. 231 (2005) 150 – 162.

[34] H. Suleman, A.S. Maulud, Z. Man, Experimental measurements and modeling of carbon dioxide solubility in aqueous AMP/MDEA and Piperazine/MDEA blends, Fluid Phase Equilib. 463 (2018) 142 – 148.

[35] E.E. Isaacs, F.D. Otto, A.E. Mather, Solubility of hydrogen sulfide and carbondioxide in an aqueous diisopropanolamine solution, J. Chem. Eng. Data 22 (1977) 71 – 73.

[36] K.P. Shen, M.H. Li, Solubility of carbon dioxide in aqueous mixtures of monoethanolamine with methyldiethanolamine, J. Chem. Eng. Data 37 (1992) 96-100.

[37] M.K. Park, O.C. Sandall, Solubility of carbon dioxide and nitrous oxide in 50 mass % methyldiethanolamine, J. Chem. Eng. Data 46 (2001) 166 – 168.

[38] A.Chakma, A. Meisen, Solubility of CO_2 in aqueous methyldiethanolamine and N,N-Bis(hydroxyethyl)piperazine solutions, Ind. Eng. Chem. Res. 26 (1987) 2461 – 2466.

[39] S.W. Rho, K.P. Yoo, Solubility of CO_2 in aqueous methyldiethanolamine solutions, J. Chem. Engg. Data 42 (1997) 1161 – 1164.

[40] P.Y. Chung, A.N. Soriano, R.B. Leron, M.H. Li, Equilibrium solubility of carbon dioxide in the amine solvent system of (triethanolamine + piperazine + water), J. Chem. Thermodyn 42 (2010) 802 – 807.

[41] Z. Xu, S. Wang, G. Qi, A.A. Trollebo, H.F. Svendsen, C. Chen, Vapour liquid equilibrium and heat of absorption of CO_2 in aqueous 2-(diethylamino)-ethanol solutions, Int. J. Greenh. Gas Control 29 (2014) 92 – 103.

[42] M. Kundu, B. P. Mandal, and S. S. Bandyopadhyay, Vapor-liquid equilibrium of CO_2 in aqueous solutions of 2-amino-2-methyl-1-propanol, J. Chem. Eng. Data 48 (2003) 789 – 796.

[43] T.T. Teng, A.E. Mather, Solubility of H_2S, CO_2 and their mixtures in an AMP solution, Can. J. Chem. Eng. 67 (1989) 846 – 850.

[44] S.K. Dash, A.N. Samanta, S.S. Bandyopadhyay, Experimental and theoretical investigation of solubility of carbon dioxide in concentrated aqueous solution of 2-Amino-2-methyl-1-propanol and piperazine, J. Chem. Thermodyn. 51 (2012) 120-125.

[45] Y. Liang, H. Liu, W. Rongwong, Z. Liang, R. Idem, P. Tontiwachwuthikul, Solubility, absorption heat and mass transfer studies of CO_2 absorption into aqueous solution of 1-dimethylamino-2-propanol, Fuel 144 (2015) 121 – 129.

[46] G.F. Versteeg, W.P.M. Van Swaaij, On the Kinetics between CO_2 and alkanolamines both in aqueous and non-aqueous solutions-II. tertiary amines, Chem. Eng. Sci. 43 (1988) 587 – 591.

[47] Barth, C. Tondre, G. Lappal, J.J. Delpuech, Kinetic study of carbon dioxide reaction with tertiary amines in aqueous solutions, J. Phys. Chem. 85 (1981) 3660 – 3679.

[48] A.K. Chakraborty, G. Astarita, K.B. Bischoff, CO_2 absorption in aqueous solutions of hindered amines, Chem. Eng. Sci. 41 (1986) 997 – 1003.

[49] S. Xu, Y.W. Wang, F.D. Otto, A.E. Mather, Kinetics of the reaction of carbon dioxide with 2-amino-2-methyl-1-propanol solutions, Chem. Eng. Sci. 51 (1996) 841 – 850.

[50] M.H. Li, K.P. Shen, Densities and solubilities of solutions of carbon dioxide in water + monoethanolamine + N-methyldiethanolamine, J. Chem. Eng. Data 37 (1992) 288–290.

[51] M.H. Li, B.C. Chang, Solubilities of carbondioxide in water + monoethanolamine + 2-amino-2-methyl-1-propanol, J. Chem. Eng. Data 39 (1994) 448 – 452.

[52] M. Kundu, S.S. Bandyopadhyay, Solubility of CO_2 in water + diethanolamine + 2-amino-2-methyl-1-propanol, J. Chem. Eng. Data 51 (2006) 398 – 405.

[53] M. Kundu, S.S. Bandyopadhyay, Solubility of CO_2 in water + diethanolamine + N-methyldiethanolamine, Fluid Phase Equilib. 248 (2006) 158 – 167.

[54] G. Kumar, M. Kundu, Solubility of CO_2 in aqueous blends of (N-methyl-2-ethanolamine + N-methyldiethanolamine) and (N-methyl-2-ethanolamine + 2-amino-2-methyl-1-propanol), J. Chem. Eng. Data 57 (2003) 3203-3209.

[55] Tong, G.C. Maitland, M.J.P. Trusler, P.S. Fennell, Solubility of carbondioxide in aqueous blends of 2-amino-2-methyl-1-propanol and piperazine, Chem. Eng. Sci. 101 (2013) 851 – 864.

[56] S.K. Dash, S.S. Bandyopadhyay, Studies on the effect of addition of piperazine and sulfolane into aqueous solution of N-methyldiethanolamine for CO_2 capture and VLE modelling using eNRTL equation, Int. J. Greenh. Gas Control 44 (2016) 227–237.

[57] S. Bishnoi, G.T. Rochelle, Thermodynamics of piperazine / methyldiethanolamine / water/ carbon dioxide, Ind. Eng. Chem. Res. 41 (2002) 604 – 612.

[58] Y.C. Chang, R.B. Leron, M.H. Li, Equilibrium solubility of carbon dioxide in aqueous solutions of (diethylenetriamine + piperazine), J. Chem. Thermodyn. 64 (2013) 106 – 113.

[59] B.K. Mondal, S.S. Bandyopadhyay, A.N. Samanta, Equilibrium solubility measurement and Kent-Eisenberg modeling of CO_2 absorption in aqueous mixture of N-methyldiethanolamine and hexamethylenediamine, Greenh. Gas Sci. Technol. (2016) 1-13.

[60] B.K. Mondal, S.S. Bandyopadhyay, A.N. Samanta, Experimental measurement and Kent-Eisenberg modelling of CO_2 solubility in aqueous mixture of 2-amino-2-methyl-1-propanol and hexamethylenediamine, Fluid Phase Equilib. 437 (2017) 118–126.

[61] Hafizi, M.H. Mokari, R. Khalifeh, M. Farsi, M.R. Rahimpour, Improving the CO_2 solubility in aqueous mixture of MDEA and different polyamine promoters: The effects of primary and secondary functional groups, J. Mol. Liq. (2019) 111803.

[62] M.J. Khodadadi, S. Riahi, M. Abbasi, Experimental modeling of the solubility of carbon dioxide in aqueous solution of monoethanolamine +1, 3-diaminopropane, J. Mol. Liq. 281 (2019) 415 – 422.

[63] Y.E. Kim, J.H. Choi, S.C. Nam, Y.I. Yoon, CO_2 absorption capacity using aqueous potassium carbonate with 2-methylpiperazine and piperazine, J. Ind. Eng. Chem. 18 (2012) 105 – 110.

[64] A.T. Zoghi, F. Feyzi, Equilibrium solubility of carbon dioxide in aqueous 2-((2-aminoethyl) amino) ethanol and N-methyldiethanolamine solution and modeling by electrolyte mPR-CPA EoS, J. Chem. Thermodyn. 67 (2013) 153 – 162.

[65] S.K. Dash, A.N. Samanta, S.S. Bandyopadhyay, Experimental and theoretical investigation of solubility of carbon dioxide in concentrated aqueous solution of 2-amino-2-methyl-1-propanol and piperazine, J. Chem. Thermodyn. 51 (2012) 120 -125.

[66] Y. Du, Le. Li, O. Namjoshi, K.A. Voice, A.N. Fine, G.T. Rochelle, Aqueous piperazine/N-(2-aminoethyl) piperazine for CO_2 capture, Energy Procedia 37 (2013) 1621-1638.

[67] S. Paul, A. K. Ghoshal, B. Mandal, Kinetics of absorption of carbon dioxide into aqueous solution of 2-(1-piperazinyl)-ethylamine, Chem. Eng. Sci. 64 (2009) 313-321.

[68] R. Ramazani, S. Mazinani, A. Hafizi, A. Jahanmiri, Equilibrium solubility of carbon dioxide in aqueous blend of monoethanolamine (MEA) and 2-1-piperazinyl-ethylamine (PZEA) solutions: Experimental and optimization study, Process Saf. Environ. Prot. 98 (2015) 325–332.

[69] P. Singh, J.P.M. Niederer, G.F. Versteeg, Structure and activity relationships for amine-based CO_2 absorbents-II, Chem. Eng. Res. Des. 7 (2008) 135–144.

[70] B.K. Mondal, S.S. Bandyopadhyay, A.N. Samanta, Measurement of CO_2 absorption enthalpy and heat capacity of aqueous hexamethylenediamine and its aqueous mixture with N-methyldiethanolamine, J. Chem. Thermodyn. 113 (2017) 276 – 290

Chapter 2

Mechanism of CO_2-Aqueous Amine System Reactions and Modeling Methodologies

This chapter provides a thorough examination of the fundamental chemistry of CO_2 with the aqueous amine solutions. Thermodynamic and kinetic aspects relating to the absorption of CO_2 in an aqueous amine solution have been concisely discussed. The reaction process for various amine groups is discussed and establishes rate expression, and interprets possible reaction products. The second section of the chapter covers thermodynamics and detailed explanations of the different modeling methodologies used in the current work to connect CO_2 solubility data.

2.1 Introduction

CO_2 absorption in alkanolamine solutions is caused by a chemical interaction between the CO_2 and the amines. A chemical reaction in the liquid phase raises the liquid-film absorption coefficient compared to simple physical absorption. The dissolved molecules appear to move well into the liquid's body before the chemical reaction occurs. For that purpose, the overall mass transfer rate is not considerably accelerated. However, in highly fast reactions, the dissolved molecules only move a short distance before the reaction. There are moderately rapid and fast processes, resulting in varied absorption kinetics. The types of chemical processes involved are crucial in defining the total absorption kinetics. The underlying mechanism governing CO_2's reactivity with alkanolamines is still unknown. However, significant progress has been made in gathering rate data and constructing kinetic expressions that reasonably describe experimental data. As a result, in the gas-liquid absorption system, proper knowledge

of reaction mechanisms and reaction regimes is critical for establishing a suitable reaction mechanism.

In addition to dependable solubility measuring techniques, proper mathematical models are required to forecast gas solubility across a wide variety of temperature and acid gas loading conditions. The aqueous amine system's equilibrium thermodynamics can be described as a combination of physical equilibrium in the gas-liquid phase and reaction equilibrium matching numerous intermediate reactions found in aqueous alkanolamine systems. Additionally, the thermodynamic framework and construction of precise process model development for non-rigorous modified Kent Eisenberg models are presented. The building of an ANN model, model architecture, and ANN network optimization are also covered in this chapter.

2.2 Chemistry of CO_2-aqueous alkanolamine system

The zwitter ion mechanism and the termolecular mechanism are commonly used to describe the interaction of CO_2 with a primary or secondary alkanolomaine. Still, the base catalysed hydration of CO_2 [1] illustrates the reaction of tertiary amines.

2.2.1 Zwitterion mechanism

CO_2 forms a bond with the amine functionality in the first phase, according to this two-step mechanism established by Caplow [2] and later reintroduced by Danckwerts [3]. In the second stage, an amine-proton is transferred to a second molecule. The second molecule in Caplow's article was water, but it could be any base molecule. A zwitterion is the reaction's intermediate species. Before the amine reacts with the CO_2 molecule, Caplow [2] assumes that a hydrogen bond is created between the amine and a water molecule. However, as can be shown in the work of Danckwerts [3], Versteeg et al. [4], and Kumar et al. [5], this trait has been neglected in later published material. As a result, according to this mechanism, the interaction between

CO_2 and the amine (referred to as Z_{Am}) takes place via the creation of a zwitterion as an intermediate:

$$CO_2 + Z_{Am} \underset{k_{-1}}{\overset{k_2}{\rightleftarrows}} Z^+_{Am}COO^- \tag{2.1}$$

This zwitterion undergoes deprotonation by a base (or bases) b, thereby resulting in carbamate formation:

$$Z^+_{Am}COO^- + b \xrightarrow{k_b} Z_{Am}COO^- + bH^+ \tag{2.2}$$

The base, b, can be an amine, OH^- or H_2O, although the contribution of OH^- can be neglected as its concentration is deficient compared with those of amine and H_2O [6].

The rate of reaction of CO_2 in aqueous solutions can be stated as follows using the steady-state principle and the intermediate zwitterion:

$$r_{CO_2-amine} = k_2 \left[\frac{[CO_2][Z_{Am}]}{1 + \frac{1}{\sum \left(\frac{k_b}{k_{-1}} \right)[b]}} \right] \tag{2.3}$$

For two asymptotic situations, Eq. (2.3) may be simplified as follows:

i. The term $k_{-1} / \left(k_b [b] \right) \leq 1$. This leads to simple second-order kinetics, showing that the zwitterion deprotonation reaction is quick compared to CO_2 and amine reversion rates. Eq. (2.3) is therefore simplified to

$$r_{CO_2-amine} = k_2 [CO_2][Z_{Am}] \tag{2.4}$$

ii. The term $k_{-1} / \left(k_b [b] \right) \gg 1$. It leads to complex expression:

$$r_{CO_2-a\min e} = \frac{k_2 \times k_b \times [CO_2] \times [Z_{Am}] \times [b]}{k_{-1}} \quad (2.5)$$

If the contribution of water to the deprotonation of the zwitterion is ignored, Eq. (2.5) shows that the total reaction order is three. The reaction order shifts from two to three in the transition zone between the two asymptotic situations. In the limiting scenario, where the contribution of amine to zwitterion deprotonation is significantly more outstanding than that of other bases such as H_2O and OH^-, the entire reaction is of the second order concerning amine.

The carbamate production can be written as follows if the base, b, considering in the Eq. (2.2) is the amine:

$$Z_{Am}^{+}COO^{-} + Z_{Am} \rightarrow Z_{Am}COO^{-} + Z_{Am}H^{+} \quad (2.6)$$

The total reaction that accounts for carbamate production in a solution is given by the sum of reactions represented by Eqs. (2.1) and (2.6):

$$CO_2 + 2Z_{Am} \rightleftharpoons Z_{Am}COO^{-} + Z_{Am}H^{+} \quad (2.7)$$

When the amine is sterically hindered, the zwitterion interacts with water more readily than with Am, resulting in the creation of bicarbonate:

$$Z_{Am}COO^{-} + H_2O \rightarrow HCO_3^{-} + Z_{Am}H^{+} \quad (2.8)$$

The reaction that accounts for bicarbonate generation is obtained by summation of Eqs. (2.1) and (2.8):

$$CO_2 + Z_{Am} + H_2O \rightleftharpoons HCO_3^{-} + Z_{Am}H^{+} \quad (2.9)$$

Due to their low stability, the carbamates of sterically hindered amines may also readily undergo hydrolysis, forming bicarbonates and releasing free amine molecules. This can be expressed as follows:

$$Z_{Am}^{+}COO^{-} + H_2O \rightleftharpoons HCO_3^{-} + Z_{Am} \quad (2.10)$$

The liberated amine molecules will react with CO_2 once more. As a result, bicarbonate ions will be more abundant than carbamate ions.

The reactions of water and its dissociation products with the gases and amines are necessary to understand CO_2 absorption into aqueous amine solutions. The water dissociation reaction is the most significant in aqueous chemistry.

$$H_2O \rightleftharpoons H^{+} + OH^{-} \quad (2.11)$$

In an aqueous amine solution, the following reactions can also happen at the same time:

$$Z_{Am} + H_2O \rightleftharpoons Z_{Am}H^{+} + OH^{-} \quad (2.12)$$

$$CO_2 + H_2O \rightleftarrows HCO_3^{-} + H^{+} \quad (2.13)$$

$$CO_2 + OH^{-} \rightleftharpoons HCO_3^{-} \quad (2.14)$$

The reaction (2.13), which is extremely slow (k = 0.026 s^{-1} at 298 K) [7], may normally be ignored. Even when the hydroxyl ion concentration is modest, the reaction (2.14) significantly impacts the overall reaction rate. [7] describes the forward reaction rate for reaction (2.14):

$$r_{CO_2 - OH^{-}} = k^{*}_{OH^{-}} \left[CO_2\right]\left[OH^{-}\right] \quad (2.15)$$

The sum of the reaction rates given by Eqs. (2.15) and (2.3) gives the overall rate of all CO_2 reactions in an aqueous solution:

$$r_{ov} = \frac{k_2[CO_2][Z_{Am}]}{1 + \frac{1}{\sum\left(k_b / k_{-1}\right)[b]}} + k^{*}_{OH^{-}}[CO_2][OH^{-}] \quad (2.16)$$

$$r_{ov} = k_{ov}\left[CO_2\right] \quad (2.17)$$

The observed overall reaction rate constant, which can be measured, is denoted by k_{ov} and is given by:

$$k_{ov} = \frac{k_2[Z_{Am}]}{1+\frac{1}{\left(k_b/k_{-1}\right)[b]}} + k^*_{OH^-}[OH^-] \tag{2.18}$$

The apparent reaction rate constant (k_{app}), which is employed in experimental data analysis, is calculated as follows:

$$k_{app} = k_2\left[\frac{[Z_{Am}]}{1+\frac{1}{\left(k_b/k_{-1}\right)[b]}}\right] \tag{2.19}$$

k_{app} can be obtained from k_{ov} as follows:

$$k_{app} = k_{ov} - k^*_{OH^-}[OH^-] \tag{2.20}$$

2.2.2 Termolecular mechanism

According to the termolecular process, the amine in the aqueous solution reacts concurrently with CO_2 and one molecule of base, b [8]. The proton transfers and the required bond formation between the amine molecules and CO_2 co-occur in this pathway.

$$CO_2 + Am\cdots\cdots b \rightleftharpoons AmCOO^- \cdots\cdots bH^+ \tag{2.21}$$

During the reaction, an unstable short-lived intermediate chemical complex forms. A small fraction of the intermediate combines with a water molecule or an amine molecule to create ionic products, while the complex dissociates further into free amine molecules and CO_2.

2.2.3 Base-catalysed hydration mechanism

According to Donaldson et al. [9], tertiary alkanolamines (referred to as R_3N here) cannot react directly with CO_2. On the hydration of CO_2, such amines have a base-catalytic action. This can be expressed as follows:

$$CO_2 + R_3N + H_2O \xrightarrow{k_2} R_3NH^+ + HCO_3^- \quad (2.22)$$

In aqueous solutions, the reaction with tertiary amines creates protonated amines and bicarbonate ions, resulting in enhanced CO_2 loading and reduced heat of absorption compared to primary and secondary amines.

2.3 Modeling of CO_2 solubility data

Together experimental and theoretical analysis of CO_2 solubility data is required to reasonably design a CO_2 collection unit. In aqueous amine systems, CO_2 solubility or VLE data are often reported as the total concentration of CO_2 in the aqueous amine solution vs. the total, partial pressure of the gas phase at equilibrium circumstances. However, adequate correlations are always required for interpolating and projecting the data to the intended range of operating possibilities [10].

In an absorber unit, the CO_2-amine reaction produces a variety of ionic species. The reaction equilibrium in the CO_2–amine system has been assessed using various thermodynamic models. Numerous research has been conducted and published in the open literature to anticipate equilibrium solubility values for equally single and blended aqueous amine solvents. Thermodynamic models used to forecast or model CO_2 solubility data in aqueous alkanolamine solutions can be divided into the subsequent classes [1]:

- Excess Gibbs energy-based rigorous models (gamma-phi models): The model employs the utilisation of excess Gibbs energy. Some of the most extensively used models in

this category are Electrolyte-NRTL and e-UNIQUAC [11-12]. Faramarzi et al. [13] used the e-UNIQUAC equation to model binary aqueous solutions of MEA and MDEA, as well as ternary amine blends of MEA and MDEA.

- Equation of state model (phi-phi approach): This category includes equations of state (EOS) that are used to analyse molecular interactions accurately and can be used to correlate solubility data, such as PR-EOS, PC-SAFT, and electrolyte EOS [14].
- Non-rigorous Empirical models: These methods estimate the reaction equilibrium constant's solubility data. It ignores the non-ideality of the system, resulting in fugacity, and the activity coefficient is assumed to be one. The Kent–Eisenberg model was one of the first models, and it is still used in various modified variants today [15].

2.3.1 Modified Kent-Eisenberg model

Kent and Eisenberg [15] proposed the first valuable and adaptable model. The non-ideality that exists between the aqueous amine-CO_2 systems is ignored in this model. Compared to other rigorous models, the equilibrium reaction constants are the only parameter to estimate. By calculating the equilibrium reaction constants as a function of essential operating factors, the equilibrium reaction constants may be easily determined. Failure to provide an accurate approximation of the initial guess values can also cause solubility estimation convergence difficulties in rigorous models. As a result, the KE model reduces processing time dramatically. According to Lee et al. [16], the KE model has given an excellent prediction between the experimental and predicted over a wide range of experimental conditions.

2.3.1.1 Thermodynamic framework

The following are the equations that describe the CO_2 solubility in primary, secondary, or tertiary amines aqueous system: (where ZNH_2 stands for primary amine and Z_3N stands for secondary amine)

$$ZNH^{3+} \overset{K_{11}}{\rightleftharpoons} H^{+} + ZNH_2 \tag{2.23}$$

$$Z_3NH^{+} \overset{K_{11}}{\rightleftharpoons} H^{+} + Z_3N \tag{2.24}$$

$$ZNHCOO^{-} + H_2O \overset{K_2}{\rightleftharpoons} ZNH_2 + HCO_3^{-} \tag{2.25}$$

$$H_2O + CO_2 \overset{K_3}{\rightleftharpoons} H^{+} + HCO_3^{-} \tag{2.26}$$

$$H_2O \overset{K_4}{\rightleftharpoons} H^{+} + OH^{-} \tag{2.27}$$

$$HCO_3^{-} \overset{K_5}{\rightleftharpoons} H^{+} + CO_3^{2-} \tag{2.28}$$

Where,

K_{11} = Equilibrium constant of de-protonation of amine
K_2 = Equilibrium constant of carbamate hydrolysis of amine
K_3 = Equilibrium constant of formation of bicarbonate ion
K_4 = Equilibrium constant of dissociation of water
K_5 = Equilibrium constant of dissociation of bicarbonate ion

Henry's Law can be used to calculate the concentration of CO_2 in the liquid phase.

$$P_{CO_2} = H_{CO_2}\left[CO_2\right] \tag{2.29}$$

Where, P_{CO_2} is the equilibrium CO_2 partial pressure and H_{CO_2} is Henry's law constant for CO_2 in aqueous amine solutions. The whole amine mass and electro neutrality balance equation for the primary amine can be written as:

$$m_1 = \left[ZNH_2\right] + \left[ZNH_3^{+}\right] + \left[ZNHCOO^{-}\right] \tag{2.30}$$

$$m_1 \times \alpha_{CO_2} = \left[CO_2\right] + \left[HCO_3^{-}\right] + \left[CO_3^{2-}\right] + \left[ZNHCOO^{-}\right] \tag{2.31}$$

$$\left[ZNH_3^+\right]+\left[H^+\right]-[ZNHCOO^-]+\left[HCO_3^-\right]+2\left[CO_3^{2-}\right]+\left[OH^-\right]=0 \quad (2.32)$$

All the terms in the third bracket represented in equation (2.29) – (2.31) stand for the ionic concentrations of all the species prevailing in the reaction phase.

The general method for the modified KE model is as follows [17]:

- The proposition of the possible (or confirmed) reactions of the CO_2-amine system.
- Development of the system's charge balance, chemical, and physical equilibria.
- Development of the CO_2 loading equation using the above steps, providing appropriate initial guesses of the equilibrium to be estimated according to the proposed reactions.
- Solving the non-linear equation to estimate the concentration of all ionic species stated in reaction equilibria.
- Calculation of the unknown equilibrium constants, K_i associated with chemical reactions by reducing the AAD between the calculated and experimental CO_2 loading data.

The equilibrium constants for reactions (2.26-2.28) can be found in the public domain. The solvent explicit equilibrium constants specified in reactions (2.23–2.25) must be regressed and determined to fit the experimental solubility data. The equilibrium model and Henry's law constant were originally expressed as a function of temperature alone, as seen below:

$$ln\ K\ = l+\frac{m}{T}+n.\ln T+o.T \quad (2.33)$$

where T is temperature and l, m, n, and o are the coefficients.

Many variables, such as CO_2 partial pressure and amine concentration, have recently been studied in various logarithmic and square forms to account for the multiple non-idealities associated with prediction [18-24]. The equilibrium constants related to deprotonation and carbamate hydrolysis were employed in this study as a function of the variables listed below:

$$K_{11} = g + (h \times M) + (k \times T) + (l \times M \times T) + (n \times T^2) + (p \times P_{CO_2}) + (q \times P_{CO_2}^2) \quad (2.34)$$

$$k_2 = g + (h \times M) + (k \times T) + (l \times M^2) + (n \times m \times T) + (p \times T^2) + (q \times P_{CO_2}) + (r \times P_{CO_2}^2) \quad (2.35)$$

Where g, h, k, l, n, p, q, and r, are parametric coefficients linked with the equilibrium constants and originate through optimization.

2.3.2 Artificial neural network model

2.3.2.1 Neural network modeling

A neural network is a type of artificial intelligence that can simulate any complex data, including highly non-linear systems. A neural network's input layer, hidden layer(s), and output layer are all made up of neurons as shown in Fig.2.1. Every neuron in the previous and subsequent levels is linked to the prior and subsequent layers. A transfer function is used to calculate each neuron's output based on its input. In the field of CO_2 capture processes, neural network modeling has been widely used for various property predictions and process intensification [25-26]. It can accommodate any multivariate system's nonlinearity by making minor adjustments such as normalising i/p and o/p data. It usually does not necessitate a thorough understanding of the system's technical aspects. For any system with input 'p,' a neuron calculates the output 'm' using the following equation:

$$Y_i = f\left(\sum_{i=1}^{n}\left(w_i X_i + b_i\right)\right) \quad (2.36)$$

Here X_i and Y_i denote the i^{th} neuron's i/p and o/p, one-to-one, f represents the transfer function, w_i is the weight coefficient, and b_i indicates the bias associated with each weighting coefficient. Weights and biases are automatically modified for a network to imitate a specific task. This is known as training, and it involves using a proper training algorithm to process the network's weights and biases. The training aims to reduce the difference between the modeled output and the actual or experimental value. The Levenberg-Marquardt (LM) back-propagation method is utilised as the training function in this ANN design [26-27].

For moderate-sized networks, the LM technique is regarded as the fastest algorithm when the network functions comprise many data sets. The exclusive property of memory reduction distinguishes it. Hyperbolic tangent sigmoid and linear functions are used as transfer functions for the hidden and output layers.

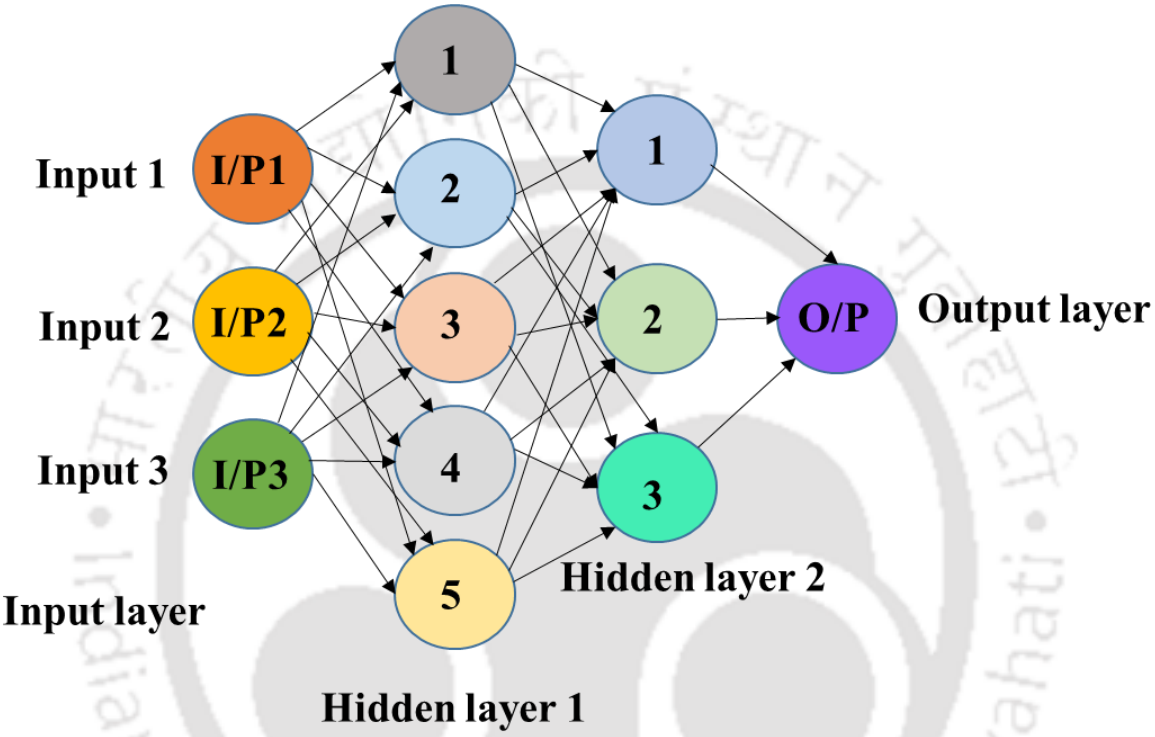

Figure 2.1 The feed-forward network with two unseen layers, each with five and three neurons, has a network structure.

$$f_{hiden}(x) = \frac{2}{1+e^{-2x}} - 1 \tag{2.37}$$

$$f_{output}(x) = x \tag{2.38}$$

Where $f_{hiden}(x)$ and $f_{output}(x)$ are the transfer functions used for the hidden and output layers, respectively. The hyperbolic tangent sigmoid function is employed in the hidden layer, while the linear function is used in the output layer. The training procedure's primary goal is to

reduce the difference between the experimental and predicted values. The following statistical parameter is used to analyse the performance and validation of the constructed network:

$$\text{Mean square error } (MSE) = \frac{1}{N}\sum_{i=1}^{N}\left(Y_i^{\exp} - Y_i^{pre}\right)^2 \tag{2.39}$$

$$\%\text{AAD} = \frac{1}{N}\sum_{i=1}^{N}\left(\frac{Y_i^{\exp} - Y_i^{pre}}{Y_i^{pre}}\right)^2 \times 100 \tag{2.40}$$

Where 'N' stands for the number of data points, $Y_i^{\exp}$ is the experimental value of output variable, Y_i^{pre} is the network predicted value of output variable.

2.3.2.2 Analysis and acquirement of solubility data

Detailed experimental CO_2 solubility data under various operating conditions is critical for optimising a specific neural network. The total number of data sets that have been moved into the network can be categorized into three:

Training data sets: These are sent into the network via the training phase, and the network is then optimised based on the resulting error.

Validation data sets: These are used to compute network generalisation and end the training process when the generalisation does not improve further.

Testing data sets: These have no bearing on the training process and give an objective evaluation of network performance during and after training.

The majority of the researchers in this discipline used 70% of the complete data sets for training. As a result, in the current method, networks are constructed using 70% of data for training, 15% for validation, and 15% for testing [28]. Because all of the input and output property data sets are known with various units and ranges, the input and output data sets are normalised in the field of 0-1 before training the ANN network.

$$Y_i = \frac{X_i - X_{\min}}{X_{\max} - X_{\min}} \tag{2.41}$$

The maximum value of different input variables X_i is represented by $X_{\max}$, and the minimum value is expressed as $X_{\min}$ respectively in the training and test data sets. Y_i is the input and output variable's normalised value in the range of (0-1). With the variation in the number of neurons, the ideal architecture of the ANN was determined through trial and error. A small number of neurons can cause substantial network defects, whereas a large number can cause over-fitting [29]. The minimum error criteria are used to determine the network's optimal structure (i.e. %AAD and MSE).

The black box aspect of the artificial neural network model and the network's inexplicable behavior are the model's key drawbacks. In addition, no formal rule exists for determining the structure of an artificial neural network. Experience and trial and error are used to create an appropriate network structure. Furthermore, to make better predictions, ANN modeling necessitates a lot more data than conventional models.

NOTATIONS

CO_2	Carbon dioxide
Z_{Am}	Amine
b	Base
k^{-1}	Backward rate constant in Eq. (2.1), s^{-1}
k_2	Second order forward reaction rate constant, m3 mol^{-1} s^{-1}
k_{ov}	Observed overall reaction rate constant, s^{-1}
k_{app}	Apparent reaction rate constant, s^{-1}
r	Reaction rate, kmol m^{-3} s^{-1}
R_3N	Tertiary alkanolamine
[ ]	Concentration, kmol m^{-3}
K_{11}	Equilibrium constant of de-protonation of amine
K_2	Equilibrium constant of carbamate hydrolysis of amine
K_3	Equilibrium constant of formation of bicarbonate ion
K_4	Equilibrium constant of dissociation of water
K_5	Equilibrium constant of dissociation of bicarbonate ion
P_{CO2}	Equilibrium partial pressure of CO_2
H_{CO2}	Henry's law constant for CO_2 in aqueous amine solutions
ANN	Artificial neural network
w_i	Weight coefficient
f	Transfer function
MSE	Mean square error
N	No of data points

References

[1] Z. Liang, W. Rongwong, H. Liu, Recent progress and new developments in post-combustion carbon-capture technology with amine based solvents, Int. J. Greenh. Gas Control 40 (2015) 26-54. M.

[2] Caplow, Kinetics of carbamate formation and breakdown, J. American Chem. Soc. 90 (1968) 6795-6803.

[3] P. Danckwerts, The reaction of CO_2 with ethanolamines, Chem. Eng. Sci. (1979) 443-446.

[4] G. Versteeg, L.V. Dijck, W.P.M. Swaaij, On the kinetics between CO_2 and alkanolamines both in aqueous and non-aqueous solutions- An overview, Chem. Eng. Com. 144 (1996)113-158.

[5] P. Kumar, J. Hogendoorn,, G. Versteeg,, P. Feron, Kinetics of the reaction of CO_2 with aqueous potassium salt of taurine and glycine, AIChE Journal 49(2003)203-213.

[6] S. Xu, Y. W. Wang, F. D. Otto, and A. E. Mather, Kinetics of the Reaction of CO_2 with 2-Amino-2-methyl-1-propanol Solutions, Chem. Eng. Sci, 51, 841 – 850 (1996).

[7] B. R. W. Pinsent, L. Pearson, and F. W. J. Roughton, The Kinetics of Combination of Carbon Dioxide with Hydroxide Ions, J. Chem. Soc, Faraday Trans, 52, 1512 – 1520 (1956).

[8] J.E. Crooks, J.P. Donnellan, Kinetics and mechanism of the reaction between carbon dioxide and amines in aqueous solution, J. Chem. Soc. Perkin Transactions 2 (1989) 331-333.

[9] T.L. Donaldson, Y.N. Nguyen. Carbon dioxide reaction kinetics and transport in aqueous amine membranes, Ind. Eng. Chem. Fund. 19 (1980) 260-266.

[10] G. Kumar, Vapour liquid equilibrium of carbon dioxide in newly proposed blends of alkanolamine, (2013) Ph D dissertation. NIT Rourkela.

[11] S.K. Dash, A.N. Samanta, S.S. Bandyopadhyay, Vapour liquid equilibria of carbon dioxide in dilute and concentrated aqueous solutions of piperazine at low to high pressure, Fluid Phase Equilib. 300 (2011) 145-154.

[12] A. Haghtalab, H. Eghbali, A. Shojaeian, Experiment and modeling solubility of CO_2 in aqueous solutions of diisopropanolamine + 2-amino-2-methyl-1-propano + piperazine at high pressures, J. Chem. Thermodyn. 71 (2014) 71–83.

[13] L. Faramarzi, G.M. Kontogeorgis, K. Thomsen, E.H. Stenby, Extended UNIQUAC model for thermodynamic modeling of CO_2 absorption in aqueous alkanolamine solutions, Fluid Phase Equilib. 282 (2009)121–132.

[14] F. Diab, E. Provost, N. Laloue, P. Alix, W. Furst, Effect of the incorporation of speciation data in the modeling of CO_2–DEA–H_2O system, Fluid Phase Equilib. 353 (2013) 22–30.

[15] R.L. Kent, B. Eisenberg, Better data for amine treating, Hydrocarbon Process. 55 (1976) 87-90.

[16] I.J. Lee, F.D. Otto, A.E. Mather, The measurement and prediction of the solubility of the mixtures of carbon dioxide and hydrogen sulphide in a 2.5 N monoethanolamine solutions, Can. J. Chem. Eng., 54 (1976) 803-805.

[17] S. J. Hwang, H .K. Kwang, S. Lee, Prediction of VLE for aqueous blended amines using VLE models of single amines, International Journal of Greenhouse Gas Control 49 (2016) 250–258.

[18] H. Pahlavanzadeh, S. Nourani, M. Saber, Experimental analysis and modeling of CO_2 solubility in AMP (2-amino-2-methyl-1-propanol) at low CO_2 partial pressure using the models of Deshmukh-Mather and the artificial neural network, Journal of Chemical Thermodynamics 43 (2011) 1775-1783.

[19] Z. Y. Yang, A. N. Soriano, A. R. Caparanga, M. H. Li, Equilibrium solubility of carbon dioxide in (2-amino-2-methyl-1-propanol + piperazine + water), Journal of Chemical Thermodynamics 42 (2010) 659–665.

[20] M. H. Li, K. P. Shen, Calculation of equilibrium solubility of carbon dioxide in aqueous mixtures of monoethanolamine with methyldiethanolamine, Fluid Phase Equilibria 85 (1993) 129–140.

[21] D. M. Austgen, G. T. Rochelle, X. Peng, C. C. Chen, Model of vapor-liquid equilibria for aqueous acid gas-alkanolamine systems using the electrolyte-NRTL equation, Industrial and Engineering Chemistry Research 28 (1989) 1060–1073.

[22] D. M. Austgen, G. T. Rochelle, C. C. Chen, Model of vapor-liquid equilibria for aqueous acid gas-alkanolamine systems. 2. Representation of hydrogen sulfide and carbon dioxide solubility in aqueous MDEA and carbon dioxide solubility in aqueous mixtures of MDEA with MEA or DEA, Industrial and Engineering Chemistry Research 30 (1991) 543–555.

[23] W. Hu, A. Chakma, Modelling of equilibrium solubility of CO_2 and H_2S in aqueous amino methyl propanol (AMP) solutions, Chemical Engineering Communications 94 (1990) 53–61.

[24] W. Hu, A. Chakma, Modelling of equilibrium solubility of CO_2 and H_2S in aqueous diglycolamine (DGA) solutions, Canadian Journal of Chemical Engineering 68 (1990) 523–525.

[25] J. S. Torrecilla, J. Palomar, J. Garcia, E. Rojo, F. Rodriguez. Modelling of carbon dioxide solubility in ionic liquids at sub and supercritical conditions by neural networks and mathematical regressions. Chemometrics and Intelligent Laboratory Systems 93 (2008) 149-159.

[26] M. Mirarab, M. Sharifi, M. A. Ghayyem, F. Mirarab. Prediction of solubility of CO_2 in ethanol-[EMIM] [Tf2N] ionic liquid mixtures using artificial neural networks based on genetic algorithm. Fluid Phase Equilibria 371 (2014) 6–14.

[27] M. Mirarab, M. Sharifi, B. Behzadi, M.A. Ghayyem, Intelligent prediction of CO_2 capture in propyl amine methyl imidazole alanine ionic liquid: an artificial neural network model, Sep. Sci. Technol. 50 (1) (2014) 26–37.

[28] H. Pahlavanzadeh , S. Nourani, M. Saber, Experimental analysis and modeling of CO_2 solubility in AMP (2-amino-2-methyl-1-propanol) at low CO_2 partial pressure using the models of Deshmukh–Mather and the artificial neural network, J. Chem. Thermodyn. 43 (2011) 1775-1783

[29] G. Chen, X. Luo, H. Zhang, K. Fu, Z. Liang, W. Rongwong, P. Tontiwachwuthikul, R. Idem, Artificial neural network models for the prediction of CO_2 solubility in aqueous amine solutions, Int. J. Greenh. Gas Control 39 (2015) 174-184.

Chapter 3

Measurement and correlations of physicochemical properties of the novel solvent tris(2-aminoethyl) amine and its blend with N-methyldiethanolamine and 2-amino 2-methyl-1-propanol

This chapter discusses the thermophysical properties of tris(2-aminoethyl) amine and its blend with N-methyldiethanolamine and 2-amino 2-methyl-1-propanol. All measurements were carried out at 0.1 MPa throughout a temperature range of (293.15 to 333.15) K. The density and viscosity values were then correlated with Redlich - Kister and Grunberg - Nissan models as a function of temperature and amine concentration. Excess molar volumes, kinematic viscosity deviations, the diffusivity of CO_2/N_2O in proposed solvents have all been calculated using the experimental data.

3.1 Introduction

Increased greenhouse gas emissions have become an object of research in recent years [1,2]. Among all greenhouse gasses, CO_2 has an excessive influence due to its omnipresence. Among all greenhouse gasses, CO_2 has an excessive influence due to its omnipresence. To effectively handle global warming to provide a sustainable solution, research must be concentrated on limiting the composition of CO_2 in the atmosphere [3]. More recently, numerous alkanolamine solvents have been proposed to effectively remove CO_2 from the flue, natural, and synthesis gas streams. The major conventional solvents, namely primary amine (monoethanolamine, MEA), secondary amine (diethanolamine, DEA), tertiary amine (*N*-methyl diehanolamine,

MDEA), and also the amine (2-amino-2-methyl-1-propanol, AMP), which is sterically hindered, have been used for several industrial gas treatment units [4,5]. Still, these types of amines also have various downsides like degradation of the solvent, higher energy requirement for regeneration, and eroding to the equipment leads to the economically unfavorable utilization of them [6–8]. To overcome these problems, investigators have proposed blended solvents as striking to remove any acidic impurities in the sour gas streams. Many researchers have proposed several activators like piperazine (PZ), 1-(2-aminoethyl)piperazine (PZEA), 1-methyl piperazine, and bis(3-aminopropyl)amine, (APA)[9–13] to blend with these available commercial alkanolamines solvents because of possible increase in total CO_2 loading capacity, and reduced cost of the regeneration [14–24]. In the current work, we propose a novel activator tris(2-aminoethyl) amine or (2,2',2"-Triaminotriethylamine, TAEA). It has three primary and one tertiary amine groups, which have high thermal stability and, on the other hand, low vapour pressure, which may provide a higher capacity of CO_2 per mole of amine. In addition, it is expected that the activator, as mentioned earlier, plays the role of a rate promoter due to primary amine groups. For these reflections, this paper deals with eliminating CO_2 from gas streams using the activator TAEA blended with traditionally used aqueous MDEA and AMP solutions.

The physicochemical properties such as viscosity, density of the new blends (i.e. aqueous solution of activated TAEA with MDEA and AMP), as well as Henry's law constant ($K_{H\text{-}CO2}$), and CO_2 diffusivity in these solvents, are crucial for the process design of gas treating units and the manufacture of gas treating equipment. Awareness of the physical parameters is highly beneficial to operate process equipment like pumps and heat exchangers. The density of the solution, viscosity, and physical solubility of CO_2 are helpful for mass transfer rate modeling of absorber and stripper. This is due to the apparent reason that liquid-film mass transfer factor will affect these properties

Herein, we measured the physiochemical properties of TAEA and their blends with MDEA and AMP. This work aims at some new correlations that rely on the data obtained from experiments to relate the diffusivity, viscosity, and density of novel aqueous solutions. Henry's law constant of N_2O have also been measured in these solutions regarding amine concentration and temperature at atmospheric pressure. Measured experimental viscosities have been used to calculate the diffusivity of CO_2 into these solutions using a modified-Stokes-Einstein equation. CO_2 and the solvent go through a chemical reaction, as mentioned earlier, rendering the determination of the diffusivity of CO_2 in amine solutions and estimation of the $K_{H\text{-}CO2}$ become cumbersome. Therefore, usage of a non-reacting gas such as N_2O as a substitute to CO_2 approximates the diffusivity of CO_2 and also the estimation of $K_{H\text{-}CO2}$ in these solvents. This analogy is given by Eqs. 3.1 and 3.2.

$$K_{HCO_2-Am} = K_{HN_2O-Am}\left(\frac{K_{HCO_2-Water}}{K_{HN_2O-Water}}\right) \tag{3.1}$$

$$D_{CO_2-Am} = D_{N_2O-Am}\left(\frac{D_{CO_2-Water}}{D_{N_2O-Water}}\right) \tag{3.2}$$

Here $k_{H,CO_2\text{-}Am}$ is the Henry's law constant of CO_2 in amine and $D_{CO_2\text{-}Am}$ is one-to-one CO_2 diffusivity in amine solutions. The viscosities and densities of binary and tertiary systems have been correlated using the Redlich-Kister equation, Grunberg and Nissan, respectively. The physical solubility of N_2O of binary and tertiary systems has been correlated using a temperature-dependent Arrhenius type equation.

3.2 Experimental unit

3.2.1 Materials

The analytical grade AMP (0.95< purity), TAEA (0.96< purity), and MDEA (0.99< purity) were purchased from Sigma Aldrich and used without any further purification. A double

distillation unit (Borosil, 3362 Series) has been used for making distilled water. The amine solutions were prepared with distilled water that had been steam degassed. An auto titrator (DL 50, Mettler Toledo) with hydrochloric acid (HCl, 37 wt%, Merck) was used to determine the amine content in the solution. The composition of the amine solutions had a 0.001 % uncertainty. The weighing balance (Wensar, Model: HPB510, Accuracy: 0.001 mg) was used to weigh the amine solutions. The nitrous oxide (0.99< purity) and carbon dioxide (0.99<purity) were purchased from Assam Air Products, India, with a testified purity license. The impurities present in the AMP (purity>0.95) and TAEA (purity>0.96) are mostly water and traces of other components. Detailed specification of the chemicals is given in Table 3.1.

Table 3.1 Description of used chemicals in this work.

Chemical Name	Chemical formula	Molar mass, $g.mol^{-1}$	Molecular structure	Source	Mass fraction Purity	CAS no	Method of analysis
2,2',2"-Triaminotriethylamine	$C_6H_{18}N_4$	146.23	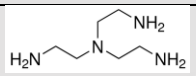	Sigma Aldrich	0.96	4097-89-6	GC
n-methyldiethanolamine (MDEA)	$C_5H_{13}NO_2$	119.16	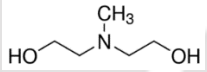	Sigma Aldrich	0.99	105-59-9	GC
2-amino-2-methyl-1-proponol (AMP)	$C_4H_{11}NO$	89.14	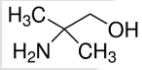	Sigma Aldrich	0.95	124-68-5	HClO4 titration
Nitrous oxide	N_2O	44.013	$N^+=N^-=O$	Assam air products, Guwahati	0.99	10024-97-2	GC
Carbon dioxide	CO_2	44.01	$O=C=O$	Assam air products, Guwahati	0.99	124-38-9	GC
Hydrogen chloride (0.1 N)	HCl	36.46	H-Cl	Merck specialities private limited, Mumbai	-	7647-01-0	Titration with NaOH
Impurities are mostly water in AMP and TAEA							

3.2.2 Apparatus and Procedure

3.2.2.1 Physiochemical properties

A digital densitometer (Anton Paar DMA-4500 M model) was used to measure the densities of the amine. In detail, a U-shaped tube (made of borosilicate glass) has taken where the sample was placed. Then the tube was excited to vibrate at its characteristic frequency relating to the density of the sample. This frequency is converted into density by the densitometer. The density values are reported in the temperature range of (293.15 - 333.15) K. The densitometer automatically controls temperature with a resolution of 0.01 K and an accuracy of 0.03 K. Finally, the experimental uncertainty was as low as 2.5 $kg.m^{-3}$ in the measurement of density. The mean of three measures of density data is reported.

An Ostwald viscometer was used to determine the experimental viscosity. A thermostated bath was used to submerge the viscometer. The temperature of the bath was maintained within the accuracy of 0.3 K of the desired level using a refrigerated and heating bath circulator (RW 2025G, Jeio Tech). The average of three measurements was provided for each value. The calculated experimental uncertainty for viscosity was 0.17 mPa.s.

To validate the density and viscosity measurements, the density and viscosity of pure MDEA, 20 wt%, and 30 wt% aqueous MDEA solutions were measured at 288.15, 313.15, and 333.15 K, and a comparison is drawn with previous studies in the literature[25]. The results are given in Table A1.1 (Appendix-1). After validating our experimental protocol, a similar procedure was followed to measure the density and viscosity of the novel aqueous solutions of TAEA and activated with MDEA and AMP solutions at several temperatures viz. (293.15 - 333.15) K.

3.2.2.2 Henry's Law Constant ($K_{H\text{-}N2O}$)

The stirred cell experimental apparatus designed and developed in this study shown in Fig. 3.1 is used for the measurement of N_2O solubility. It consists of three major sections, viz. the charge section, a cell section, and vacuum/vent manifold. The charge section consists of three different reservoirs viz. R1, R2, and R3 with volumes ~ ($2.25 \cdot 10^{-3}$, $2.25 \cdot 10^{-3}$ and $1.5 \cdot 10^{-4}$)

m^3 and two pressure transducers viz. LP1 and HP1 ranges ($0 – 3.33 \cdot 10^3$ and $0 – 13.8 \cdot 10^3$) kPa. Depending on the requirement of the experiment, one or more of the reservoirs and pressure transducers may be isolated completely. The low-pressure transducer is of higher accuracy and was used whenever the experimental conditions allowed.

The cell section comprises a stirred cell with a jacket around it. A water circulator with a temperature controller is used to circulate water in the jacket during absorption studies to control the temperature inside the cell accurately. The heater is also provided around the jacket for high temperatures above 373.15 K. A thermocouple is used to measure the temperature inside the cell via a thermowell. An impeller is offered to stir the cell contents and is connected to a motor via a hermetically sealed shaft. The rotation speed of the impeller can also be changed via an rpm controller. The cell is isolated from the charge section via a feed valve. Finally, a safety valve is provided on the cell to prevent over-pressurisation. The volume of the stirred cell is about 850 cm^3. As in the case of the charge section, two transducers viz. LP2 and HP2 range ($0 – 3.33 \cdot 10^3$ and $0 – 13.8 \cdot 10^3$) kPa are also provided in the cell section for accurate measurement of the cell pressure.

The solubility measurement principle is based on the mass balance of the gas injected into the cell. Initially, about 10^{-4} m^3 of the desired solvent is transferred into a well-cleaned cell. The cell is cooled down to a low temperature of about 278.15 K to minimize the vapour pressure of the solvent and evacuated. Evacuation is achieved by opening the cell section to the vacuum/vent manifold connected to a dry vacuum pump and a rotary vane vacuum pump. The evacuated cell is then isolated from the vacuum manifold and allowed to reach the experimental temperature in order to ensure the complete equilibrium of the cell contents at the observed temperature, the cell contents are allowed to equilibrate for an additional two hours. The temperature and the pressure of the cell are recorded. This pressure corresponds to the vapour pressure P^{Sat} of the solvent at the experimental temperature.

The charge section is evacuated completely by opening it to the vent/vacuum manifold. In this case, the gas of interest, N_2O is charged into the charge section to a pre-determined target pressure, P_{Charge}. The temperature and pressure of the charge section are recorded. The gas from the charge section is then injected into the cell by opening the isolation valve V_6 for a concise duration of ~ 5 seconds and closed after that. The pressure P_{Final} and temperature of the charge section are noted again. If the volume of the charge section is known accurately, then using the molar density of the gas phase, the number of moles transferred from the charge section into the cell section can be accurately calculated using the temperature and the two pressures P_{Charge} and P_{Final}.

After injection, the cell contents are stirred at about 1200 rpm and allowed to equilibrate. The impellers are mounted on the shaft such that contents of both the gas and the liquid phases are stirred well enough. During the equilibration, the pressure of the gas inside the cell decreases as it is dissolved in the solvent. Once equilibrium is reached, there would be no further change in pressure. Usually, about 60-80 minutes was necessary to reach equilibrium. After equilibration, the cell's final temperature and pressure $P_{Equlibrium}$ are noted. If the volume of the vapour space in the cell is known accurately, then a mass balance using the two pressures $P_{Equlibrium}$ and P^{Sat} yields the moles of N_2O present in the vapour phase inside the cell. The difference between the moles transferred from the charge section and the moles present in the cell section at equilibrium will give the moles of N_2O dissolved in the liquid solvent.

As outlined earlier, the technique is based on mass balance, and it is vital to have accurate temperature, pressure, and volume measurements. All temperatures were measured accurately to 273.25 K, using thermocouples. The pressure measurements were performed using high-accurate Baratron transducers (Make: MKS and Model: 627F, 750C). The volume measurements were performed using helium pycnometry, and the protocol was similar to solubility measurements but consisted of using helium as the gas and did not involve the liquid

solvent during the measurements. The volume of the vapour space in the cell after the liquid is introduced obtained by subtracting the liquid volume from the empty volume of the cell. The volumes of the various section in the apparatus were measured using helium pycnometry. In addition, the mole balances also require the densities of the gas phase in the charge and the cell sections. The density of the charge section is straightforward since it involves only the density of the pure gas (N_2O) at the desired temperature and pressure. In this work, the pure gas density was taken from the NIST Chemistry Webbook (NIST, 2019) [27]. A similar experimental work was also published in our earlier publication [26]. Henry's constant in other units calculated from the experiments (kPa.m^3. kmol^{-1}) may be obtained by simple manipulation given in Eq. 3.3

$$K_{H-N2O}/kPa.m^3.kmol^{-1} = \frac{1}{K_{H-N2O}/kmol.kg^{-1}.kPa^{-1} \times densityofsolvent/kg.m^{-3}} \quad (3.3)$$

The experimental protocol was validated by measuring K_H of CO_2 and N_2O in water and compared with the literature [25, 27-28]. The results of the validation experiments are presented in Tables A1.2 and A1.3 (Appendix-1). These findings suggest that the experimental equipment used in this study is suitable for determining the physical solubility of N_2O.

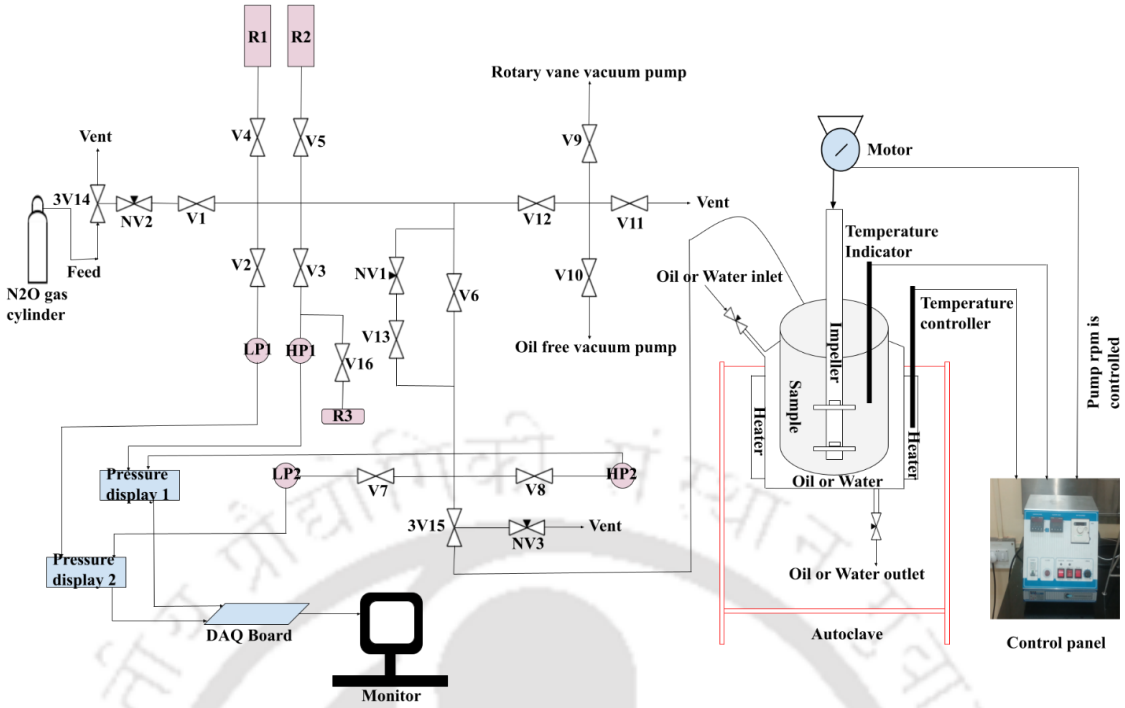

Figure 3.1 Block diagram of the stirred cell apparatus. DAQ board = Data acquisition board, 3V = 3-way valve, NV = Needle valve, V = 2-way valve, LP = Low pressure transducer, HP = High pressure transducer, R = Reservoir.

3.3 Results and discussion

3.3.1 Physiochemical properties

The measured physicochemical properties of TAEA and their blends with MDEA and AMP solutions are shown in Figs. 3.2 and 3.3 and Tables 3.2 and 3.3. The experimental results indicate that measured densities and viscosities of studied solutions increased with increase in mole fraction of TAEA in the amine solutions.

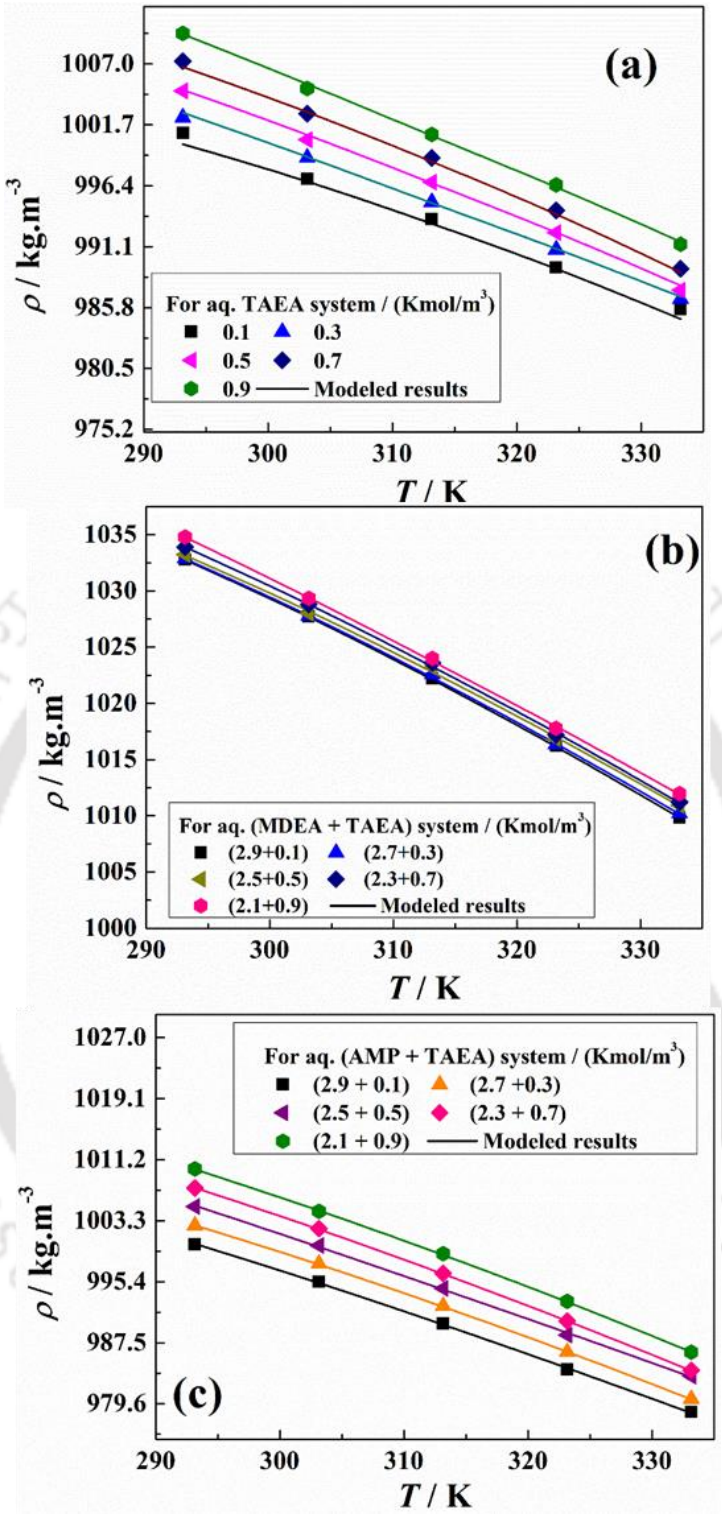

Figure 3.2 Comparison of experimental and model-predicted density of (a) For aq. TAEA System / Kmol.m^{-3} ■ 0.1, ▲ 0.3, ◀ 0.5, ◆ 0.7, ⬢ 0.9; (b) For aq. (MDEA+TAEA) System / Kmol.m^{-3} ■ (2.9+0.1), ▲ (2.7+0.3), ◀ (2.5+0.5), ◆ (2.3+0.7), ⬢ (2.1+0.9); and (c) For aq. (AMP+TAEA) System / Kmol.m^{-3} ■ (2.9+0.1), ▲ (2.7+0.3), ◀ (2.5+0.5), ◆ (2.3+0.7), ⬢ (2.1+0.9); Line is to read modeled results.

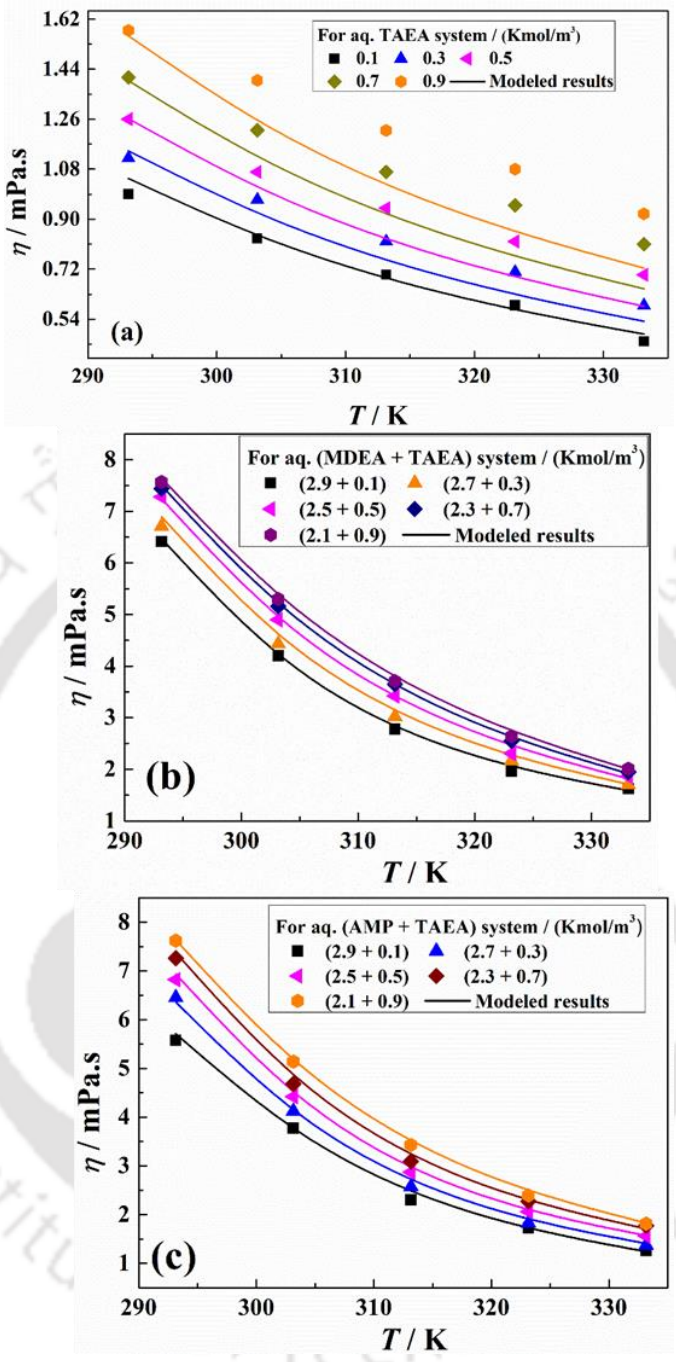

Figure 3.3 Comparison of experimental and model-predicted viscosity of (a) For aq. TAEA System / Kmol.m^{-3} ■ 0.1, ▲ 0.3, ◀ 0.5, ◆ 0.7, ⬢ 0.9 ; (b) For aq. (MDEA+TAEA) System / Kmol.m^{-3} ■ (2.9+0.1), ▲ (2.7+0.3), ◀ (2.5+0.5), ◆ (2.3+0.7), ⬢ (2.1+0.9); and (c) For aq. (AMP+TAEA) System / Kmol.m^{-3} ■ (2.9+0.1), ▲ (2.7+0.3), ◀ (2.5+0.5) , ◆ (2.3+0.7), ⬢ (2.1+0.9); Line is to read modeled results.

Table 3.2 Experimentally measured density (ρ / kg.m^{-3}) of aq. TAEA, aq. (MDEA + TAEA), and aq. (AMP + TAEA) systems from (293.15 K to 333.15) K at 0.1 MPa.[a]

Concentration / (kmol.m^{-3})	**ρ / kg.m^{-3}**				
	T / K				
	293.15	303.15	313.15	323.15	333.15
	(a) aq. TAEA				
0.1	1000.9	996.9	993.5	989.3	985.6
0.3	1002.4	998.9	994.9	990.9	986.5
0.5	1004.7	1000.4	996.7	992.3	987.3
0.7	1007.3	1002.7	998.8	994.3	989.2
0.9	1009.7	1004.9	1000.9	996.5	991.3
	(a) aq. (MDEA (1) +TAEA (2))				
2.9 + 0.1	1032.8	1027.7	1022.2	1016.2	1009.8
2.7 + 0.3	1032.9	1027.8	1022.6	1016.3	1010.2
2.5 + 0.5	1033.3	1028.0	1023.2	1016.9	1010.9
2.3 + 0.7	1033.9	1028.8	1023.6	1017.2	1011.2
2.1 + 0.9	1034.8	1029.4	1024.0	1017.8	1011.9
	(b) aq. (AMP (1) + TAEA (2))				
2.9 + 0.1	1000.2	995.4	989.9	983.9	978.5
2.7 + 0.3	1002.7	997.7	992.2	986.3	980.2
2.5 + 0.5	1005.1	1000.1	994.5	988.5	983.2
2.3 + 0.7	1007.5	1002.3	996.5	990.3	983.9
2.1 + 0.9	1010.0	1004.5	999.0	992.9	986.3

[a]The standard uncertainties *u* are *u*(*T*) = 0.3 K, *u*(*P*) = 0.01 MPa, *u*(ρ) = 2.5 kg·m^{-3}, *u*(*c*)=0.001 kmol.m^{-3}. Solvent is water.

Table 3.3 Experimentally measured viscosity (η / mPa.s) of aq. TAEA, aq. (MDEA + TAEA), and aq. (AMP + TAEA) systems at 0.1 MPa and temperature ranging from 293.15 K to 333.15 K.[a]

Concentration / (kmol.m^{-3})	T / K				
	293.15	303.15	313.15	323.15	333.15
	(a) aq. TAEA (1)				
0.1	0.988	0.833	0.701	0.590	0.462
0.3	1.123	0.972	0.816	0.713	0.590
0.5	1.259	1.072	0.941	0.817	0.699
0.7	1.408	1.222	1.067	0.950	0.810
0.9	1.579	1.403	1.222	1.075	0.921
	(b) aq. (MDEA (1) +TAEA (2))				
2.9 + 0.1	6.415	4.203	2.779	1.962	1.626
2.7 + 0.3	6.714	4.436	3.024	2.164	1.701
2.5 + 0.5	7.277	4.902	3.416	2.310	1.860
2.3 + 0.7	7.443	5.158	3.652	2.551	1.954
2.1 + 0.9	7.575	5.303	3.712	2.639	2.011
	(c) aq. ((AMP (1) + TAEA (2))				
2.9 + 0.1	5.569	3.767	2.304	1.722	1.260
2.7 + 0.3	6.450	4.119	2.575	1.820	1.371
2.5 + 0.5	6.823	4.424	2.865	2.058	1.564
2.3 + 0.7	7.264	4.680	3.089	2.268	1.774
2.1 + 0.9	7.617	5.135	3.431	2.387	1.814

[a]The standard uncertainties u are $u(T)$ = 0.3 K, $u(P)$ = 0.01 MPa, $u(\eta)$ = 0.17 mPa.s, $u(c)$=0.001 kmol.m^{-3}. Solvent is water

A Redlich–Kister type equation for excess molar volume is used to correlate the densities of the liquid mixtures. The Redlich–Kister equation has the following expression for a binary system.[29–34]

$$V_{jk}^{E}/\mathrm{m}^3\cdot\mathrm{kmol}^{-1}=x_j x_k\sum_{i=0}^{n}A_i\left(x_j-x_k\right)^i \tag{3.4}$$

x indicates the mole fraction. A_i represents a pair of temperature-dependent parameters, where A_i *is* denoted by:

$$A_i=a+b\left(T/\mathrm{K}\right)+c\left(T/\mathrm{K}\right)^2 \tag{3.5}$$

For the binary system, its assume that the excess volume of liquid mixtures is

$$V^E=V_{12}^E \tag{3.6}$$

From the observed fluids density, the excess volume of liquid mixtures can be determined by the following expression,

$$V^E=V_m-\sum x_i V_i^0 \tag{3.7}$$

V*m* represents the liquid mixture's molar volume, where V_i^0 is pure fluids at the system temperature, respectively. The V*m* can be estimated using the formula given below:

$$V_m=\frac{\sum x_i M_i}{\rho_m} \tag{3.8}$$

Where M_i is the pure component *i* molar mass , ρ_m is the measured liquid density, and x_i is the pure component *i* mole fraction. A general set of parameters that are predominantly temperature-dependent has been established with the help of experimental data. TAEA, MDEA or AMP, and H_2O have been chosen as the first, second, and third components for our suitability. The densities, viscosity, and $k_{H,\mathrm{N_2O}}$ pure TAEA were experimentally measured as represented in Table 3.4. The experimental data used to derive Henry's law constants in Table 3.4 is given in Table A1.4 (Appendix-1). The density and viscosity of the pure MDEA and

AMP were measured and compared with the literature[19] Table A1.5 (Appendix-1). The determined parameters over the temperature range (293.15 - 333.15) K are presented in Tables 3.5. The measured excess molar volumes of aqueous TAEA and blended with MDEA and AMP in the range of 293.15 K to 333.15 K are given in Table A1.6 (Appendix-1).

Table 3.4 Viscosity η, density ρ, *and* k_{H,N_2O} of Pure TAEA from (293.15 to 333.15) K at 0.1 MPa.[a]

Temperature (K)	Density ($kg.m^{-3}$)	Viscosity (mPa.s)	k_{H,N_2O} ($kPa{\cdot}m^3{\cdot}kmol^{-1}$)
293.15	976.3	12.47	2206
303.15	964.1	7.83	2465
313.15	953.2	5.36	2687
323.15	943.6	3.78	2834
333.15	934.2	3.14	-

[a]The standard uncertainties u are $u(T)$ = 0.3 K, $u(P)$ = 0.01 MPa, $u(\rho)$ = 2.5 $kg{\cdot}m^{-}3$, $u(\eta)$ = 0.17 mPa.s, $u(c)$=0.001 $kmol.m^{-3}$. The combined expanded uncertainties for solubility measurements Uc ($H_{N2O\text{-}TAEA}$) = 12.96 $kPa{\cdot}m^3{\cdot}kmol^{-1}$ (0.95 level of confidence, k=2).

Table 3.5 Binary interaction parameters (A_0, A_1, and A_2) of the Redlich-Kister equation for the excess volume.

Parameters		System				
		TAEA+H_2O	MDEA+TAEA	MDEA+H_2O	AMP+TAEA	AMP+H_2O
A_0	*a*	-124.348	$5.004 \cdot 10^{-11}$	$-1.253 \cdot 10^{-10}$	$2.992 \cdot 10^{-12}$	$-3.979{\cdot}10^{-12}$
	b	0.800	$1.568 \cdot 10^{-8}$	$-3.905 \cdot 10^{-8}$	$9.356{\cdot}10^{-10}$	$-1.261{\cdot}10^{-9}$
	c	-0.001	$4.930 \cdot 10^{-6}$	$-1.566 \cdot 10^{-6}$	$2.932{\cdot}10^{-7}$	$-4.223{\cdot}10^{-7}$
A_1	*a*	-283.717	$1.079 \cdot 10^{-11}$	$3.484 \cdot 10^{-11}$	$5.606{\cdot}10^{-13}$	$-1.137{\cdot}10^{-12}$
	b	1.826	$3.377 \cdot 10^{-9}$	$1.068 \cdot 10^{-8}$	$1.754{\cdot}10^{-10}$	$-3.380{\cdot}10^{-10}$
	c	-0.003	$1.060 \cdot 10^{-6}$	$2.280 \cdot 10^{-6}$	$5.502{\cdot}10^{-8}$	$-1.363{\cdot}10^{-7}$
A_2	*a*	-162.023	$9.304 \cdot 10^{-13}$	$3.972 \cdot 10^{-11}$	$4.345{\cdot}10^{-14}$	$5.387{\cdot}10^{-12}$
	b	1.042	$2.912 \cdot 10^{-10}$	$1.263 \cdot 10^{-8}$	$1.360{\cdot}10^{-11}$	$1.664{\cdot}10^{-9}$
	c	-0.002	$9.135 \cdot 10^{-8}$	$4.2514 \cdot 10^{-6}$	$4.266{\cdot}10^{-9}$	$5.302{\cdot}10^{-7}$
AAD (%)		0.030	1.035		1.118	

The experimental viscosity values were associated using Grunberg and Nissan model for ternary solutions, as shown below[13–16,21].

$$\ln(\eta/mPa\,.\,s)=\sum x_i \ln \eta_i + \sum\sum x_i x_j G_{ij} \quad (3.9)$$

Gij in Eq. (3.9) is represented as a function of temperature, which is shown in Eq. (3.10).

$$G_{ij} = a + b(T/K) + c(T/K)^2 \quad (3.10)$$

Table 3.6 shows the parameters for viscosity that were derived using regression analysis of the experimental data from this study. The predicted densities and viscosities from the correlation are highly close to the actual data with the average absolute deviation, AAD (%) among the correlated and the experimental density and Viscosity data for the (TAEA+H_2O), (MDEA+TAEA+H_2O), (AMP+TAEA+H_2O), systems being about 0.030, 1.035 and 1.118 for density correlation and for viscosity it is around 9.602, 2.162 and 1.765, respectively. The kinematic viscosity deviations, Δv with mole fractions for aqueous TAEA and blended with MDEA and AMP solutions over the entire temperature range (293.15 - 333.15) K are given in Table 3.7. As shown in Table A1.6, the values of excess molar volumes are negative in the whole temperature range. It suggests that the structural contribution of different size molecules present in the solutions provides a geometrical effect to fit each other's structure and strong dipole-dipole interaction among the components. Also, it involves hydrogen bonding formation in the solution[35]. It also signifies the contraction volume occurred by strong intermolecular interaction in the system upon mixing. Similarly, Table 3.7 shows that increasing the mole fraction of TAEA in the solution viscosity deviations also increases, leading to the strong interaction between the molecules in the solutions.

Table 3.6 Grunberg-Nissan model parameters for (i) TAEA (1) + H_2O (2), (ii) MDEA (1) + TAEA (2) + H_2O (3), and (iii) AMP (1) + TAEA (2) + H_2O (3) systems

Parameters		(i) TAEA + H_2O	(ii) MDEA + TAEA + H_2O	(iii) AMP + TAEA + H_2O
	a	$-1.174 \cdot 10^{3}$	$-4.886 \cdot 10^{4}$	$1.392 \cdot 10^{5}$
G_{12}	*b*	7.325	320.095	-885.560
	c	$-1.106 \cdot 10^{-2}$	-0.517	1.409
	a	-	$2.031 \cdot 10^{3}$	$-7.500 \cdot 10^{3}$
G_{23}	*b*	-	-13.158	48.025
	c	-	0.021	-0.077
	a	-	541.671	239.486
G_{31}	*b*	-	-3.171	-1.179
	c	-	0.005	$1.500 \cdot 10^{-3}$
AAD (%)		9.602	2.162	1.765

Table 3.7 Kinematic Viscosity Deviations, Δv / $m^2.s^{-1}$, for (i) TAEA + H_2O, (ii) MDEA + TAEA + H_2O, and (iii) AMP + TAEA + H_2O from (293.15 to 333.15) K

Concentration / (kmol.m^{-3})	293.15 K	303.15 K	313.15 K	323.15 K	333.15 K
	(i) aq. TAEA (1)				
0.1	$-1.742 \cdot 10^{-2}$	$2.962 \cdot 10^{-2}$	$4.523 \cdot 10^{-2}$	$4.197 \cdot 10^{-2}$	$-7.701 \cdot 10^{-3}$
0.3	$1.0538 \cdot 10^{-1}$	$1.647 \cdot 10^{-1}$	$1.624 \cdot 10^{-1}$	$1.605 \cdot 10^{-1}$	$1.222 \cdot 10^{-1}$
0.5	$2.363 \cdot 10^{-1}$	$2.595 \cdot 10^{-1}$	$2.789 \cdot 10^{-1}$	$2.685 \cdot 10^{-1}$	$2.318 \cdot 10^{-1}$
0.7	$3.757 \cdot 10^{-1}$	$4.028 \cdot 10^{-1}$	$4.044 \cdot 10^{-1}$	$3.960 \cdot 10^{-1}$	$3.401 \cdot 10^{-1}$
0.9	$5.341 \cdot 10^{-1}$	$5.752 \cdot 10^{-1}$	$5.493 \cdot 10^{-1}$	$5.222 \cdot 10^{-1}$	$4.476 \cdot 10^{-1}$
	(ii) aq. (MDEA + TAEA)				
2.9 + 0.1	-1.140	$-8.835 \cdot 10^{-1}$	$-4.661 \cdot 10^{-1}$	$-2.897 \cdot 10^{-1}$	$7.092 \cdot 10^{-2}$
2.7 + 0.3	$-5.238 \cdot 10^{-1}$	$-4.393 \cdot 10^{-1}$	$-9.876 \cdot 10^{-2}$	$-7.230 \cdot 10^{-3}$	$1.945 \cdot 10^{-1}$
2.5 + 0.5	$3.517 \cdot 10^{-1}$	$2.339 \cdot 10^{-1}$	$4.133 \cdot 10^{-1}$	$2.205 \cdot 10^{-1}$	$4.013 \cdot 10^{-1}$
2.3 + 0.7	$8.461 \cdot 10^{-1}$	$7.036 \cdot 10^{-1}$	$7.755 \cdot 10^{-1}$	$5.433 \cdot 10^{-1}$	$5.452 \cdot 10^{-1}$
2.1 + 0.9	1.311	$1.0069 \cdot 10$	$9.677 \cdot 10^{-1}$	$7.163 \cdot 10^{-1}$	$6.525 \cdot 10^{-1}$

			(iii) aq. (AMP + TAEA)		
2.9 + 0.1	-7.147	-4.154	-1.715	$-5.544 \cdot 10^{-1}$	$-1.995 \cdot 10^{-1}$
2.7 + 0.3	-5.692	-3.451	-1.285	$-3.799 \cdot 10^{-1}$	$-4.715 \cdot 10^{-2}$
2.5 + 0.5	-4.732	-2.788	$-8.318 \cdot 10^{-1}$	$-6.142 \cdot 10^{-2}$	$1.889 \cdot 10^{-1}$
2.3 + 0.7	-3.684	-2.162	$-4.495 \cdot 10^{-1}$	$2.317 \cdot 10^{-1}$	$4.451 \cdot 10^{-1}$
2.1 + 0.9	-2.708	-1.328	$7.181 \cdot 10^{-2}$	$4.323 \cdot 10^{-1}$	$5.275 \cdot 10^{-1}$

3.3.2 N_2O and CO_2 (Physical) Solubility

Figs. 3.4 & 3.5 show data on N_2O solubility and anticipated CO_2 solubility in aqueous solutions using the N_2O analogy of novel solvents (TAEA+H_2O), (MDEA+TAEA+H_2O), and (AMP+TAEA+H_2O) for temperatures (293.15 - 323.15) K, as well as Table 3.8. The experimental data used to derive the Henry's law constants in Table 3.8 is given in Tables A1.7-A1.9 (Appendix-1).

Table 3.8 Experimental N_2O and estimated CO_2 solubility (k_{H,CO_2} / kPa·m^3·kmol^{-1}) in (i) aq. TAEA, (ii) aq. (MDEA + TAEA) and (iii) aq. (AMP + TAEA) from (293.15 to 323.15) K.[a]

Concentration / (kmol.m^{-3})	k_{H,N_2O} / kPa·m^3·kmol^{-1}				k_{H,CO_2} / (kPa·m^3·kmol^{-1})			
	293.15	303.15	313.15	323.15	293.15	303.15	313.15	323.15
				(i) aq. TAEA				
0.1	4047	4571	5257	6211	3027	3328	3731	4305
0.3	4348	5075	5729	6698	3252	3694	4066	4643
0.5	4643	5540	6440	7204	3472	4033	4571	4993
0.7	5025	5790	6878	7514	3758	4215	4882	5208
				(ii) aq. (MDEA + TAEA)				
2.9 + 0.1	5961	6511	7161	7732	4458	4740	5083	5359
2.7 + 0.3	6300	7101	7509	8127	4712	5169	5330	5633
2.5 + 0.5	6652	7306	7880	8470	4975	5318	5593	5871
2.3 + 0.7	6921	7628	8285	8779	5176	5553	5881	6085
				(iii) aq. (AMP + TAEA)				

2.9 + 0.1	4948	5936	6633	7722	3701	4321	4708	5353
2.7 + 0.3	4850	5803	6475	7682	3627	4224	4596	5325
2.5 + 0.5	4810	5649	6428	7655	3597	4112	4563	5306
2.3 + 0.7	4754	5529	6248	7422	3555	4025	4435	5145

[a]The standard uncertainties u are $u(T)$ = 0.3 K, $u(P)$ = 0.01 MPa, $u(c)$=0.001 kmol.m^{-3}. The combined expanded uncertainties for solubility measurements Uc ($H_{N2O\text{-}TAEA}$) =37.1 kPa·m^3·kmol^{-1}, Uc ($H_{N2O\text{-}MDEA+TAEA}$) =37.3 kPa·m^3·kmol^{-1}, Uc ($H_{N2O\text{-}AMP+TAEA}$) =41.2 kPa·m^3·kmol^{-1} with (0.95 level of confidence, k=2). Solvent is water.

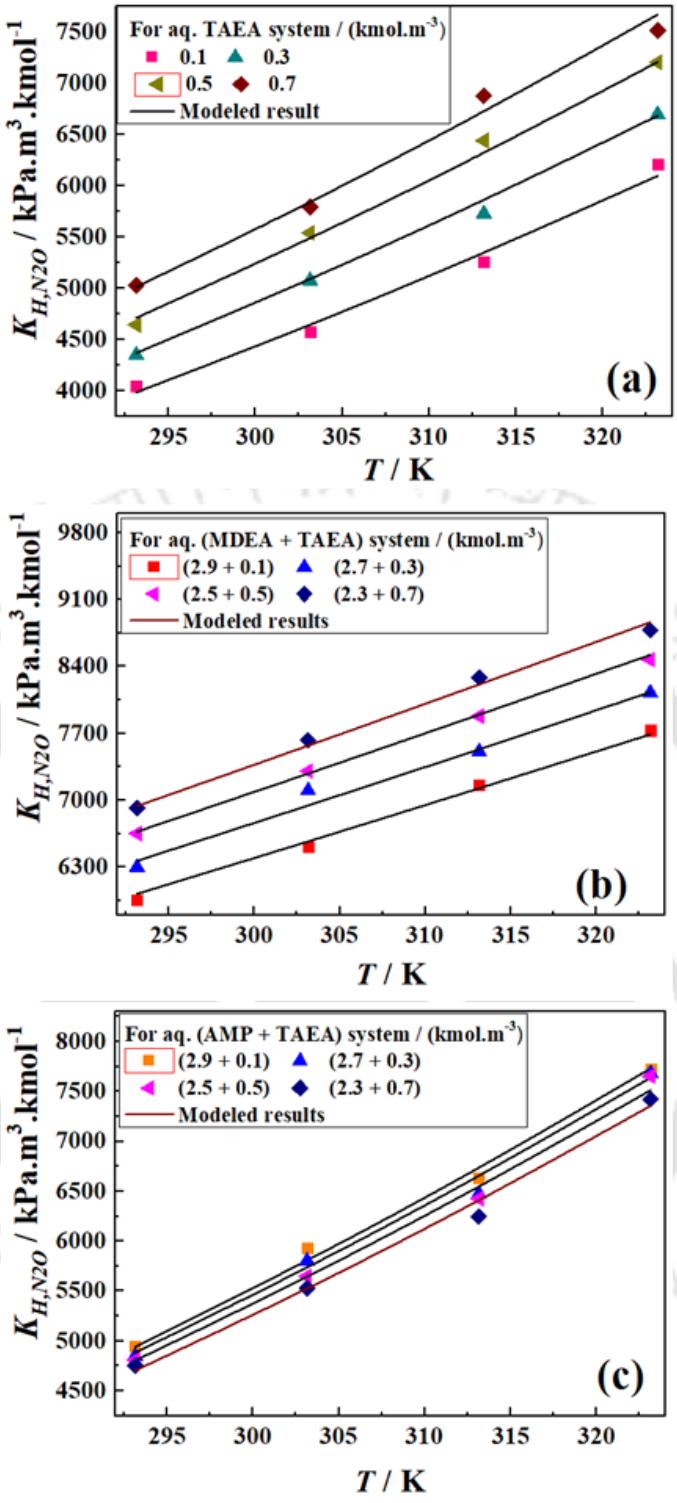

Figure 3.4 Analysis and comparison of experimental and model-predicted Henry's constant $K_{H,\,N2O}$ / kPa.m^3.kmol^{-1} in (a) For aq. TAEA System / Kmol.m^{-3} ■ 0.1, ▲ 0.3, ◀ 0.5, ◆ 0.7; (b) For aq. (MDEA+TAEA) System / Kmol.m^{-3} ■ (2.9+0.1), ▲ (2.7+0.3), ◀ (2.5+0.5), ◆ (2.3+0.7); and (c) For aq. (AMP+TAEA) System / Kmol.m^{-3} ■ (2.9+0.1), ▲ (2.7+0.3), ◀ (2.5+0.5), ◆ (2.3+0.7); line is to read modeled results.

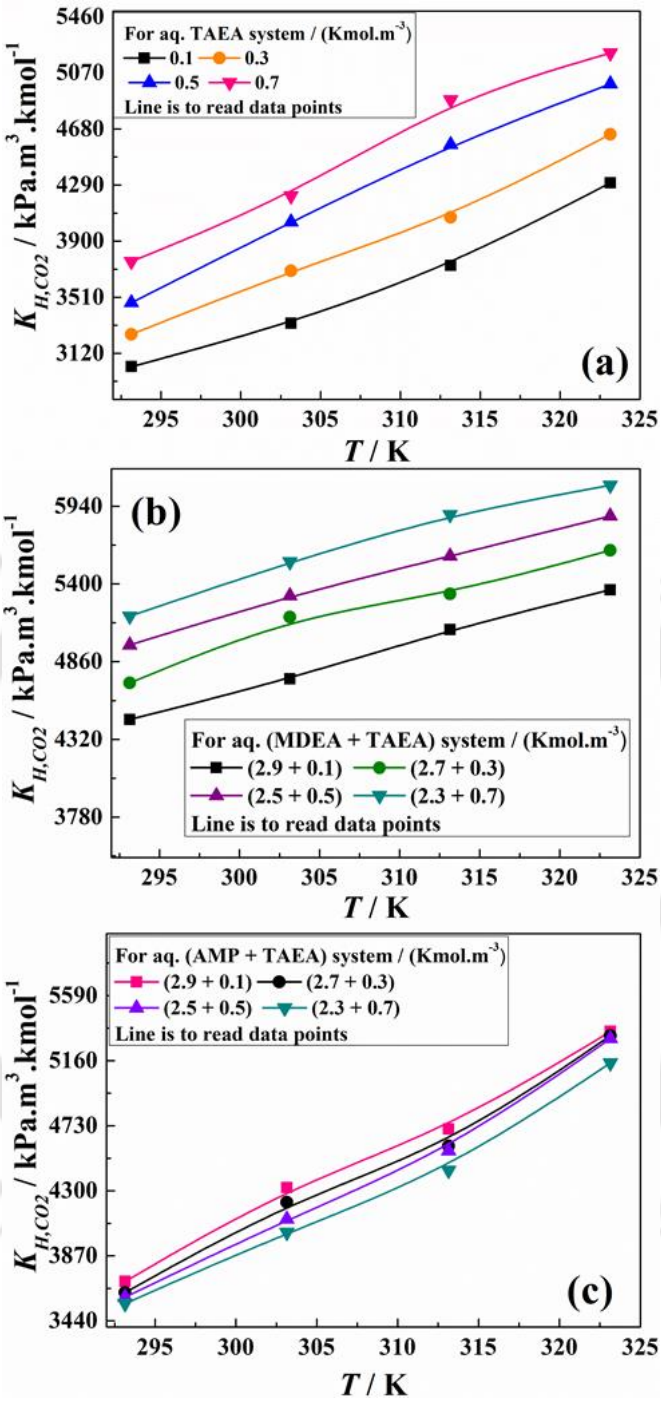

Figure 3.5 N_2O analogy model-predicted Henry's constant $K_{H,\,CO2}$ / kPa.m^3.kmol^{-1} in (a) For aq. TAEA System / Kmol.m^{-3} ■ 0.1, ● 0.3, ▲ 0.5, ▼ 0.7; (b) For aq. (MDEA+TAEA) System / Kmol.m^{-3} ■ (2.9+0.1), ● (2.7+0.3), ▲ (2.5+0.5), ▼ (2.3+0.7); and (c) For aq. (AMP+TAEA) System / Kmol.m^{-3} ■ (2.9+0.1), ● (2.7+0.3), ▲ (2.5+0.5), ▼ (2.3+0.7); Line is to read data points.

The calculated $K_{H\text{-}N2O}$ of N_2O in aqueous novel solvent TAEA and activated with MDEA is directly proportional to changes in temperature and mole percent of TAEA in the mixture because of the exothermic nature in the gas absorption. Whereas in the TAEA activated with AMP, the results show that the calculated $K_{H\text{-}N2O}$ of N_2O in these solutions is directly proportional to changes in temperature but inversely proportional to the mole percent of TAEA. Thus, it shows that the activator has more affinity towards N_2O. To correlate the solubility data, the Arrhenius type equation is proposed at various concentrations (molarity) of TAEA (M_1) solutions and their blends with MDEA/AMP (M_2) solutions, and different temperatures (T) as follows[9,10];

$$K_{H-N2O}/kPa.m^3.kmol^{-1} = (a + b \cdot M_1 + c \cdot M_2) \cdot exp\left(\frac{-d}{T/K}\right) \quad (3.11)$$

H_{N2O} represents the $K_{H\text{-}N2O}$ and T in the above equation, represents the temperature, and (a, b, c, d) are the constants, which is applicable for the binary system of TAEA and water when the concentration of MDEA or AMP is zero. The values are shown in Table 3.9 for binary and ternary solutions, respectively. The AAD (%) values for the solutions of aqueous TAEA and their blends with MDEA and AMP solutions were obtained as 1.259, 0.654, and 1.121, respectively. These deviations indicate excellent agreement with our experimental results.

Table 3.9 Estimated parameters of Arrhenius type equation for N_2O Solubility in (i) aq. TAEA, (ii) aq. (MDEA + TAEA) and (iii) aq. (AMP + TAEA)

	Systems		
Parameters	TAEA + H_2O	MDEA + TAEA + H_2O	AMP + TAEA + H_2O
a	$3.746 \cdot 10^5$	$-1.862 \cdot 10^5$	$1.463 \cdot 10^7$
b	$1.675 \cdot 10^5$	$1.107 \cdot 10^5$	$-4.721 \cdot 10^6$
c	0.000	89402.000	$-4.672 \cdot 10^6$
d	1343.300	772.260	1412.100
AAD (%)	1.259	0.654	1.121

3.3.3 Diffusivity

The viscosity of aqueous amine solutions can be correlated to diffusivity by modified Stokes-Einstein relation[18] as shown in Eq. 3.12.

$$\left(D_{N_2O} \times \mu^{0.80}\right)_{Amine} = Cons\tan t = \left(D_{N_2O} \times \mu^{0.80}\right)_{Water} \tag{3.12}$$

The above modified Stokes-Einstein equation states that product of diffusivity of N_2O in an amine solution and $\mu^{0.8}$ of the liquid is constant, where μ is the measured viscosity of the amine solution. Diffusivity of CO_2 and N_2O in water can be obtained by the following expressions[36] Eqs. 3.13 and 3.14, respectively, and viscosity of water was taken from the open literature,

$$D_{CO_2} = 2.35\ .\ 10^{-6} \times \exp(-2119/T),\ \ m^2.s^{-1} \tag{3.13}$$

$$D_{N_2O} = 5.07\ .\ 10^{-6} \times \exp(-2371/T),\ \ m^2.s^{-1} \tag{3.14}$$

Fig. 3.6 and Table A1.10 (Appendix-1) show the predicted CO_2 diffusivity in the aqueous solution using the N_2O analogy of (TAEA+ H_2O), (MDEA+TAEA+ H_2O), and (AMP+TAEA+ H_2O) for temperatures ranging from (293.15 - 333.15) K.

As we can see from Fig. 6, the diffusivity values are increasing with the increase in temperature because the viscosity decreases with the rising temperature. Also, it has been observed that diffusivity decreases with increasing mole fraction TAEA in the solution

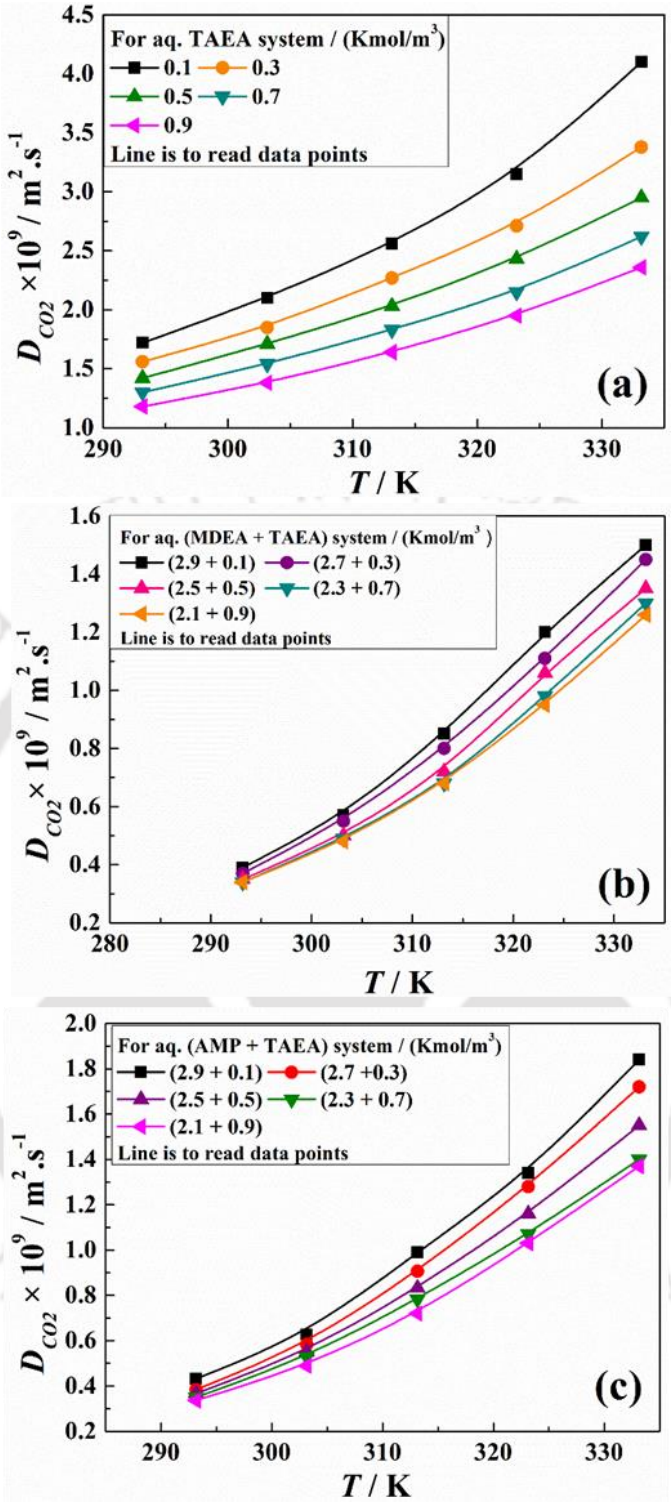

Figure 3.6 Stokes-Eisenstein model-predicted diffusivity of CO_2 in (a) For aq. TAEA System / Kmol.m^{-3} ■ 0.1, ● 0.3, ▲ 0.5, ▼ 0.7, ◀ 0.9; (b) For aq. (MDEA+TAEA) System / Kmol.m^{-3} ■ (2.9+0.1), ● (2.7+0.3), ▲ (2.5+0.5), ▼ (2.3+0.7), ◀ (2.1+0.9); and (c) For aq. (AMP+TAEA) System / Kmol.m^{-3} ■ (2.9+0.1), ● (2.7+0.3), ▲ (2.5+0.5), ▼ (2.3+0.7), ◀ (2.1+0.9); Line is to read data points.

References

[1] R.A. Kerr, Global warming is changing the world, Science (80-.). 316 (2007) 188–190.

[2] T. Sema, M. Edali, A. Naami, R. Idem, P. Tontiwachwuthikul, Solubility and diffusivity of N_2O in aqueous 4-(diethylamino)-2-butanol solutions for use in postcombustion CO_2 capture, Ind. Eng. Chem. Res. 51 (2012) 925–930.

[3] Y.N. Helei Liu, Zhiwu Liang, Teerawat Sema, Wichitpan Rongwong, Chen Li, and P.T. Raphael Idem, Kinetics of CO_2 Absorption into a Novel 1-Diethylamino-2-propanol Solvent Using Stopped-Flow Technique, AIChE J. 60 (2014) 3502–3510.

[4] R.B. Kohl, A. L, Nielsen, Gas Purification, 5th ed., Gulf Publishing Company: Houston, 1997.

[5] T. Chakravarty, U.K. Phukan, R.H. Weiland, Reaction of Acid Gases With Mixtures of Amines., Chem. Eng. Prog. 81 (1985) 32–36.

[6] B. Sreenivasulu, D. V. Gayatri, I. Sreedhar, K. V. Raghavan, A journey into the process and engineering aspects of carbon capture technologies, Renew. Sustain. Energy Rev. 41 (2015) 1324–1350.

[7] S. Garg, G. Murshid, F.S. Mjalli, A. Ali, W. Ahmad, Experimental and correlation study of selected physical properties of aqueous blends of potassium sarcosinate and 2-piperidineethanol as a solvent for CO_2 capture, Chem. Eng. Res. Des. 118 (2017) 121–130.

[8] Paul T Anastas, John Charles Warner, Green chemistry : theory and practice, 1998.

[9] S. Paul, A.K. Ghoshal, B. Mandal, Physicochemical properties of aqueous solutions of 2-(1-Piperazinyl)- ethylamine, J. Chem. Eng. Data. 55 (2010) 1359–1363.

[10] B. Das, B. Deogam, Y. Agrawal, B. Mandal, Measurement and Correlation of the

Physicochemical Properties of Novel Aqueous Bis(3-aminopropyl)amine and Its Blend with N-Methyldiethanolamine for CO_2 Capture, J. Chem. Eng. Data. 61 (2016) 2226–2235.

[11] G. Murshid, A.M. Shariff, K.K. Lau, M.A. Bustam, F. Ahmad, Physical properties of piperazine (PZ) activated aqueous solutions of 2-amino-2-hydroxymethyl-1,3-propanediol (AHPD + PZ), J. Chem. Eng. Data. 57 (2012) 133–136.

[12] A. V. Rayer, K.Z. Sumon, A. Henni, P. Tontiwachwuthikul, Physicochemical properties of {1-methyl piperazine (1) + water (2)} system at T = (298.15 to 343.15) K and atmospheric pressure, J. Chem. Thermodyn. 43 (2011) 1897–1905.

[13] A.A. Khan, G.N. Halder, A.K. Saha, Comparing CO_2 removal characteristics of aqueous solutions of monoethanolamine, 2-amino-2-methyl-1-propanol, methyldiethanolamine and piperazine through absorption process, Int. J. Greenh. Gas Control. 50 (2016) 179–189.

[14] A. Samanta, S.S. Bandyopadhyay, Absorption of carbon dioxide into aqueous solutions of piperazine activated 2-amino-2-methyl-1-propanol, Chem. Eng. Sci. 64 (2009) 1185–1194.

[15] S. Bishnoi, G.T. Rochelle, Absorption of carbon dioxide into aqueous piperazine: Reaction kinetics, mass transfer and solubility, Chem. Eng. Sci. 55 (2000) 5531–5543.

[16] G. Xu, C. Zhang, S. Qin, Y. Wang, Kinetics Study on Absorption of Carbon Dioxide into Solutions of Activated Methyldiethanolamine, *Ind. Eng. Chem. Res*, **1992**, *31*, 921–927.

[17] H. Machida, H. Yamada, Y. Fujioka, S. Yamamoto, CO_2 solubility measurements and modeling for tertiary diamines, J. Chem. Eng. Data. 60 (2015) 814–820.

[18] F. Bougie, M.C. Iliuta, Solubility of CO_2 in and density, viscosity, and surface tension of aqueous 2-amino-1,3-propanediol (serinol) solutions, J. Chem. Eng. Data. 59 (2014) 355–361.

[19] S. Xu, F.D. Otto, A.E. Mather, Physical Properties of Aqueous AMP Solutions, J. Chem. Eng. Data. 36 (1991) 71–75.

[20] M.H. Li, Y.C. Lie, Densities and Viscosities of Solutions of Monoethanolamine + N-methyldiethanolamine + Water and Monoethanolamine + 2-Amino-2-methyl-1-propanol + Water, J. Chem. Eng. Data. 39 (1994) 444–447.

[21] S.J. Yoon, H.S. Lee, H. Lee, J.I. Baek, J.H. Yoon, H.M. Eum, Densities, viscosities, and surface tensions of aqueous 2-amino-2-ethyl-1,3-propanediol solutions, J. Chem. Eng. Data. 47 (2002) 30–32.

[22] Y.-W.W. Guo-Wen Xu, Cheng-Fang Zhang, Shu-Jun Qin, Kinetics Study on Absorption of Carbon Dioxide into Solutions of Activated Methyldiethanolamine, Ind. Eng. Chem. Res. 31 (1992) 921–927.

[23] H.T.K. Niklas O. Braun, Ulf A. Persson, Densities and Viscosities of Mono(ethylene glycol) + 2-Amino-2-methyl-1-propanol + Water, J. Chem. Eng. Data. 46 (2001) 805–808.

[24] Jeom-In Baek, Ji-Ho Yoon, Solubility of Carbon Dioxide in Aqueous Solutions of 2-Amino-2-methyl-1,3-propanediol, J. Chem. Eng. Data. 43 (1998) 635–637.

[25] H.A. Al-Ghawas, D.P. Hagewiesche, G. Ruiz-Ibanez, O.C. Sandall, Physicochemical Properties Important for Carbon Dioxide Absorption in Aqueous Methyldiethanolamine, J. Chem. Eng. Data. 34 (1989) 385–391.

[26] R. Tellagorla, S.C. Balchandani, S. Gumma, B. Mandal, Equilibrium CO_2 solubility of

novel tris(2-aminoethyl) amine as a promoter to N-methyldiethanolamine and 2-amino-2-methyl-1-propanol, Elsevier B.V., 2021.

[27] https://webbook.nist.gov/cgi/cbook.cgi?ID=C10024972&Units=SI&Mask=10#Solubility (accessed on 13.Nov. 2018).

[28] G. F . Versteeg, L. A. J. Van Dijck, W. P. M. van Swaaij, On the kinetics between CO_2 and alkanolamines both in aqueous and non-aqueous solutions, An overview. Chem. Eng. Commun, 1996, 144, 113–158.

[29] S. Paul, B. Mandal, Density and viscosity of aqueous solutions of (2-piperidineethanol +piperazine) from (288 to 333) K and surface tension of aqueous solutions of (N-methyldiethanolamine + piperazine), (2-amino-2-methyl-1-propanol + piperazine), and (2-piperidineethanol + , J. Chem. Eng. Data. 51 (2006) 2242–2245.

[30] Subham Paul and Bishnupada Manda, Density and Viscosity of Aqueous Solutions of 2-Piperidineethanol, (2-Piperidineethanol + Monoethanolamine), and (2-Piperidineethanol + Diethanolamine) from (288 to 333) K Subham, J. Chem. Eng. Data. 51 (2006) 1808–1810.

[31] B.P. Mandal, M. Kundu, S.S. Bandyopadhyay, Density and Viscosity of Aqueous Solutions of (N -Methyldiethanolamine + Monoethanolamine), (N -Methyldiethanolamine + Diethanolamine), (2-Amino-2-methyl-1-propanol + Monoethanolamine), and (2-Amino-2-methyl-1-propanol + Diethanolamine), J. Chem. Eng. Data. 48 (2003) 703–707.

[32] Subham Paul and Bishnupada Mandal, Density and Viscosity of Aqueous Solutions of 2-Piperidineethanol, (2-Piperidineethanol + Monoethanolamine), and (2-Piperidineethanol + Diethanolamine) from (288 to 333) K, J. Chem. Eng. Data. 51 (2006) 1406–1410.

[33] A.K.G. and B.M. Subham Paul, Physicochemical Properties of Aqueous Solutions of 2-Amino-2-hydroxymethyl-1,3-propanediol, J. Chem. Eng. Data. 54 (2009) 444–447.

[33] Z. Idris, L. Ang, D.A. Eimer, J. Ying, Density measurements of unloaded and CO2-loaded 1-dimethylamino-2-propanol at temperatures (298.15 to 353.15) K, J. Chem. Eng. Data. 60 (2015) 1419–1425.

[34] D.B. Karuna Kumar, K.R. Reddy, G.S. Rao, G.V.R. Rao, C. Rambabu, Thermodynamic and spectroscopic study of molecular interactions in the binary liquid mixtures of N-methyl-2-pyrrolidone and some substituted benzenes at different temperatures, J. Mol. Liq. 174 (2012) 100–111.

[35] D. B. K. Kumar, K. R. Reddy, G. S. Rao, G. R. Rao, C. Rambabu, Thermodynamic and Spectroscopic study of molecular interaction in the binary liquid mixtures of N-methyl-2-pyrrolidone and some substituted benzenes at different temperatures, *J. Mol. Liq.* 2012, 174, 100-111.

[36] G.F. Versteeg, W.P.M. van Swaal, Solubility and Diffusivity of Acid Gases (CO_2, N_2O) in Aqueous Alkanolamine Solutions, J. Chem. Eng. Data. 33 (1988) 29–34.

Chapter 4

Equilibrium CO_2 solubility of novel tris(2-aminoethyl) amine as a promoter to *N*-methyldiethanolamine and 2-amino-2-methyl-1-propanol

This chapter includes a comprehensive experimental, and theoretical investigation of CO_2 equilibrium solubility in aqueous (TAEA+MDEA) and (TAEA+AMP) blends over a wide temperature and pressure range. Modified Kent-Eisenberg equilibrium model with gas-phase non-ideality and Feed forward neural network model were used to model the experimental vapor-liquid equilibrium data (VLE). In addition, qualitative ^{13}C NMR and FTIR studies were carried out to evaluate the suggested chemical scheme.

4.1 Introduction

Global warming and climate change issues have been raised over the years due to the massive release of greenhouse gases [1–4]. Among the greenhouse gases, CO_2 has an outsized role due to its abundance. To overcome this problem and maintain a sustainable environment, different countries have developed various ways to reduce or control CO_2 in the atmosphere [5–10]. Absorption-regeneration technology helped with various improved alkanolamine solvents towards the mitigation of CO_2, and it is considered a feasible technology so far. The most commonly used solvents such as primary (monoethanolamine, MEA), secondary (diethanolamine, DEA), tertiary (N-methyldiethanol amine, MDEA), and sterically hindered (2-amino-2-methyl-1-propanol, AMP) amines have been proposed for various industrial gas treating units [11-12]. Since various amines have their specific drawbacks when used for CO_2 absorption-desorption scale-like degradation of the solvent, corrosion, low absorptive capacity, high energy requirement for reduction of CO_2, etc.[13–19], researchers introduced a cyclic

amine as a promoter to blend with commercial solvents like MEA, MDEA, AMP to improve absorption capacity and decrease the energy required for the regeneration of CO_2 [8,20,21]. Novel activated amine solvent development is promising for a sustainable future due to higher energy demand in the conventional amine blend-based CO_2 capture process. Activated amine solvents play a pivotal role in boosting CO_2 capture efficiency, and focus in this area is necessary. Herein, we propose a novel cyclic amine (tris(2-aminoethyl) amine, TAEA) activator to MDEA and AMP solutions to remove CO_2 from gas streams. This novel promoter has three secondary and tertiary groups with high thermal stability and low vapour pressure. It is expected that this activator will act as a rate promoter with a high CO_2 absorption capacity.

This study measured the equilibrium CO_2 solubility in aqueous solutions of novel solvents such as (TAEA + MDEA + H_2O) and (TAEA + AMP + H_2O). The measured experimental solubility data is correlated using a modified Kent Eisenberg (KE) thermodynamic model [22]. Various modified thermodynamics models such as Deshmukh-Mather [23], electrolyte NRTL [24], and Pitzer model [25] are also used in the literature to account for the non-ideality of CO_2-amine systems and to predict the CO_2 solubility in amine-based solutions. However, compared to all other models, the KE model deals with effortlessness and reduces the computation time [26]. In the KE model, the activity coefficients related to all the species in the electrolyte system are assumed to be unity; the only parameter for regression is the equilibrium constants [27]. Distant from the KE model, an artificial neural network (ANN) model is also applied in the present work to model the equilibrium solubility of the blended amine systems [28].

4.2 Experimental section

4.2.1 Materials

Reagent grade MDEA (mass fraction purity > 0.99), AMP (mass fraction purity > 0.95) and TAEA (mass fraction purity > 0.96) were acquired from Sigma Aldrich and used without

further cleansing. Distilled water degassed by steaming was used for making the amine solutions. The amine contents of the solutions were determined by acidimetric titration with standard HCl using an autotitrator (DL 50, Mettler Toledo). The uncertainty in the composition of the amine solutions was valued as ± 0.01 %. The carbon dioxide (mass fraction purity > 0.999) was obtained from Assam Air Products, India. The purity of CO_2 was reported as obtained from the same vendor with certified purity. Description of the chemicals is represented in Table 4.1.

Table 4.1 List of chemicals used in this work.

Chemical Name	Formula	Molecular Weight (g/mol)	Source	Purity (%)	CAS no	Purification method
Tris(2-aminoethyl) amine (TAEA)	$(NH_2CH_2CH_2)_3N$	146.23	Sigma Aldrich	96	4097-89-6	None
n-methyldiethanolamine (MDEA)	$CH_3N(C_2H_4OH)_2$	119.16	Sigma Aldrich	99	105-59-9	None
2-amino-2-methyl-1-propanol (AMP)	$C_4H_{11}NO$	89.14	Sigma Aldrich	95	124-68-5	None

4.2.2 Experimental Methodology

4.2.2.1 CO_2 solubility measurement

A schematic diagram of the developed experimental setup for measuring the CO_2 solubility has given in Fig. 4.1. A similar procedure was explained in chapter-3 was followed for calculating the CO_2 solubility in aqueous amine solutions.

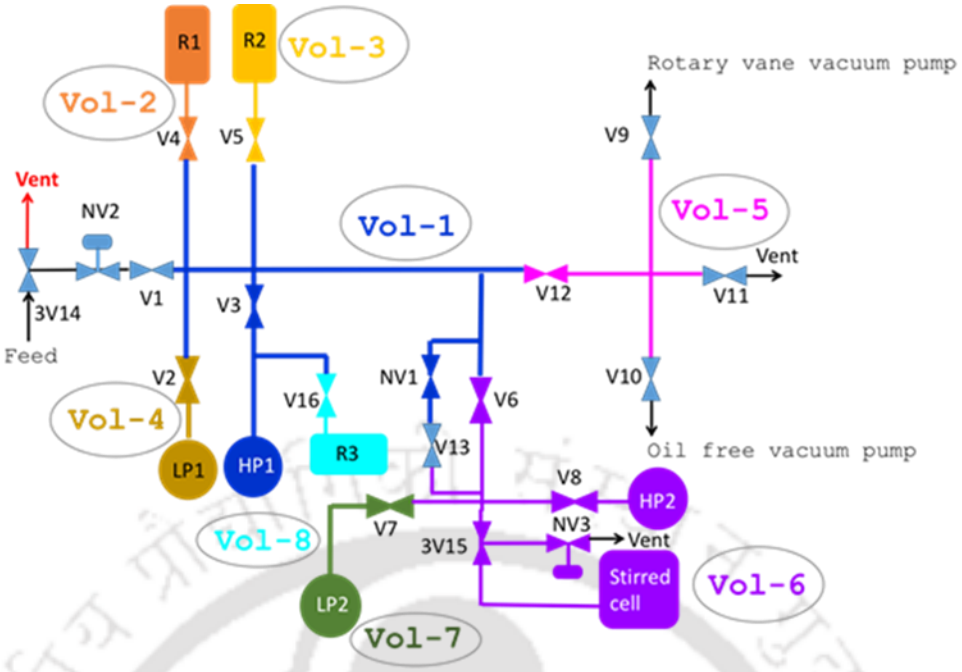

Vol-1: Volume section b/w V1, V2, V3, V4, V5, V12, V6 and NV1.
Vol-2: Volume section above V4.
Vol-3: Volume section above V5.
Vol-4: Volume section below V2.
Vol-5: Volume section b/w V9, V10, V11 and V12.
Vol-6: Volume section below 3V15.
Vol-7: Volume section b/w NV1, V6, HP2 and 3V15.
Vol-8: Volume section below V3.
LP1, LP2: Low pressure transducers.
HP1, HP2: High pressure transducers.
V1 to V13 and V16: 2-way valves.
NV1, NV2 and NV3: Needle valves.
3V14, 3V15: 3-way valves.
R1, R2 and R3: Reservoir 1, 2 & 3.

Figure 4.1 Flow diagram of the stirred cell apparatus

The experiments for CO_2 were performed in the (0 to 10) bar range and temperatures in the range of (293.15-323.15) K. To validate the experimental protocol, the equilibrium loading of CO_2 in 14.7 wt% MEA solution at different partial pressures were measured. The results were compared with literature data [30]. The results are shown in Fig. 4.2. These results indicate the suitability of the experimental apparatus developed in this work to measure solubility for CO_2.

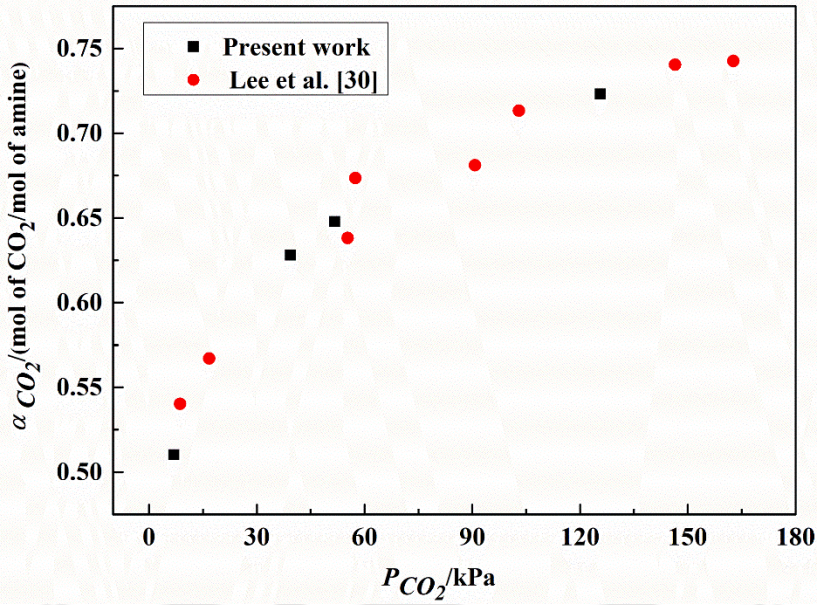

Figure 4.2 Solubility of CO_2 in 14.7 wt% aqueous MEA solution at 313.15 K and compared with the literature data

4.2.2.2 Standard uncertainty in the solubility measurement

The standard uncertainty related to the calculation of equilibrium CO_2 loading data can be ascertained by the theory of error propagation [31]. This theory states that the standard uncertainty u(y), which corresponds to the output variable measured, can be expressed as a summation of all the uncertainties with respective input variables u (x_i). The functional relation in mathematical form is given below:

$$u^2(y) = \sum_{i=1}^{n} \left(\frac{\partial f}{\partial x_i} u(x_i) \right)^2 \tag{4.1}$$

Variables like temperature, pressure, composition, and reactor volume of the inlet solution together describe the standard uncertainty in the measurement of CO_2 loading. The maximum standard uncertainty associated with measured loading data (αCO_2) in the present system is estimated in the vicinity of $\pm 5\%$.

4.3 Modeling of CO_2 solubility

The equilibrium CO_2 solubility data in aqueous (TAEA + MDEA + H_2O) and (TAEA + AMP + H_2O) has been modeled using modified Kent-Eisenberg model [22] and artificial neural network (ANN) model [27].

4.3.1 Modified Kent-Eisenberg model

Phase and chemical equilibrium processes are both presents during the absorption of CO_2 in aqueous (TAEA+MDEA+H_2O) and (TAEA+AMP+H_2O) solutions. Henry's law constant represents the physical solubility of CO_2, whereas reaction equilibrium constants represent the chemical equilibrium considering reversible reactions in the liquid phase. The steric hindrance effect accounts for the low stability of the intermediate, AMP-carbamate, which then undergoes hydrolysis forming a free amine molecule along with bicarbonate species. The liquid phase reaction consisted of protonation of both the amines, carbamate formation by TAEA, and other reactions. The equilibrium reactions for (TAEA+MDEA+H_2O) and (TAEA+AMP+H_2O) can be expressed using reactions R 4.1 to R 4.8:

Physical Solubility

$$CO_2(g) \xleftarrow{H_{CO2}} CO_2(aq) \qquad \text{(R4.1)}$$

Dissociation of bicarbonate ion

$$HCO_3^-(g) \xleftarrow{K_1} CO_3^{2-} + H^+ \qquad \text{(R4.2)}$$

Formation of bicarbonate ion

$$CO_2 + H_2O \xleftarrow{K_2} HCO_3^- + H^+ \qquad \text{(R4.3)}$$

Dissociation of water

$$H_2O \xleftrightarrow{K_3} OH^- + H^+ \quad \text{(R4.4)}$$

Deprotonation of TAEA

$$TAEAH^+ \xleftrightarrow{K_4} TAEA + H^+ \quad \text{(R4.5)}$$

Carbamate hydrolysis of TAEA

$$TAEACOO^- + H_2O \xleftrightarrow{K_5} TAEA + HCO_3^- \quad \text{(R4.6)}$$

Deprotonation of MDEA

$$MDEAH^+ \xleftrightarrow{K_6} MDEA + H^+ \quad \text{(R4.7)}$$

Deprotonation of AMP

$$AMPH^+ \xleftrightarrow{K_7} AMP + H^+ \quad \text{(R4.8)}$$

In the modified Kent-Eisenberg model, the activity coefficients of the species in the liquid phase are assumed to be unity. The concentration-based apparent equilibrium constants of reactions R 4.2- R 4.8 are expressed as:

$$K_1 = \frac{\left[CO_3^{2-}\right]\left[H^+\right]}{\left[HCO_3^-\right]} \quad (4.2)$$

$$K_2 = \frac{\left[HCO^{3-}\right]\left[H^+\right]}{\left[CO_2\right]} \quad (4.3)$$

$$K_3 = \left[H^+\right]\left[OH^-\right] \quad (4.4)$$

$$K_4 = \frac{\left[TAEA\right]\left[H^+\right]}{\left[TAEAH^+\right]} \quad (4.5)$$

$$K_5 = \frac{[TAEA]\left[HCO_3^-\right]}{\left[TAEACOO^-\right]} \tag{4.6}$$

$$K_6 = \frac{[MDEA]\left[H^+\right]}{\left[MDEAH^+\right]} \tag{4.7}$$

$$K_7 = \frac{[AMP]\left[H^+\right]}{\left[AMPH^+\right]} \tag{4.8}$$

Where, (K_1-K_7) are the equilibrium constants corresponding to the reaction R (4.2) – R (4.8). The CO_2 partial pressure, P_{CO_2}, at equilibrium, is related to the physically dissolved CO_2 concentration, $[CO_2]$, in the solvent phase by Henry's law expression. Vapour phase equilibrium can be expressed as:

$$P_{CO_2} = H_{CO_2}\lfloor CO_2 \rfloor \tag{4.9}$$

The overall mass balance and charge balance of various molecular and ionic species present in the liquid phase can be described as:

TAEA balance:

$$[TAEA]_t = m_1 = [TAEA]\left[TAEAH^+\right]\left[TAEACOO^-\right] \tag{4.10}$$

MDEA balance:

$$[MDEA]_t = m_2 = [MDEA]\left[MDEAH^+\right] \tag{4.11}$$

AMP balance:

$$[AMP]_t = m_2 = [AMP]\left[AMPH^+\right] \tag{4.12}$$

CO_2 balance:

$$\alpha_{CO_2} \times (m_1 + m_2) = [CO_2] + [HCO_3^-] + [CO_3^{2-}] + [TAEACOO^-] \quad (4.13)$$

Where, α_{CO2} is the CO_2 loading and m_1, as well as m_2, represents initial TAEA and MDEA or AMP molar concentration, respectively.

Electroneutrality balance for aqueous (TAEA + MDEA):

$$[H^+] + [TAEAH^+] + [MDEAH^+] - [HCO_3^-] + 2[CO_3^{2-}] + [OH^-] + [TAEA(COO^-)] = 0 \quad (4.14)$$

Electroneutrality balance for aqueous (TAEA + AMP):

$$[H^+] + [TAEAH^+] + [AMPH^+] - [HCO_3^-] + 2[CO_3^{2-}] + [OH^-] + [TAEA(COO^-)] = 0 \quad (4.15)$$

Where the terms in the third bracket relate to the concentration of ionic species in the reaction medium, the system of equations (4.2) - (4.12) and either of (4.14) and (4.15) can be used to derive a polynomial equation which is expressed in terms of $[H^+]$. The linear polynomial equation accompanied with the coefficients can be described as follows:

$$A[H^+]^6 + B[H^+]^5 + C[H^+]^4 + D[H^+]^3 + E[H^+]^2 + F[H^+] + G = 0 \quad (4.16)$$

Where,

$$A = K_5$$
$$B = K_5.\left(K_6 + K_4 + m_1 + m_2\right)$$
$$C = K_6.K_5.\left(m_1 + K_4\right) + K_2.\left[CO_2\right]\left(K_4 - K_5\right) + K_5.\left(m_2.K_4 - K_3\right)$$
$$D = K_2.K_4.\left(K_6.\left[CO_2\right] + m_2 - K_5.\left[CO_2\right] - m_1.\left[CO_2\right]\right) - K_5.\left(K_2.K_6.\left[CO_2\right] - K_2.K_4.\left[CO_2\right]\right) - K_3.K_5.\left(K_6 + K_4\right)$$
$$E = K_2.\left[CO_2\right]\left(-K_4.K_5.K_6 - K_2.K_4.\left[CO_2\right] - 2.K_1.K_5.K_6 - 2.K_1.K_4.K_5 - K_3.K_4 - m_1.K_4.K_6\right) - K_3.K_4.K_5.K_6$$
$$F = K_2.K_4.\left[CO_2\right]\left(-2.K_1.K_5.K_6 - 2.K_1.K_2.\left[CO_2\right] - K_3.K_6 - K_2.K_6.\left[CO_2\right]\right)$$
$$G = -2.K_1.K_2{}^2.K_4.K_6.\left[CO_2\right]^2$$

Furthermore, equations (4.2) – (4.16) can be used to get the modified form of loading equation as given below,

$$\alpha_{CO_2} = \frac{P_{CO_2}}{H_{CO_2}.\left(m_1 + m_2\right)}\left[1 + \frac{K_2}{\left[H^+\right]} + \frac{K_1.K_2}{\left[H^+\right]^2} + \frac{m_1.K_2.K_4}{K4.K5.\left[H^+\right] + K_5.\left[H^+\right]^2 + K_2.K_4.\left[\frac{P_{CO_2}}{H_{CO_2}}\right]}\right] \quad (4.17)$$

Where α_{CO2} is the estimated CO_2 loading in the aqueous amine solution and m_1, m_2 represents the concentration of TAEA and MDEA in molarity scale, respectively. The real root of the equation (4.16) is used to calculate the estimated CO_2 loading value from equation (4.17). In the above model, the equilibrium constants (K_1-K_3), K_6, and K_7 can be considered as a function of temperature and expressed as follows:

$$\ln K = a_i + b_i / T + C_i \ln T \quad (4.18)$$

Where a_i, b_i, and c_i are the coefficients of the above expression and are reported in Table 4.2.

Table 4.2 Coefficients of the equilibrium constants used in the present work.

K_i / kmol.m^{-3}	a_i	b_i	c_i	T / K	Ref.
K_1	220.067	-12431.7	-35.4819	273-498	[22]
K_2	235.485	-12092.1	-36.7816	273-498	[22]
K_3	140.932	-13445.9	-22.4773	273-498	[22]
K_6	87.3972	-8483.95	-13.8328	298-333	[23]
K_7	-3.68672	-6754.686	0	273-328	[32]

Henry's constant for physical solubility, H_{CO2}, has been taken from the work of Hsu et al. [34] as given below.

$$\ln H_{CO_2} / \frac{kPa\,.m^3}{kmol} = 20.2669 - \frac{1.38306\times10^4}{T} + \frac{0.06913\times10^8}{T^2} - \frac{0.015589\times10^{11}}{T^3} + \frac{0.012\times10^{13}}{T^4} \quad (4.19)$$

The equilibrium constants K_4 and K_5 are regressed using the least square fitting in the MATLAB® platform. These constants refer to the deprotonation and carbamate hydrolysis reaction of TAEA, respectively. The algorithm for the data regression system is shown in Fig. 4.3. The equilibrium constants estimated by the Kent-Eisenberg model in their work [33] were correlated in terms of temperature only. There are various modifications proposed so far by different researchers [22,27,28] in the estimation of equilibrium constants. In some modified versions, equilibrium constants are considered a function of CO_2 loading, amine concentration, and temperature [27]. In the present work, K_4 and K_5 are expressed in terms of temperature, CO_2 partial pressure, and amine concentration [28].

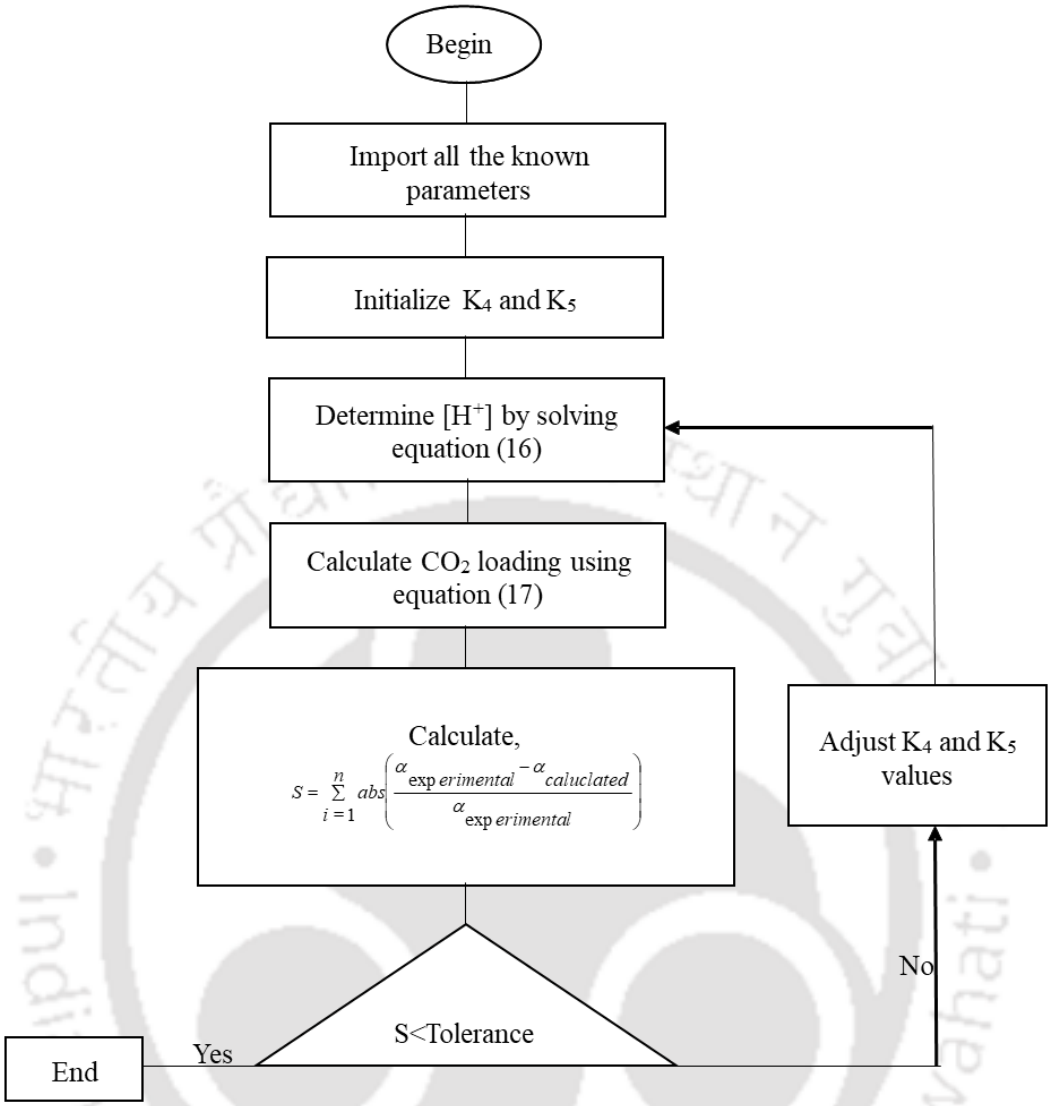

Figure 4.3 Algorithm for regression of equilibrium constants from experimental data

4.3.2 Artificial neural network

Owing to the adaptability of implementation and advantages over other simple models, ANN models are well known in the application to correlating the solubility of CO_2 in a variety of solvents [34,35]. Here, the applicability of the artificial neural network (ANN) model has also been investigated in the present work to correlate the equilibrium CO_2 solubility in (TAEA+MDEA+H_2O) and in (TAEA+MDEA+H_2O) systems.

In this work, we consider a multilayer feedforward neural network to correlate the available solubility data. The ANN network comprises various layers like input layers, one or more

hidden layers with functions, and ultimately an output layer. Processing units known as neurons are bound by a set of processing units. The neurons in the hidden layer and output layer must be trained to determine the output of the network. Information at the input layer is processed at each neuron in the hidden layer using a transfer function and then transferred to the output layer as given by Eq. (4.20)

$$Y_i = f\left(\sum_{i=1}^{n}\left(W_i X_i + b_i\right)\right) \tag{4.20}$$

Where x_i and y_i represent the input and output of the i^{th} neuron, respectively, f is the transfer function, w_i is the weight coefficient, and b_i is the bias associated with each weight coefficient. For a network to simulate a specific task, weights and biases are adjusted automatically. This process is called training, in which a suitable training algorithm is used to process the weights and biases of the network. The objective of the training is to minimize the error between the modeled output and the actual or experimental value. The ANN architecture used in this work consists of the Levenberg-Marquardt backpropagation algorithm as a training function [36]. The transfer function implemented for hidden and output layers is hyperbolic tangent sigmoid functions and linear functions, respectively. The performance of the above developed neural network model is tested based on the following parameter as mentioned below:

$$Mean\ square\ error\ (MSE) = \frac{1}{N}\sum_{i=1}^{n}\left(Y_i^{\exp} - Y_i^{\mathrm{mod}}\right)^2 \tag{4.21}$$

$$Average\ absolute\ deviation\ (\%AAD) = \frac{1}{N}\sum_{i=1}^{n}\frac{\left|Y_i^{\exp} - Y_i^{\mathrm{mod}}\right|}{Y_i^{\exp}} \times 100 \tag{4.22}$$

$$Correlation\ coefficient\ (R^2) = \frac{\sum_{i=1}^{n}\left(Y_i^{\exp} - Y_{avg}\right)^2 - \sum_{i=1}^{n}\left(Y_i^{\exp} - Y_i^{\mathrm{mod}}\right)^2}{\sum_{i=1}^{n}\left(Y_i^{\exp} - Y_{avg}\right)^2} \tag{4.23}$$

Where '*N*' represents the number of data points Y_i^{exp} and Y_i^{mod} stands for experimental and network predicted value of output variable, respectively, and Y_{avg} denotes the average value of the experimental output. The input parameters used in the network are temperature (*T*/K), equilibrium CO_2 partial pressure (P_{CO_2} / kPa), and concentration of TAEA (m_1/kmol.m^{-3}) and MDEA or AMP (m_2/kmol.m^{-3}), respectively. The CO_2 loading (α_{CO2}) has been chosen as the output variable.

4.4 Results and discussion

4.4.1 CO_2 Solubility measurement

From the sections above, it can be understood that the validation of the experimental set-up and the steps for measuring solubility have been performed. The measured data is in good agreement with that from previous studies on the equilibrium solubility of CO_2 in an aqueous 14.7% mass percentage of MEA at 313.15 K [30]. The comparison of data is represented in Fig. 4.2. From the figure, it could be inferred that the current work is in line with the solubility data available from literature for experiments with MEA at similar conditions.

We then measured the solubility of CO_2 in (TAEA + MDEA + H_2O) and (TAEA + AMP + H_2O) at temperatures 293.15, 303.15, 313.15, and 323.15 K and in the CO_2 partial pressure range of 2-500 kPa. The amine solution compositions experimented with are TAEA: MDEA or AMP = 0.1:2.9; 0.3:2.7; 0.5:2.5; and 0.7:2.3, respectively. Tables 4.3 and 4.4 contain the solubility data of experiments conducted concerning each loading.

Figs. 4.4 and 4.5 explain the CO_2 loading vs. the partial pressure of the CO_2 for blended systems (TAEA + MDEA + H_2O) and (TAEA + AMP + H_2O). As shown in Fig. 4.4, the CO_2 loading increases with an increase in P_{CO2} at any experimental temperature and the amine concentration. This can be attributed to the rise in the partial pressure of the CO_2 causes the

increase in the collisions between the gas molecules and liquid surface. Hence, more gas molecules absorbed on the amine surface lead to higher CO_2 loading [37]. Furthermore, Fig. 4.4 explains the decrease in CO_2 loading with an increase in the temperature at constant pressure due to the exothermic nature of the process [27]

Table 4.3 CO_2 solubility data in aqueous solutions of (TAEA + MDEA + H_2O) solutions at different temperatures and partial pressures

Concentration / mol/l	*T*/ 293.15 K		*T*/ 303.15 K		*T*/ 313.15 K		*T*/ 323.15 K	
	P/ kPa	α_{CO2}	*P*/ kPa	α_{CO2}	P/ kPa	*P*/ kPa	α_{CO2}	*P*/ kPa
MDEA(2.9)+TAEA (0.1)+H_2O	4.3	0.34	9	0.44	29	0.54	37	0.46
	12	0.59	46	0.71	97	0.77	96	0.65
	113	0.94	142	0.90	240	0.88	196	0.77
	240	0.99	324	0.97	427	0.94	310	0.84
	372	1.02	485	1.00	561	0.96	434	0.89
	589	1.04	587	1.01	647	0.97	557	0.91
MDEA(2.7)+TAEA (0.3)+H_2O	6	0.59	10	0.58	20	0.57	29	0.50
	40	0.86	74	0.87	87	0.80	87	0.70
	164	1.00	191	0.98	196	0.91	191	0.82
	284	1.04	345	1.03	333	0.97	319	0.89
	437	1.07	466	1.05	445	0.99	443	0.93
	570	1.09	564	1.07	568	1.02	551	0.95
MDEA(2.5)+TAEA (0.5)+H_2O	3	0.61	7	0.60	14	0.58	21	0.54
	36	0.92	50	0.88	60	0.81	84	0.76
	116	1.05	162	1.01	147	0.93	190	0.88
	245	1.12	302	1.08	262	1.00	328	0.95
	356	1.15	404	1.10	375	1.03	444	0.99
	468	1.18	537	1.13	510	1.07	554	1.01
MDEA(2.3)+TAEA (0.7)+H_2O	2	0.65	4	0.63	7	0.60	10	0.54
	27	0.95	46	0.93	42	0.83	56	0.77
	105	1.10	144	1.07	121	0.97	145	0.90
	216	1.17	257	1.13	233	1.05	266	0.98
	329	1.22	393	1.17	349	1.10	381	1.03
	454	1.25	512	1.20	486	1.13	498	1.06

Table 4.4 Equilibrium loading of CO_2 in aqueous solutions of (TAEA + AMP + H_2O) at temperatures T from (293.15- 323.15) K at different partial pressures

Concentration / mol/l	*T*/ 293.15 K		*T*/ 303.15 K		*T*/ 313.15 K		*T*/ 323.15 K	
	P/ kPa	α_{CO2}	*P*/ kPa	α_{CO2}	P/ kPa	*P*/ kPa	α_{CO2}	*P*/ kPa
AMP(2.9)+TAEA (0.1)+H_2O	4	0.34	16	0.47	29	0.54	39	0.48
	12	0.59	58	0.75	98	0.76	93	0.69
	111	0.93	177	0.95	240	0.88	198	0.81
	238	0.99	360	0.98	428	0.93	318	0.88
	371	1.02	509	1.01	564	0.96	448	0.91
	583	1.05	618	1.02	648	0.97	577	0.93
AMP(2.7)+TAEA (0.3)+H_2O	7.8	0.62	8	0.60	18	0.56	26	0.50
	38	0.87	79	0.90	84	0.79	83	0.69
	162	1.01	203	1.00	193	0.91	186	0.83
	279	1.06	379	1.04	329	0.96	312	0.91
	434	1.09	506	1.06	441	0.99	439	0.94
	568	1.11	617	1.07	562	1.01	545	0.97
AMP(2.5)+TAEA (0.5)+H_2O	5	0.66	5	0.59	12	0.59	20	0.56
	35	1.00	46	0.87	56	0.81	79	0.77
	137	1.10	133	1.03	136	0.95	186	0.90
	278	1.16	270	1.09	257	1.01	322	0.97
	393	1.18	380	1.11	371	1.06	440	1.01
	508	1.19	512	1.14	507	1.10	546	1.04
AMP(2.3)+TAEA (0.7)+H_2O	3	0.66	2	0.60	11	0.59	14	0.55
	26	0.98	43	0.88	42	0.83	53	0.79
	103	1.12	118	1.04	115	0.97	139	0.94
	214	1.18	219	1.12	228	1.06	259	1.03
	325	1.23	366	1.15	342	1.11	375	1.08
	448	1.26	486	1.17	497	1.14	492	1.10

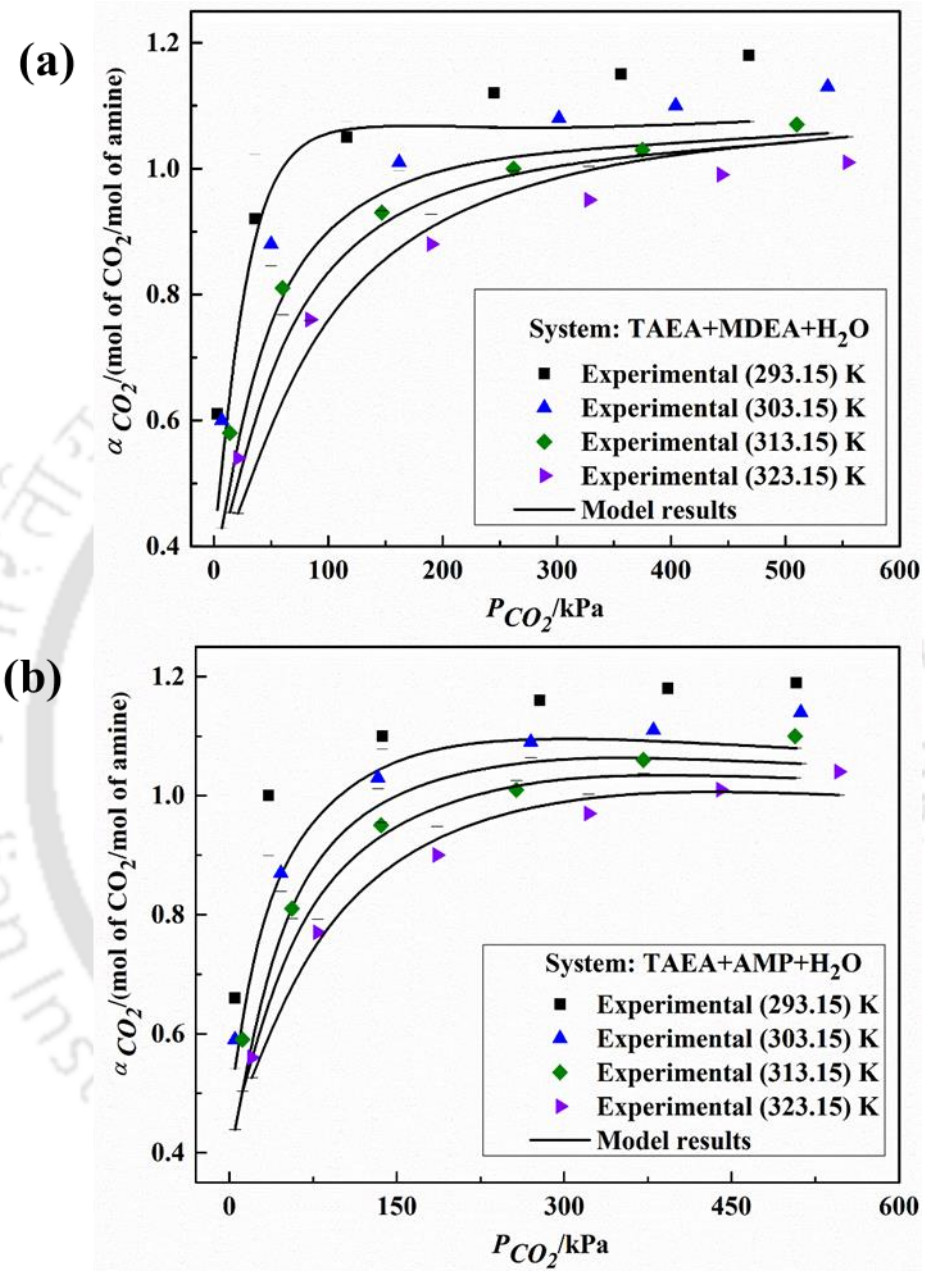

Figure 4.4 Effect of temperature on the CO_2 solubility in aqueous solutions of (a) (0.5 M TAEA + 2.5 M MDEA + H_2O) and (b) (0.5 M TAEA + 2.5 M AMP + H_2O)

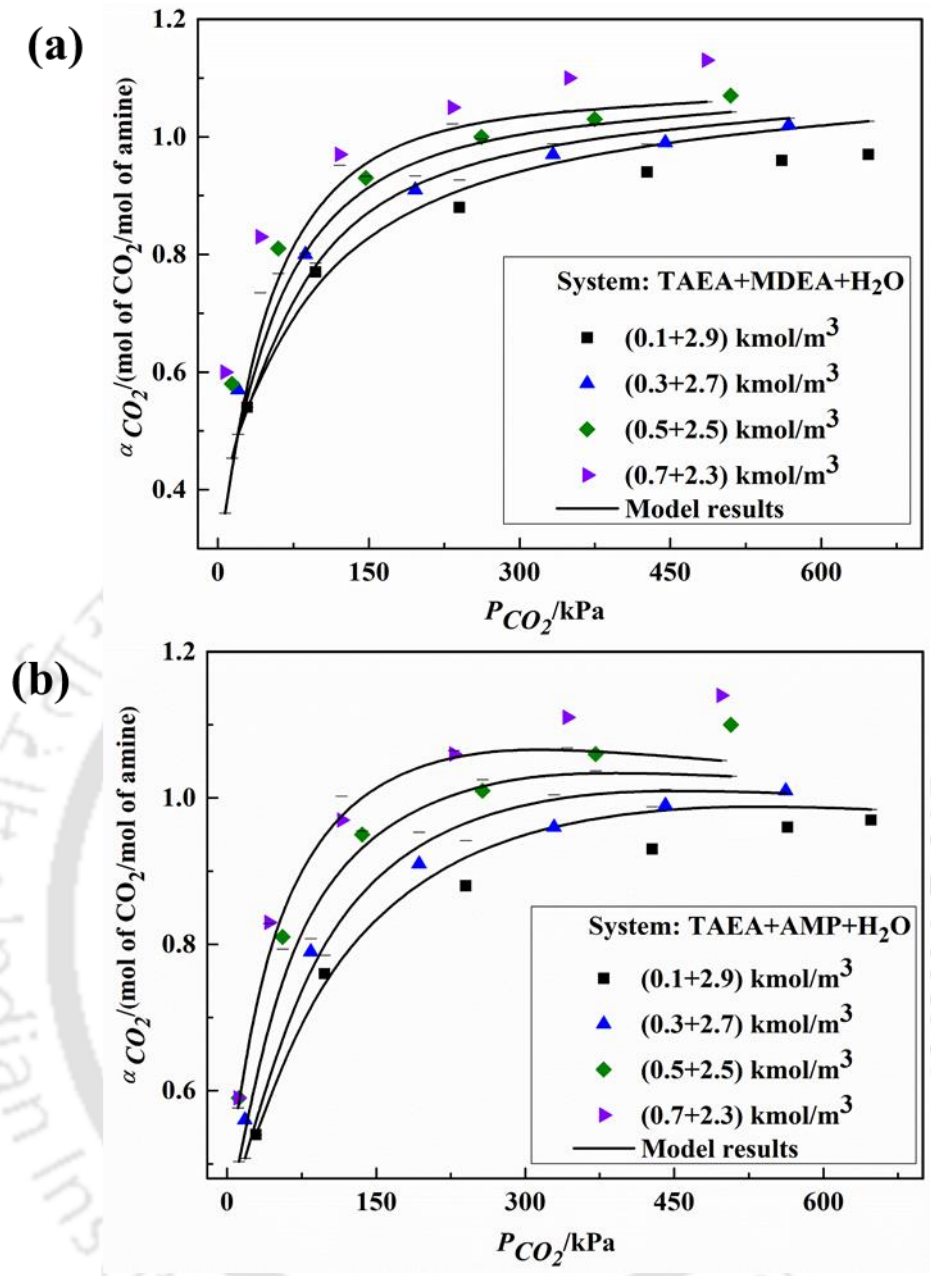

Figure 4.5 Effect of solvent concentration on the CO_2 solubility in aqueous solutions of (a) (TAEA + MDEA + H_2O) and (b) (TAEA + AMP + H_2O) at 313.15 K

Fig. 4.5 represents the effect of TAEA concentration on CO_2 loading for blended systems (TAEA + MDEA + H_2O) and (TAEA + AMP + H_2O). As shown in Fig.4.5, the CO_2 loading increases with an increase in the TAEA concentration in the solution while keeping the constant amine concentration. Ramazani et al. [38] were also observed similar results for the system of aqueous (AEP + MEA).

In this work, solubility data has been modeled using different approaches described in the previous sections. In the modified KE approach, the coefficients of the equilibrium constants (K_4 and K_5) for the ternary system (TAEA + MDEA + H_2O) and the (TAEA + AMP + H_2O) is represented as (K'_4 and K'_5) have been regressed to fit the experimental CO_2 loading data to obtain the estimated data. A non-linear optimization technique is used to reduce the error gap between the experimental and estimated data. The corresponding objective function which is used for optimization in the present work can be defined as:

$$S = \frac{1}{N}\sum_{i=1}^{N}\left|\frac{\alpha_i^{\exp} - \alpha_i^{\mathrm{mod}}}{\alpha_i^{\exp}}\right| \tag{4.24}$$

The above equation $\alpha_i^{\exp}$ α_i^{mod} stands for experimental and estimated α_{CO2}, respectively, and N represents the total number of data sets used in the developed model. The reaction equilibrium constants (K_4 and K_5) and (K'_4 and K'_5) can be estimated as:

$$K_4 = -2.63\times10^{-8} + 2.75\times10^{-9}(m1\times m2) + 8.1\times10^{-11}(T) - 3.8\times10^{-12}(m1\times m2\times T) - 1.27\times10^{-14}(T^2) + 4.88\times10^{-13}(P_{CO_2}) - 6.8\times10^{-16}(P_{CO_2}^2) \tag{4.25}$$

$$K_5 = 7.25\times10^{4} - 9.34\times10^{1}(m1\times m2) + 1.84\times10^{2}(T) - 2.37\times10^{-12}(m1^2\times m2^2) - 2.77\times10^{1}(m1\times m2\times T) + 2.88\times10^{-1}(T^2) + 1.28\times10^{1}(P_{CO_2}) + 2.47\times10^{-4}(P_{CO_2}^2) \tag{4.26}$$

$$K'_4 = 2.24\times10^{-10} - 1.68\times10^{-9}(m1\times m2) - 1.12\times10^{-11}(T) + 8.85\times10^{-12}(m1\times m2\times T) + 1.17\times10^{-14}(T^2) - 4.1\times10^{-12}(P_{CO_2}) + 6.02\times10^{-15}(P_{CO_2}^2) \tag{4.27}$$

$$K'_5 = 1.42\times10^{4} - 1.96\times10^{2}(m1\times m2) + 2.46\times10^{1}(T) + 8.7\times10^{-1}(m1^2\times m2^2) + 3.02(m1\times m2\times T) + 2.26\times10^{-2}(T^2) + 3.81\times10^{-2}(P_{CO_2}) - 1.61\times10^{-4}(P_{CO_2}^2) \tag{4.28}$$

The CO_2 loading values were estimated using the above equilibrium constants and compared with the experimental data. The comparison between the calculated and the experimental data is presented in Fig.4.6. Fig 4.6(a) represents the (TAEA+MDEA+H_2O) system, and Fig.4.6(b) depicts the (TAEA+AMP+H_2O) system. Fig.4.6 indicates that the experimental and predicted values agreeing under the examined range of temperature and composition. The average absolute deviation (in%) between the model and experimental results for (TAEA+MDEA+H_2O) and (TAEA+AMP+H_2O) is 7.49 and 5.12, respectively. The equilibrium concentrations of various species present in the liquid phase as a function of the CO_2 loading were estimated using the proposed modified KE model and concentration profiles presented in Fig.4.7. The equilibrium concentrations of different constituent species available in the liquid phase are further predicted functional to CO_2 loading using a modified KE model applied to all the systems. The concentration profile of diverse species for CO_2 loaded aqueous (TAEA (0.5) +MDEA (2.5)) M at 303.15 K presented in Fig. 4.7(a) and for CO_2 loaded (TAEA (0.5) +AMP (2.5)) M at 323.15 K presented in Fig. 4.7(b) respectively. It is evident from the speciation plot obtained from the equations (R 4.3, R 4.5, R 4.7, R 4.8) that both TAEA and MDEA or AMP disappear gradually with CO_2 loading, and the main reaction products are protonated TAEA, protonated MDEA, or AMP, and bicarbonate ion. The presence of [TAEACOO−] shown in eq. R 4.6 also shows a decreasing trend concerning α_{CO2}, indicating its hydrolysis to form more bicarbonate type species. The general trend of the majority of species concerning the change in α_{CO2} is the same. The only significant difference is the presence of protonated species [MDEAH+] and [AMPH+] at higher loadings. The dissociation and formation of [HCO^-_3] to CO_3^{2-} species (R_2-R_3) leads to an intermediate profile of both the species with a very low concentration as a function of CO_2 loading.

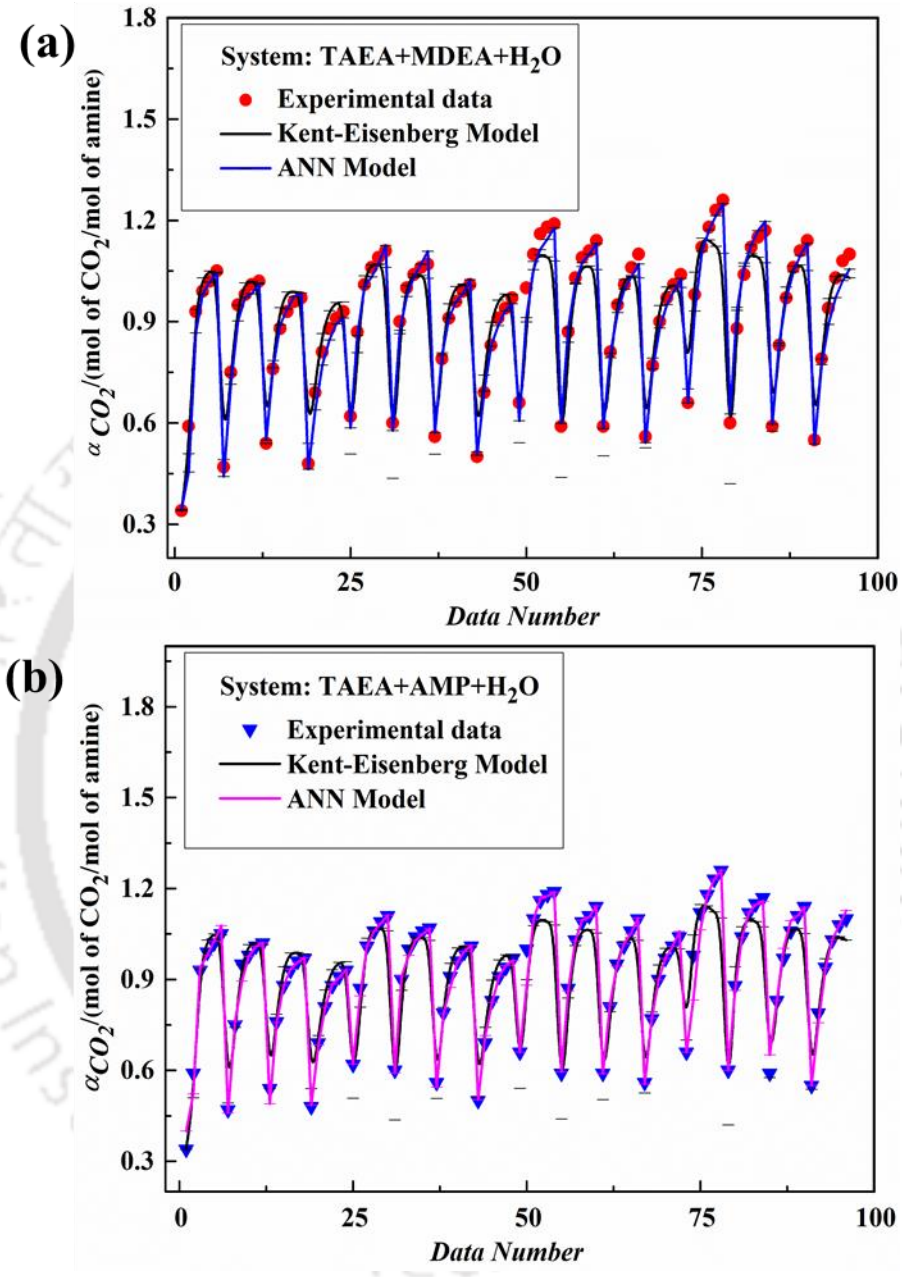

Figure 4.6 Cross plot for the comparison of experimental solubility data with model data (a) (TAEA + MDEA + H_2O) and (b) (TAEA + AMP + H_2O)

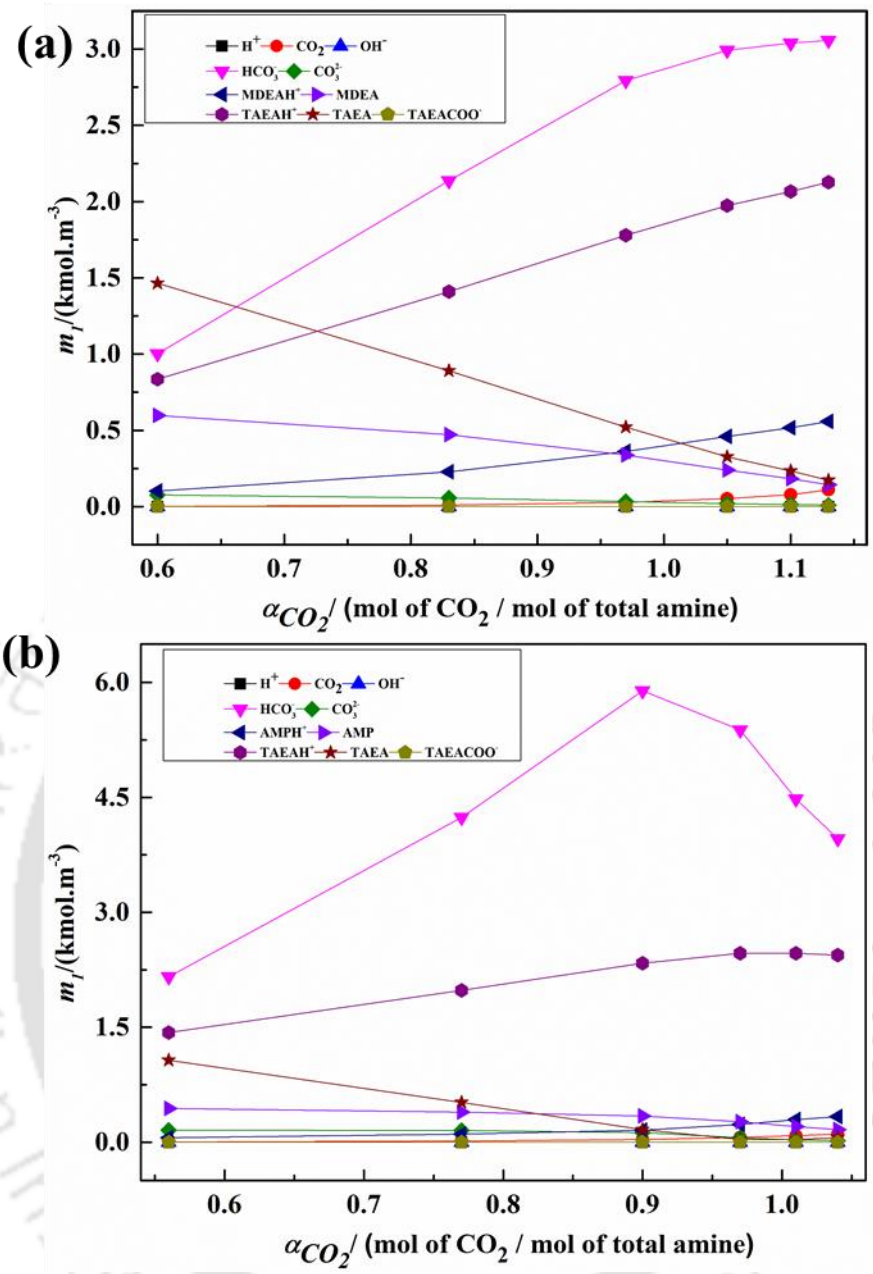

Figure 4.7 Model (modified KE) estimated speciation profile of aqueous solutions (a) (0.5 M TAEA + 2.5 M MDEA + H_2O) at 303.15 K and (b) (0.5 M TAEA + 2.5 M AMP + H_2O) at 323.15 K

The pH of the CO_2-loaded amine solvents can be predicted using the modified KE model. For the design of the CO_2 capture techniques, one should have the proper knowledge about the pH of the solvents. According to the literature reported data for other solvent systems, the pH range with respect to the change in α_{CO2} is within 7–12 [27]. Fig. 4.8 presents the estimated pH of the CO_2-loaded aqueous solution (0.7 M TAEA + 2.3 M MDEA + H_2O) using a modified KE

model at different experimental operating temperatures. An observation found in Fig. 4.8 is that the gradual reduction in the pH value with the increase in the temperature and CO_2 loading for a fixed concentration of amine solvent. This can be attributed to increasing the α_{CO2} leads to an increase in the acidic nature of the solution, then the pH of the solvent system decreases. Furthermore, an increase in temperature causes higher ionization that leads to an increase in H^+ ion concentration [27].

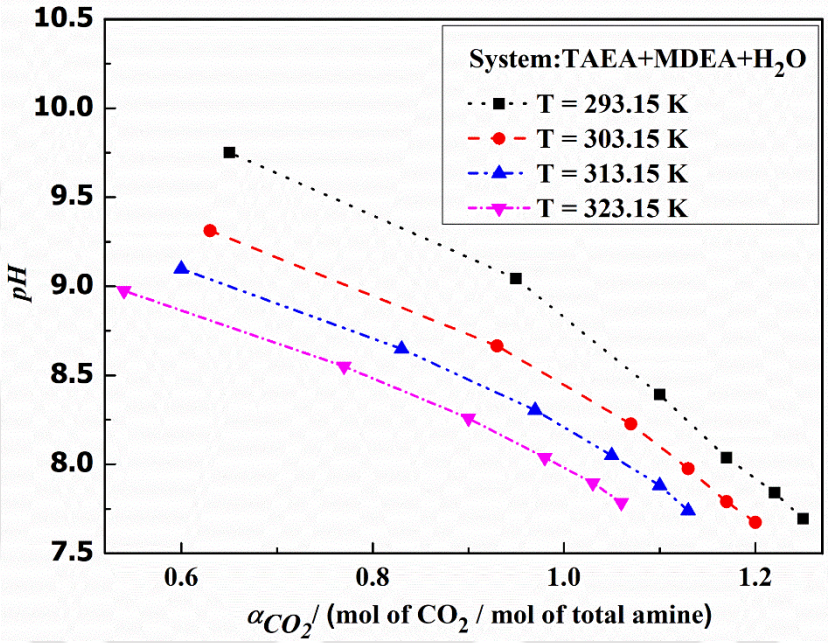

Figure 4.8 Estimation of pH as a function of CO_2 loading in aqueous solution of (0.7 M TAEA + 2.3 M MDEA + H_2O) using modified KE Model

The feed-forward ANN model was also used to model the equilibrium CO_2 loading data for aqueous (TAEA + MDEA +H_2O) and (TAEA + AMP +H_2O) blends. The optimized architecture of the ANN model can be obtained by varying the number of neurons. A low number of neurons may result in a significant error in the network, while a large number may lead to over-fitting [28]. The minimum error criteria (% AAD and MSE) and correlation coefficient (R^2) are the parameters to understand the optimum structure of the network. The variation of MSE of the total data set with the number of neurons presented in Fig. 4.9(a) for

(TAEA + MDEA +H_2O) and 4.9(b) for (TAEA + AMP +H_2O) systems. Similarly, in Fig. 10 it represents the % AAD with no of neurons in the hidden layer for ANN model for (a) (TAEA + MDEA + H_2O) and (b) (TAEA + AMP + H_2O) systems. Based on the error analysis, the optimized neurons have been determined to be 8. The solubility data of systems through the ANN model is presented in Fig. 4.6, and the ANN estimated data is in good agreement with the experimental data. The % AAD and MSE between the experimental and model-predicted loading data are for the (TAEA + MDEA +H_2O) system found to be 1.538, 0.000417. For the system (TAEA + AMP +H_2O), they are 2.696 and 0.00114, respectively, which further confirms the accuracy of the ANN model to predict the CO_2 solubility in aqueous (TAEA + MDEA +H_2O) and (TAEA + AMP +H_2O) systems.

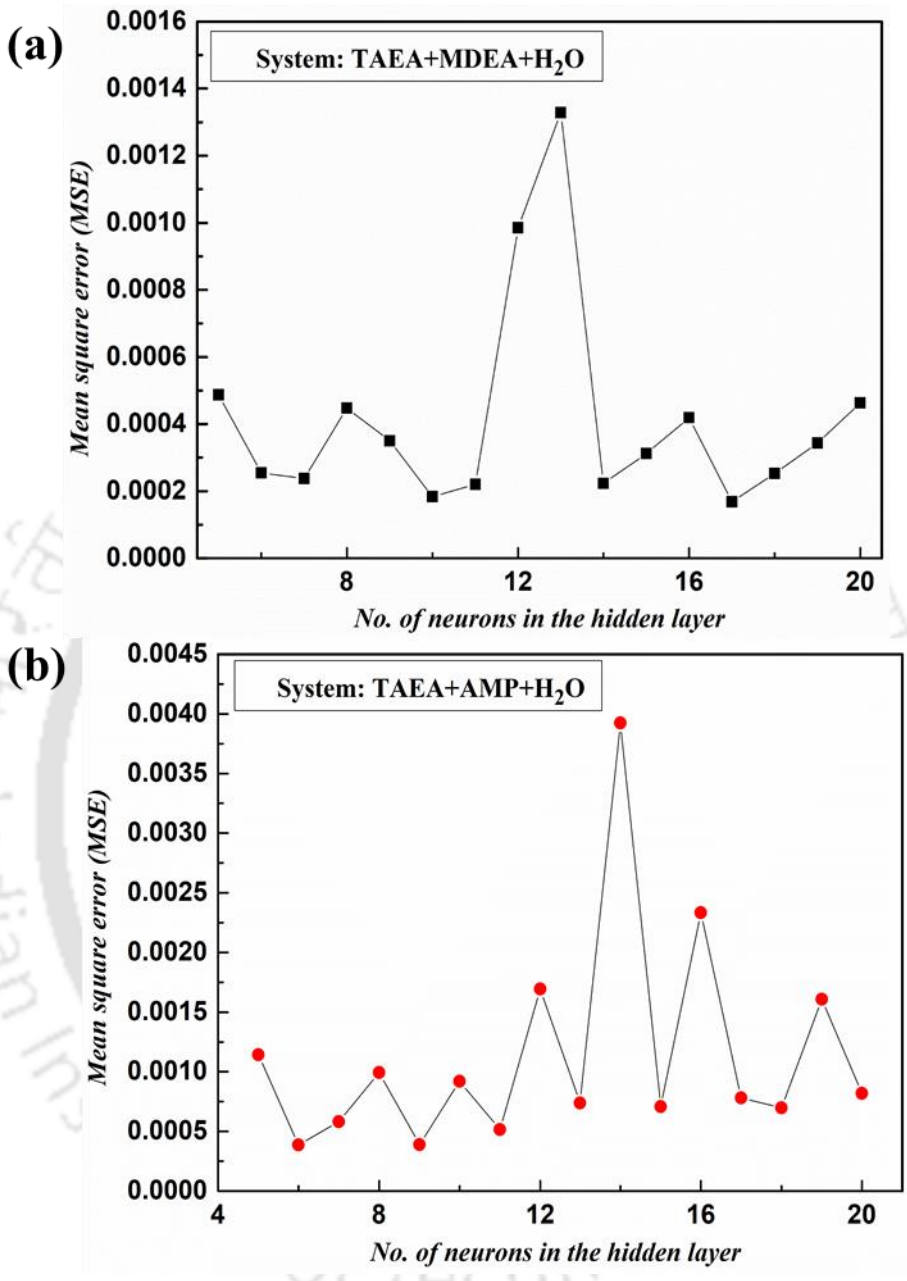

Figure 4.9 Variation of MSE (Mean square error) with number of neurons in the hidden layer for ANN model for (a) (TAEA + MDEA + H_2O) and (b) (TAEA + AMP + H_2O) systems

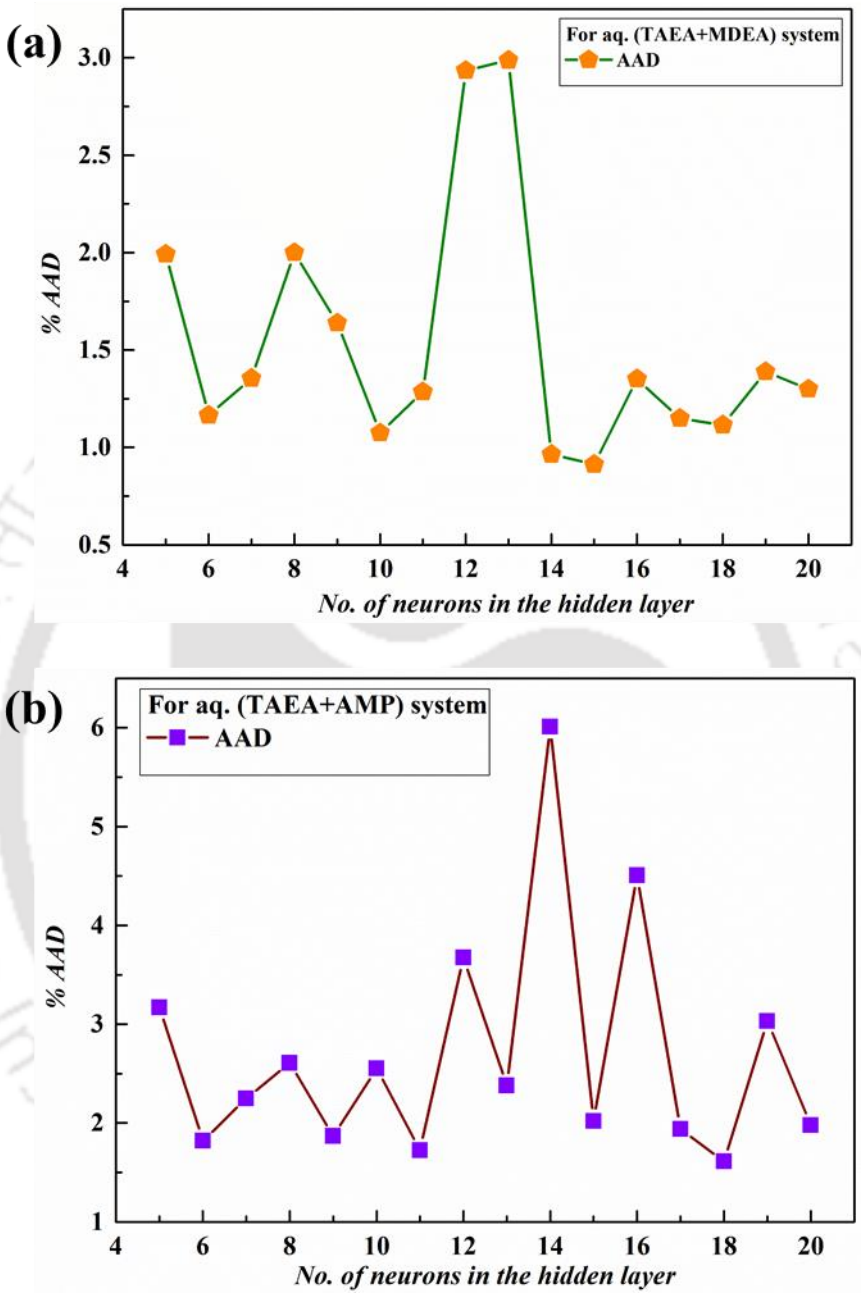

Figure 4.10 Variation of % AAD with number of neurons in the hidden layer for ANN model for (a) (TAEA + MDEA + H_2O) and (b) (TAEA + AMP + H_2O) systems

The generated data corresponding to the present amine systems is also compared with the solubility data of CO_2 in the approximate equimolar concentration of conventional solvents such as aqueous MDEA, AMP, and blended solvents like MDEA-AEP, AMP-PZ, and AMP-AEP solutions available in the literature [8, 20, 32, 39, 40] and represented in Fig. 4.11. At low CO_2 pressure, the CO_2 loading in all these aqueous amines is somewhat comparable with our data. At higher CO_2 partial pressure, the loading values of (0.5 M TAEA + 2.5 M AMP) and (0.5 M TAEA + 2.5 M MDEA) are showing greater absorption capacity compared with the other literature data for single and blended solvents throughout the experimental pressure range. Fig. 4.11 also shows quite higher loadings for the TAEA-AMP blend compared to the TAEA-MDEA because of the higher rate of reaction of AMP towards CO_2.

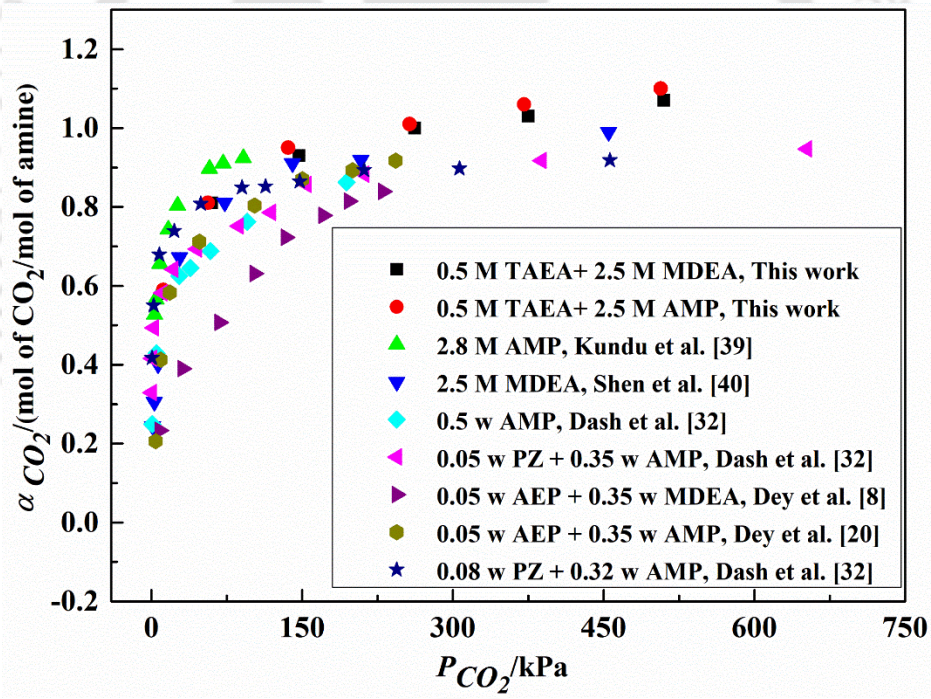

Figure 4.11 Comparison of TAEA based blends with other conventional single and blended solvents at T= 313.15 K and total concentration of 3 M

4.4.2 FTIR-ATR and NMR study

The unloaded and loaded carbonated blended amine systems are further characterized using FTIR- ATR spectroscopy (Model: Perkin Elmer Inc., Germany). The measurements were carried within the wavenumber 2000 to 800 cm^{-1}. The scales of both the unloaded and loaded blended amine systems are shown in Fig. 4.12. The unloaded system shows specific peaks at 1639 cm^{-1} and 1602 cm^{-1} which relates to (N-H) rocking vibration modes [41]. The peaks corresponding to 1330 and 1456 cm^{-1} relates to $–CH_2$ symmetric and asymmetric rocking mode. In addition, the characteristic peaks at 1028 cm^{-1} relates to C-N and C-O stretching vibration modes for blended amine solvent [41]. For the loaded system represented in Fig. 4, .12 new bands are appeared at 1355, 1467, and 1577 cm^{-1} and that will be the sign for the (COO^-) carbamate symmetric and asymmetric stretching [42]. It can be quite seeming from the spectra that there is gradual shift in the peaks corresponding to stretching modes of C-N and C-OH group from 1076 to 1026 cm^{-1} the same can be predicted to be the result of protonation of TAEA species.

In addition to the IR study, qualitative ^{13}C NMR analysis was also conducted to find the current study's proper reaction mechanism. The NMR measurement was carried out for CO_2-loaded and unloaded blended amine solvent in D_2O using a 500 MHz NMR spectrometer (Model: Ascend, Bruker) and shown in Figs. 4.13 and 4.14. The information regarding the detected peaks corresponding to the respective functional groups of the molecules was estimated by different literature sources [43, 44]. The number of peaks in the ^{13}C NMR spectra of TAEA-MDEA-H_2O-CO_2 shown in Fig. 4.14 confirmed the formation of primary and secondary carbamates. The peaks found in the low field region (160–165 ppm) commonly correspond to the peaks of carbonyl carbon of carbamate and HCO^{3-}/CO^{3}_{2-} species. However, the carbons of amine in the high field region (35–60 ppm) are shown in Figs. 4.13 and 4.14 relate to the CH_2 group of various intermediate carbamate species.

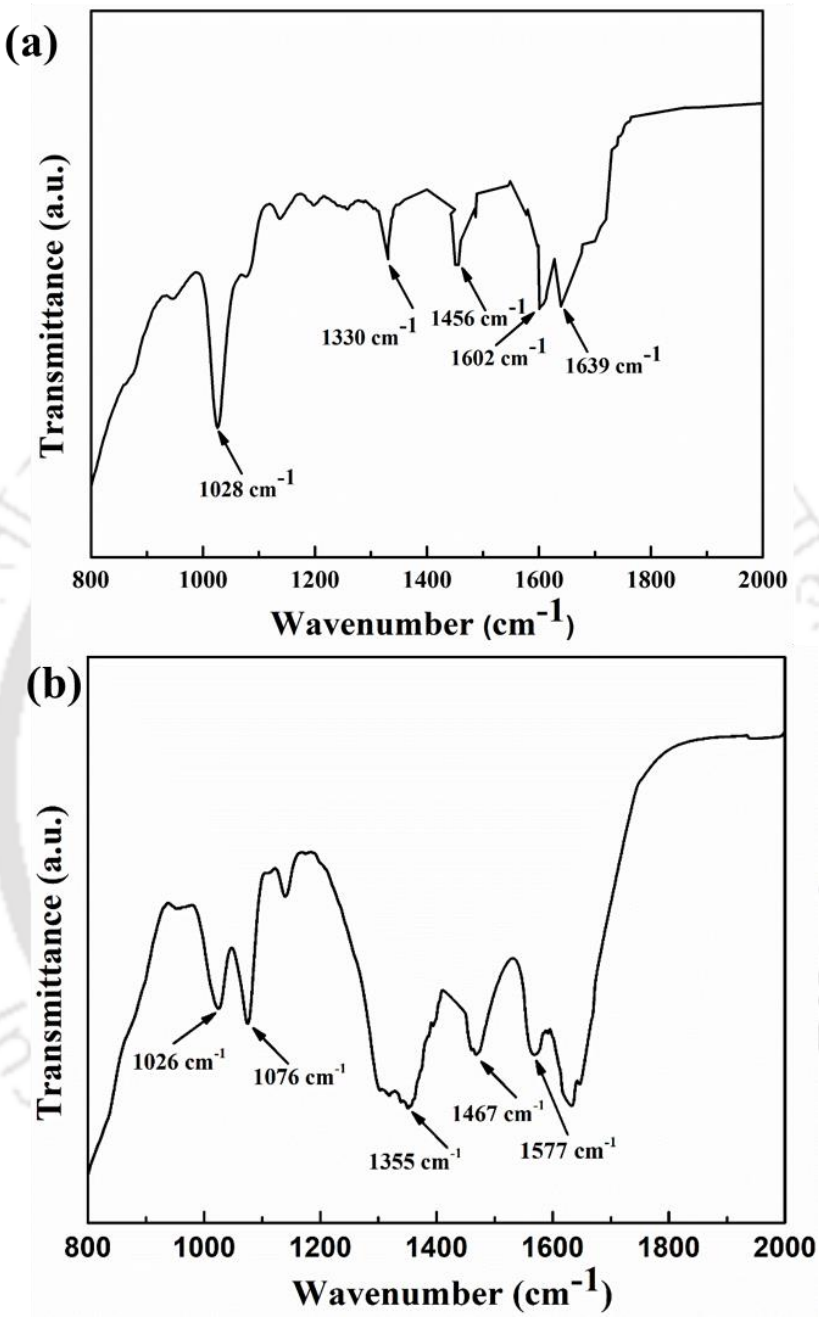

Figure 4.12 FTIR-ATR spectra of (TAEA+MDEA+H_2O) (a) unloaded amine solvent and (b) loaded amine solvent.

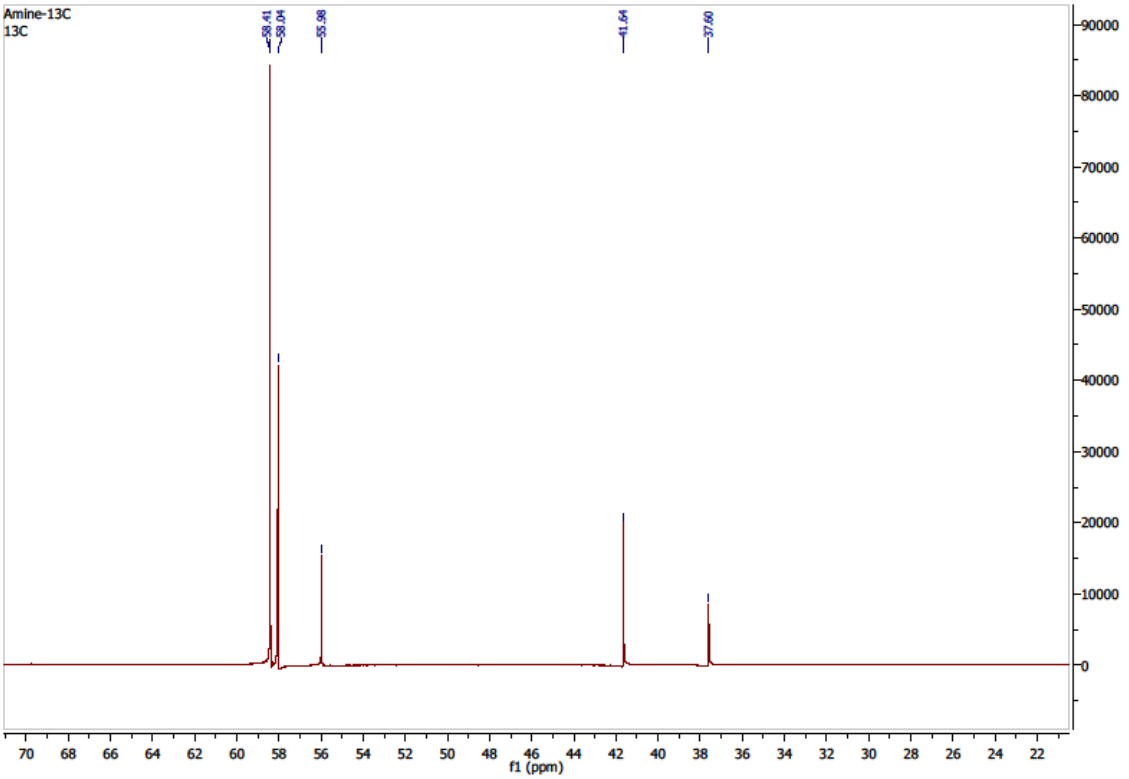

Figure 4.13 ^{13}C NMR spectra of aqueous (TAEA+MDEA+H_2O).

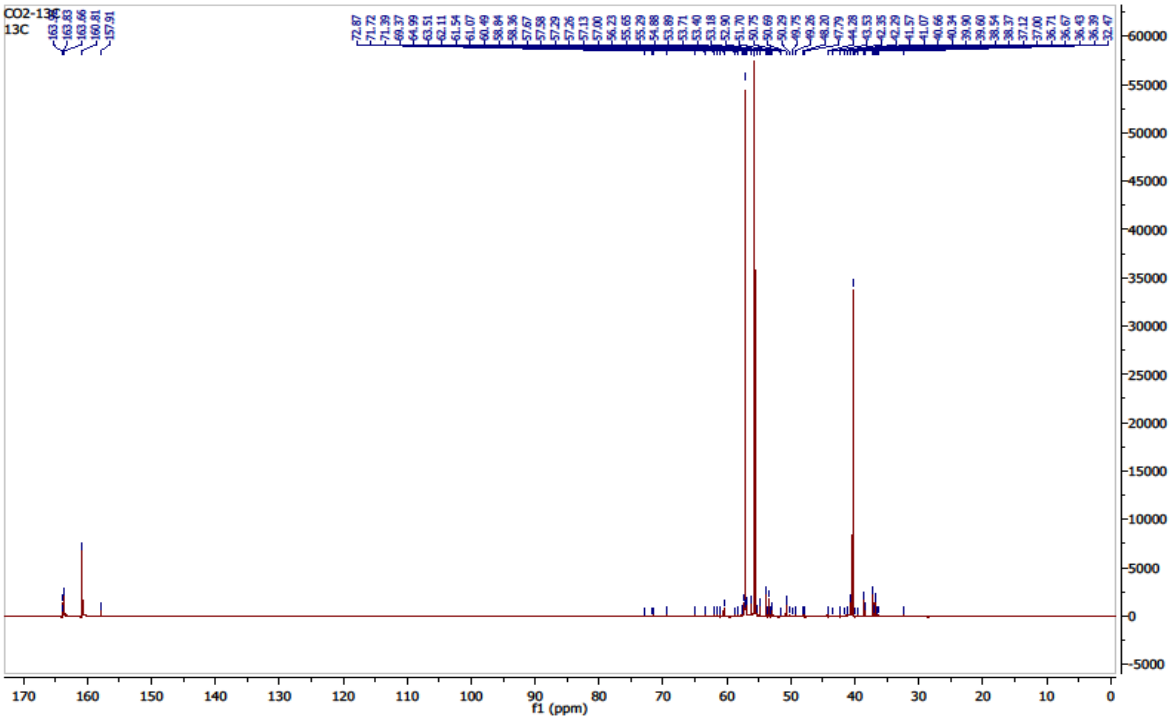

Figure 4.14 ^{13}C NMR spectra of CO_2 loaded (TAEA+MDEA+H_2O) system.

References

[1] G. Sartorl, D.W. Savage, Sterically Hindered Amines for CO_2 Removal from Gases, Ind. Eng. Chem. Fundam. 22 (1983) 239–249.

[2] S. Xu, Y.W. Wang, F.D. Otto, A.E. Mather, Representation of the equilibrium solubility properties of CO_2 with aqueous solutions of 2-amino-2-methyl-1-propanol, Chem. Eng. Process. 31 (1992) 7–12.

[3] R.A. Kerr, Global Warming Is Changing the World, Science. 316 (2007) 188–190.

[4] T. Sema, M. Edali, A. Naami, R. Idem, P. Tontiwachwuthikul, Solubility and diffusivity of N_2O in aqueous 4-(diethylamino)-2-butanol solutions for use in postcombustion CO_2 capture, Ind. Eng. Chem. Res. 51 (2012) 925–930.

[5] Y.N. Helei Liu, Zhiwu Liang, Teerawat Sema, Wichitpan Rongwong, Chen Li, and P.T. Raphael Idem, Kinetics of CO_2 Absorption into a Novel 1-Diethylamino-2-propanol Solvent Using Stopped-Flow Technique, AIChE J. 60 (2014) 3502–3510.

[6] E.S. Rubin, H. Mantripragada, A. Marks, P. Versteeg, J. Kitchin, The outlook for improved carbon capture technology, Prog. Energy Combust. Sci. 38 (2012) 630–671. https://doi.org/10.1016/j.pecs.2012.03.003.

[7] P. Tontiwachwuthikul, R. Idem, D. Gelowitz, Z.H. Liang, T. Supap, C.W. Chan, T. Sanpasertparnich, C. Saiwan, H. Smithson, Recent progress and new development of post-combustion carbon-capture technology using reactive solvents, Carbon Manag. 2 (2011) 261–263.

[8] A. Dey, S.K. Dash, B. Mandal, Equilibrium CO_2 solubility and thermophysical properties of aqueous blends of 1-(2-aminoethyl) piperazine and N-methyldiethanolamine, Fluid Phase Equilib. 463 (2018) 91–105.

[9] M.W. Arshad, P.L. Fosbøl, N. Von Solms, H.F. Svendsen, K. Thomsen, Equilibrium solubility of CO_2 in alkanolamines, Energy Procedia. 51 (2014) 217–223.

[10] N.F.N. Abdul Samat, R.B. Yusoff, M.K. Aroua, A. Ramalingam, M.A. Kassim, Solubility of CO_2 in aqueous 2-amino-1, 3-propanediol (Serinol) at elevated pressures, J. Mol. Liq. 277 (2019) 207–216.

[11] Arthur L Kohl Richard Nielsen, Gas Purification 5th Edition, 5th ed., Gulf Professional Publishing, 1997.

[12] R.H. Chakravarty, T and Phukan, U K and Weilund, Reaction of acid gases with mixtures of amines, Chem. Eng. Prog. 81 (1985) 32–36.

[13] F.L. Dong Fu, Huimin Hao, Experiment and model for the viscosity of carbonated 2-amino-2-methyl-1-propanol-monoethanolamine and 2-amino-2-methyl-1-propanol-diethanolamine aqueous solution, J. Mol. Liq. 188 (2013) 37–41.

[14] M.. Ahmady, A. and Hashim, M.A. and Aroua, Kinetics of carbon dioxide absorption into aqueous MDEA+bmimBF 4 solutions from 303 to 333K, Chem. Eng. J. 200 (2012) 317–328.

[15] J.M. Navaza, D. Gómez-Díaz, M.D. La Rubia, Removal process of CO_2 using MDEA aqueous solutions in a bubble column reactor, Chem. Eng. J. 146 (2009) 184–188.

[16] A.S. Dana Mohammadnazar, Nessacities of Studying HSE Management Position and Role in Iran Oil Industry, J. Chem. Rev. 1 (2019) 252–259.

[17] H. Guo, L. Hui, S. Shen, Monoethanolamine+2-methoxyethanol mixtures for CO_2 capture: Density, viscosity and CO_2 solubility, J. Chem. Thermodyn. 132 (2019) 155–163.

[18] I. Adeyemi, M.R.M. Abu-Zahra, I. Alnashef, Experimental Study of the Solubility of

CO_2 in Novel Amine Based Deep Eutectic Solvents, Energy Procedia. 105 (2017) 1394–1400.

[19] M. Xiao, H. Liu, H. Gao, Z. Liang, CO_2 absorption with aqueous tertiary amine solutions: Equilibrium solubility and thermodynamic modeling, J. Chem. Thermodyn. 122 (2018) 170–182.

[20] A. Dey, S.K. Dash, S.C. Balchandani, B. Mandal, Investigation on the inclusion of 1-(2-aminoethyl) piperazine as a promoter on the equilibrium CO_2 solubility of aqueous 2-amino-2-methyl-1-propanol, J. Mol. Liq. 289 (2019) 111036.

[21] B. Das, B. Deogam, Y. Agrawal, B. Mandal, Measurement and Correlation of the Physicochemical Properties of Novel Aqueous Bis(3-aminopropyl)amine and Its Blend with N-Methyldiethanolamine for CO_2 Capture, J. Chem. Eng. Data. 61 (2016) 2226–2235.

[22] M.Z. Haji-Sulaiman, M.K. Aroua, A. Benamor, Analysis of equilibrium data of CO_2 in aqueous solutions of diethanolamine (DEA), methyldiethanolamine (MDEA) and their mixtures using the modified Kent Eisenberg model, Chem. Eng. Res. Des. 76 (1998) 961–968.

[23] A. Benamor, M.K. Aroua, Modeling of CO_2 solubility and carbamate concentration in DEA, MDEA and their mixtures using the Deshmukh-Mather model, Fluid Phase Equilib. 231 (2005) 150–162.

[24] S.K. Dash, A. Samanta, A.N. Samanta, S.S. Bandyopadhyay, Vapour liquid equilibria of carbon dioxide in dilute and concentrated aqueous solutions of piperazine at low to high pressure, Fluid Phase Equilib. 300 (2011) 145–154.

[25] Á.P.S. Kamps, E. Meyer, B. Rumpf, G. Maurer, Solubility of CO_2 in aqueous solutions

of KC1 and in aqueous solutions of K_2CO_3, J. Chem. Eng. Data. 52 (2007) 817–832.

[26] Y.H. Hsu, R.B. Leron, M.H. Li, Solubility of carbon dioxide in aqueous mixtures of (reline + monoethanolamine) at T = (313.2 to 353.2) K, J. Chem. Thermodyn. 72 (2014) 94–99.

[27] B.K. Mondal, S.S. Bandyopadhyay, A.N. Samanta, Experimental measurement and Kent-Eisenberg modelling of CO_2 solubility in aqueous mixture of 2-amino-2-methyl-1-propanol and hexamethylenediamine, Fluid Phase Equilib. 437 (2017) 118–126.

[28] S. Garg, A.M. Shariff, M.S. Shaikh, B. Lal, H. Suleman, N. Faiqa, Experimental data, thermodynamic and neural network modeling of CO_2 solubility in aqueous sodium salt of l-phenylalanine, J. CO_2 Util. 19 (2017) 146–156.

[29] https://webbook.nist.gov/cgi/fluid.cgi?TUnit=K&PUnit=bar&DUnit=mol%2Fl&HUnit=k%20%20J%2Fmol&WUnit=m%2Fs&VisUnit=uPa*s&STUnit=N%2Fm&Type=IsoTherm&RefSt%20ate=DEF&Action=Page&ID=C124389

[30] D.R.Y. Hyun Seung Lee, Myoung Do Seo, Jeong Won Kang, Measurement and correlation of the solubility of carbon dioxide in the mixtures of aqueous monoethanolamine solution and benzoic acid, J. Chem. Eng. Data. 57 (2012) 3744–3750.

[31] S.Z. Ali T. Zoghi, Farzaneh Feyzi, Equilibrium solubility of carbon dioxide in a 30wt.% aqueous solution of 2-((2-aminoethyl)amino)ethanol at pressures between atmospheric and 4400kPa: An experimental and modelling study, J. Chem. Thermodyn. 44 (2012) 66–74.

[32] S.K. Dash, A.N. Samanta, S.S. Bandyopadhyay, Experimental and theoretical investigation of solubility of carbon dioxide in concentrated aqueous solution of 2-

amino-2-methyl-1-propanol and piperazine, J. Chem. Thermodyn. 51 (2012) 120–125.

[33] E.B. KENT R.L., Better data for amine treating, Hydrocarb. Process. 55 (1976) 87–90.

[34] H. Saghafi, M. Arabloo, Modeling of CO_2 solubility in MEA, DEA, TEA, and MDEA aqueous solutions using AdaBoost-Decision Tree and Artificial Neural Network, Int. J. Greenh. Gas Control. 58 (2017) 256–265.

[35] M.E. Hamzehie, S. Mazinani, F. Davardoost, A. Mokhtare, H. Najibi, B. Van der Bruggen, S. Darvishmanesh, Developing a feed forward multilayer neural network model for prediction of CO_2 solubility in blended aqueous amine solutions, J. Nat. Gas Sci. Eng. 21 (2014) 19–25.

[36] M. Mirarab, M. Sharifi, M.A. Ghayyem, F. Mirarab, Prediction of solubility of CO_2 in ethanol-[EMIM][Tf2N] ionic liquid mixtures using artificial neural networks based on genetic algorithm, Fluid Phase Equilib. 371 (2014) 6–14.

[37] M.K. Wong, M.A. Bustam, A.M. Shariff, Chemical speciation of CO_2 absorption in aqueous monoethanolamine investigated by in situ Raman spectroscopy, Int. J. Greenh. Gas Control. 39 (2015) 139–147.

[38] R. Ramazani, S. Mazinani, A. Hafizi, A. Jahanmiri, Equilibrium solubility of carbon dioxide in aqueous blend of monoethanolamine (MEA) and 2-1-piperazinyl-ethylamine (PZEA) solutions: Experimental and optimization study, Process Saf. Environ. Prot. 98 (2015) 325–332.

[39] M. Kundu, B.P. Mandal, S.S. Bandyopadhyay, Vapour-Liquid Equilibrium of CO_2 in Aqueous Solutions of, Engineering. (2003) 789–796.

[40] M.H. Li, K.P. Shen, Calculation of equilibrium solubility of carbon dioxide in aqueous mixtures of monoethanolamine with methyldiethanolamine, Fluid Phase Equilib. 85

(1993) 129–140.

[41] G. Richner, G. Puxty, Assessing the chemical speciation during CO_2 absorption by aqueous amines using in situ FTIR, Ind. Eng. Chem. Res. 51 (2012) 14317–14324.

[42] C. Sun, P.K. Dutta, Infrared Spectroscopic Study of Reaction of Carbon Dioxide with Aqueous Monoethanolamine Solutions, Ind. Eng. Chem. Res. 55 (2016) 6276–6283.

[43] W. Böttinger, M. Maiwald, H. Hasse, Online NMR spectroscopic study of species distribution in MEA-H_2O-CO_2 and DEA-H_2O-CO_2, Fluid Phase Equilib. 263 (2008) 131–143.

[44] A.K. Chakraborty, G. Astarita, K.B. Bischoff, CO_2 absorption in aqueous solutions of hindered amines, Chem. Eng. Sci. 41 (1986) 997–1003.

Chapter 5

CONCLUSIONS AND FUTURE DIRECTIONS

The primary conclusions gained from work evaluated and reported in this dissertation are presented in this chapter. A variety of futuristic research approaches are also presented.

5.1 Conclusions

The major goal of this research was to look at the CO_2 absorption properties of a new amine activator and its blends with sterically hindered and tertiary alkanoalmines. Amine activator was chosen with care to reflect large equilibrium loading capacity, and increased degradation resistance, and also high thermal stability. As a result, tris(2-aminoethyl) amine (TAEA) was chosen as a new activator for the mixture, which also included N-methyldiethanolamine (MDEA) and 2-amino-2-methyl-1-propanol (AMP). Additionally, various thermophysical properties of the blends are also studied. Further, the critical outcomes in the investigated field are discussed.

- The current work has constructed a precise experimental facility (stirred cell shown in Fig. 3.1) for assessing equilibrium CO_2 solubility. Initial solubility measurements in 14.7 % mass fractions aqueous, aqueous MEA system validated the designed system and the experimental procedure. The findings are consistent with those found in the literature.
- Equilibrium CO_2 solubility in aqueous (TAEA + MDEA + H_2O) and (TAEA + AMP + H_2O) with different relative amine compositions was determined experimentally in a stirred cell over the temperature range of (293.15 -323.15) K. The CO_2 solubility data provided in this study in terms of partial pressure and loadings are considered to be

valuable as a solubility database for the design of gas treating units like pre or post-combustion process.

- By examining the results of ^{13}C NMR and FTIR analyses of various loaded and unloaded solutions, the reactions of CO_2 in solvent blends have been proposed. Following that, the modified KE model is used to predict the systems' reaction species profiles and pH. The results showed that carbamate hydrolysis produces protonated species and bicarbonate in all the amines involved in the reaction.
- The generated equilibrium solubility data of CO_2 in blended aqueous solutions were correlated using a modified Kent-Eisenberg model. The model is also investigated for estimating the suggested chemical processes' equilibrium constants among numerous linked molecules. The average absolute deviation (in %) between the model and experimental results for (TAEA+MDEA+H_2O) and (TAEA+AMP+H_2O) is 7.49 and 5.12, respectively.
- The feed-forward ANN model was also used to model the equilibrium CO_2 loading data for aqueous (TAEA + MDEA +H_2O) and (TAEA + AMP +H_2O) blends. The solubility data of systems through the ANN and the ANN estimated data is in good agreement with the experimental data. The % AAD between the experimental and model-predicted loading data is for the (TAEA + MDEA +H_2O) system found to be 1.538. For the system (TAEA + AMP +H_2O), it is 2.696, respectively, which further confirms the accuracy of the ANN model to predict the CO_2 solubility in aqueous (TAEA + MDEA +H_2O) and (TAEA + AMP +H_2O) systems.
- The CO_2 solubility in the aqueous solvents of (TAEA + MDEA +H_2O) and (TAEA + AMP +H_2O) findings show that CO_2 loading increases with partial pressure at any given

temperature and amine concentration for all solvent blends studied. At constant pressure and amine content, CO_2 loading also decreases as temperature rises.

- The density and viscosity of the aqueous novel solvents (TAEA+H_2O), blends of (MDEA+TAEA+ H_2O) and (AMP+TAEA+ H_2O) solutions were measured. Additionally, the experimental data were correlated with varying temperature ranges at changing the composition of the blends for CO_2 capture. The diffusivity values of these blends, as mentioned above, are calculated from the viscosity values using the modified Stokes-Einstein equation. The density and viscosity of all the above solutions show decreasing trends with increasing temperature and further increases with the increase in mole fraction of TAEA is the solution. The diffusivity values increase with the rise in temperature and decrease with the increase in the mole fraction of TAEA. In addition, all the systems show a negative excess molar volume because of their strong intermolecular force. The solubility of N_2O in these solutions was measured at (293.15 to 323.15) K at atmospheric pressure and correlated with the temperature-dependent Arrhenius type equation. The calculated henry's law constant value of N_2O in (TAEA+MDEA+H_2O) increases with an increase in temperature and increasing mole percent of TAEA in the mixture because of the exothermic nature of the gas absorption. Whereas the (TAEA+AMP+H_2O) shows that increase in temperature, the values increase and decrease with increasing the mole percent of TAEA, which indicates that the activator has more affinity towards N_2O. The percentage of deviations obtained over the density, viscosity, and solubility of N_2O is less than 10% which indicates a good agreement with experimental data. The physical solubility and diffusivity of CO_2 in (TAEA + H_2O) and blends of (MDEA + TAEA + H_2O), (AMP+TAEA+ H_2O) solutions were calculated using the N_2O analogy.

- Finally, it is also shown from the comparative study that at higher CO_2 partial pressure, the CO_2 loading in the solvent systems is greater than the CO_2 loading in other conventional aqueous amines used in CO_2 capture processes. All these evaluated properties can help design CO_2 separation processes using TAEA based solvent and its subsequent utilisation.

5.2 Future directions

- The current effort primarily focuses on generating solubility data for CO_2 partial pressures of 2-500 kPa. The generation of solubility data at regeneration pressure and temperature is an essential next step.

- The heat of absorption ($\triangle H$) is a crucial metric since it determines the amount of total heat released during absorption and the regeneration energy necessary to remove CO_2 from the solvent. As a result, this attribute should be tested experimentally using a reaction calorimeter.

- The kinetics of absorption for CO_2 in the present studied solvents should be focused on before considering the testing of solvents on an industrial or pilot scale.

- A commercial simulator, such as Aspen Plus®, should be used to simulate the absorber-regenerator unit for the aqueous amine solvent explored in these studies. Parametric influences, including relative amine composition, temperature, absorber/regenerator pressure, liquid to the gas ratio (L/G), reboiler duty, must be investigated.

- The thermophysical properties of CO_2-loaded amine solvents, in addition to unloaded solvents, are critical for the accurate design of the absorber cum

regeneration unit. As a result, these properties must be precisely measured over a wide temperature and CO_2 loading range.

- Corrosion and solvent degradation are the main concerns with amine technology's widespread adoption. Future research should focus on the oxidative and thermal degradation of all activated and aqueous amine solvents.

Appendix 1

Table A1.1 Comparison of experimental density and viscosity as a function of Temperature (*T)* and Mass fraction (*w)* for pure and aqueous *N*-methyldiethanolamine (MDEA) at a pressure of 0.1 MPa [25].[a]

MDEA, mass (*w*) %	*T* / K	Density, ρ/kg.m^{-3}		Viscosity, η/ mPa.s	
		Literature[25]	This work	Literature[25]	This work
100	288.15	1044.5	1044.1	141.9	142.0
	313.15	1026.7	1027.2	34.78	34.73
	333.15	1012.3	1012.6	14.50	14.66
20	288.15	1018.0	1016.7	2.650	2.624
	313.15	1009.1	1008.6	1.301	1.305
	333.15	999.30	999.50	0.858	0.860
30	288.15	1029.0	1030.7	4.402	4.399
	313.15	1018.0	1019.3	1.937	1.929
	333.15	1006.9	1007.1	1.207	1.218

[a]The standard uncertainties *u* are $u(T)$ = 0.3 K, $u(P)$ = 0.01 MPa, $u(\rho)$ = 2.5 kg·m^{-3}, $u(\eta)$ = 0.17 mPa.s, $u(w)$=0.01. Solvent is water.

Table A1.2 Comparison of experimental measured Henry's constant of CO_2 in water as a function of Temperature (*T)* and partial pressure of CO_2.[a]

P_{CO2} / kPa	**Solubility/** (mol.kg of solvent^{-1})	**Henry's constant H, mol.kg^{-1}.kPa^{-1}**
	T = 301.15 K	
47.6	0.0164	$3.15 \cdot 10^{-4}$-This work
105	0.0346	
212.8	0.0674	$3.145 \cdot 10^{-4}$-NIST (2019)[27]
411.2	0.1287	
	T = 313.15 K	
58.3	0.0144	$2.40 \cdot 10^{-4}$-This work
120.6	0.0275	$2.38 \cdot 10^{-4}$- Literature[25]
231.7	0.0557	
454.4	0.1073	
	T = 323.15 K	
62.3	0.0126	$1.97 \cdot 10^{-4}$-This work
128.2	0.0250	$1.96 \cdot 10^{-4}$- Literature[25]
251.9	0.0540	
484.1	0.0915	

[a]The standard uncertainties *u* are $u(T)$ = 0.3 K, $u(P)$ = 0.01 MPa, $u(c)$=0.001 kmol.m^{-3}. The combined expanded uncertainties for solubility measurements Uc ($K_{H\text{-}CO2}$) =34.37 kPa.m^3.kmol^{-1} with (0.95 level of confidence, k=2). Solvent is water.

Table A1.3 Comparison of experimental measured Henry's constant of N_2O in water as a function of Temperature (*T)* and partial pressure of N_2O.[a]

P_{N2O} / (kPa)	**Solubility/ (mol.kg of solvent^{-1})**	**Henry's constant H/ (mol.kg^{-1}. kPa^{-1})**
	T = 313.15 K	
60.5	0.0107	$1.757 \cdot 10^{-4}$-This work
131.5	0.0212	$1.653 \cdot 10^{-4}$- Literature[27]
249.7	0.0432	
464.2	0.0825	
	T = 323.15 K	
66.2	0.0088	$1.447 \cdot 10^{-4}$-This work
140.6	0.0195	$1.339 \cdot 10^{-4}$- Literature[27]
270.4	0.0392	
512.1	0.0730	
	T = 335.25 K	
66.1	0.0071	$1.089 \cdot 10^{-4}$-This work
141.6	0.0151	
285.5	0.0309	$0.953 \cdot 10^{-4}$-NIST (2019)[27]
516.8	0.0565	$1.065 \cdot 10^{-4}$- Literature[28]

[a]The standard uncertainties *u* are *u*(*T*) = 0.3 K, *u*(*P*) = 0.01 MPa, *u*(*c*)=0.001 kmol.m^{-3}. The combined expanded uncertainties for solubility measurements Uc ($K_{H\text{-}N2O}$) =60.4 kPa.m^3. kmol^{-1} with (0.95 level of confidence, k=2). Solvent is water.

Table A1.4 Equilibrium loading values of N_2O in pure TAEA as a function of Temperature (*T*), Pressure (*P*) and concentration (*M*) [a]

	T/ K							
	293.15		303.15		313.15		323.15	
	P/ kPa	Absorbed, mol/kg	*P*/ kPa	Absorbed, mol/kg	*P*/ kPa	Absorbed, mol/kg	*P*/ kPa	Absorbed, mol/kg
Pure TAEA	89.3	0.0502	91.2	0.0399	96.4	0.0307	102.4	0.0247
	287.9	0.1317	287.5	0.1190	303.6	0.1148	319.3	0.0989
	448.3	0.2027	460.5	0.1807	484.8	0.1705	494.9	0.1694
	599.8	0.2660	610.8	0.2538	640.9	0.2488	647.3	0.2346
	779.1	0.3566	794.4	0.3199	810.2	0.2994	824.8	0.2959

[a]The standard uncertainties *u* are $u(T) = 0.3$ K, $u(P) = 0.01$ MPa.

Table A1.5 Comparison of experimental density and viscosity as a function of Temperature (*T)* and Mass fraction (*w)* for pure solvents *N*-methyldiethanolamine (MDEA) and 2-amino 2-methyl-1-proponol (AMP) at a pressure of 0.1 MPa [20].[a]

MDEA, mass (*w*) %	***T* / K**	**Density, *ρ*/kg.m^{-3}**		**Viscosity, *η*/ mPa.s**	
		Literature[20]	**This work**	**Literature[20]**	**This work**
100	303.15	1031.5	1032.8	57.86	57.97
	313.15	1024.9	1027.2	34.31	34.73
	323.15	1017.4	1019.1	21.67	21.89
	333.15	1009.8	1012.6	14.39	14.66
AMP, mass %	***T* / K**	**Density, *ρ*/kg.m^{-3}**		**Viscosity, *η*/ mPa.s**	
		Literature[20]	**This work**	**Literature[20]**	**This work**
100	303.15	926.7	927.9	99.47	99.65
	313.15	917.9	919.4	46.92	47.01
	323.15	909.6	911.1	24.21	24.52
	333.15	901.1	902.3	13.99	14.35

[a]The standard uncertainties *u* are $u(T)$ = 0.3 K, $u(P)$ = 0.01 MPa, $u(\rho)$ = 2.5 kg·m^{-3}, $u(\eta)$ = 0.17 mPa.s and u(w)=0.01.

Table A1.6 Measured excess molar volume, (V_{exp}^{E} / cm^3. mol^{-1}) of aq. TAEA, aq. (MDEA + TAEA), and aq. (AMP + TAEA) systems from (293.15 K to 333.15) K

Concentration / (kmol.m^{-3})	V_{exp}^{E} / cm^3.mol^{-1}				
	T / K				
	293.15	303.15	313.15	323.15	333.15
aq. TAEA (1)					
0.1	-0.0561	-0.0320	-0.0348	-0.0330	-0.0594
0.3	-0.0933	-0.0841	-0.0846	-0.0881	-0.1059
0.5	-0.1481	-0.1318	-0.1405	-0.1433	-0.1516
0.7	-0.2093	-0.1938	-0.2050	-0.2092	-0.2200
0.9	-0.2684	-0.2560	-0.2701	-0.2818	-0.2954
aq. (MDEA (1) +TAEA (2))					
2.9 + 0.1	-0.5170	-0.4935	-0.4792	-0.4644	-0.4540
2.7 + 0.3	-0.5661	-0.5466	-0.5449	-0.5270	-0.5261
2.5 + 0.5	-0.6218	-0.6049	-0.6175	-0.5991	-0.6066
2.3 + 0.7	-0.6861	-0.6791	-0.6867	-0.6710	-0.6812
2.1 + 0.9	-0.7569	-0.7473	-0.7564	-0.7482	-0.7661
aq. (AMP (1) + TAEA (2))					
2.9 + 0.1	-0.4540	-0.4485	-0.4441	-0.4349	-0.4492
2.7 + 0.3	-0.5051	-0.5015	-0.4988	-0.4928	-0.4956
2.5 + 0.5	-0.5580	-0.5561	-0.5552	-0.5498	-0.5753
2.3 + 0.7	-0.6104	-0.6084	-0.6054	-0.5996	-0.5998
2.1 + 0.9	-0.6665	-0.6633	-0.6723	-0.6688	-0.6675

Table A1.7 Equilibrium loading values of N_2O in TAEA+H_2O as a function of temperature (*T*), pressure (*P*) and concentration (*M*) [a]

Concentration / (kmol.m^{-3})	*T*/ K							
	293.15		303.15		313.15		323.15	
	P/ kPa	Absorbed, mol/kg	*P*/ kPa	Absorbed, mol/kg	*P*/ kPa	Absorbed, mol/kg	*P*/ kPa	Absorbed, mol/kg
0.1	101.9	0.0240	104.9	0.0206	116.2	0.0160	110.3	0.0073
	294.5	0.0763	316.3	0.0657	339.1	0.0611	339.1	0.0529
	489.4	0.1190	512.9	0.1121	537.9	0.0984	536.2	0.0874
	662.8	0.1641	695.0	0.1499	725.7	0.1445	733.0	0.1219
	846.9	0.2091	902.2	0.2006	938.5	0.1777	942.6	0.1499
0.3	102.5	0.0212	110.1	0.0174	119.5	0.0178	118.9	0.0148
	314.4	0.0758	326.4	0.0637	337.0	0.0549	356.0	0.0530
	500.9	0.1194	516.4	0.1029	532.5	0.0931	565.6	0.0866
	669.4	0.1571	696.7	0.1350	714.8	0.1221	720.3	0.1115
	870.7	0.1945	903.5	0.1799	933.8	0.1668	925.4	0.1514
0.5	101.1	0.0188	113.5	0.0157	121.2	0.0157	130.3	0.0119
	292.6	0.0664	312.5	0.0592	337.3	0.0490	356.4	0.0425
	523.3	0.1137	548.4	0.0977	588.1	0.0882	559.2	0.0756
	706.5	0.1537	744.7	0.1346	767.3	0.1213	752.1	0.1041
	895.1	0.1902	942.0	0.1703	970.4	0.1524	961.9	0.1384
0.7	110.0	0.0226	113.3	0.0158	122.7	0.0132	124.3	0.0100
	318.0	0.0647	329.8	0.0591	349.3	0.0503	352.5	0.0460
	506.4	0.1015	526.9	0.0861	554.7	0.0784	554.7	0.0712
	691.3	0.1396	717.9	0.1276	758.2	0.1072	758.3	0.0997
	883.1	0.1732	922.0	0.1589	964.9	0.1448	974.7	0.1333

[a]The standard uncertainties *u* are *u*(*T*) = 0.3 K, *u*(*P*) = 0.01 MPa, *u*(*c*)=0.001 kmol.m^{-3}.

Table A1.8 Equilibrium loading values of N_2O in pure MDEA+TAEA+H_2O as a function of temperatures (*T*), pressure (*P*) and concentration (*M*) [a]

Concentration / (kmol.m^{-3})	*T*/ K							
	293.15		303.15		313.15		323.15	
	P/ kPa	Absorbed, mol/kg	*P*/ kPa	Absorbed, mol/kg	*P*/ kPa	Absorbed, mol/kg	*P*/ kPa	Absorbed, mol/kg
2. 9+0.1	99.3	0.0220	101.3	0.0154	98.4	0.0142	105.7	0.0074
	294.4	0.0530	306.0	0.0449	303.2	0.0397	327.0	0.0368
	474.8	0.0743	493.6	0.0759	491.1	0.0672	512.8	0.0632
	644.8	0.1080	672.6	0.1035	669.0	0.0936	698.3	0.0953
	837.1	0.1418	875.8	0.1351	861.2	0.1218	892.8	0.1161
2.7+0.3	104.7	0.0178	128.8	0.0174	115.2	0.0110	115.2	0.0086
	301.8	0.0475	333.2	0.0496	328.6	0.0438	329.5	0.0389
	489.0	0.0760	525.8	0.0738	520.3	0.0673	518.8	0.0649
	673.4	0.1060	702.8	0.0995	701.3	0.0956	704.2	0.0867
	866.4	0.1392	889.3	0.1240	904.0	0.1204	901.5	0.1116
2.5+0.5	110.0	0.0153	114.6	0.0154	112.4	0.0106	110.3	0.0093
	304.7	0.0468	317.8	0.0440	307.4	0.0387	316.6	0.0352
	491.5	0.0709	502.9	0.0694	499.0	0.0623	508.2	0.0606
	669.7	0.1002	653.2	0.0907	679.5	0.0855	690.0	0.0808
	849.8	0.1296	804.3	0.1085	868.8	0.1120	881.7	0.1055
2.3+0.7	100.7	0.0146	105.1	0.0138	113.2	0.0108	103.8	0.0094
	306.1	0.0406	294.1	0.0366	320.9	0.0390	311.5	0.0350
	474.5	0.0721	475.2	0.0653	509.0	0.0627	500.8	0.0569
	652.4	0.0956	657.1	0.0869	691.4	0.0845	682.9	0.0768
	848.0	0.1208	843.9	0.1090	892.5	0.1065	891.1	0.1028

[a]The standard uncertainties *u* are *u*(*T*) = 0.3 K, *u*(*P*) = 0.01 MPa, *u*(*c*)=0.001 kmol.m^{-3}.

Table A1.9 Equilibrium loading values of N_2O in pure AMP+TAEA+H_2O as a function of temperatures (*T*), pressure (*P*) and concentration (*M*) [a]

Concentration / (kmol.m^{-3})	*T*/ K							
	293.15		303.15		313.15		323.15	
	P/ kPa	Absorbed, mol/kg	*P*/ kPa	Absorbed, mol/kg	*P*/ kPa	Absorbed, mol/kg	*P*/ kPa	Absorbed, mol/kg
2.9+0.1	102.9	0.0207	101.7	0.0173	99.1	0.0149	109.1	0.0120
	298.9	0.0606	307.5	0.0501	304.4	0.0442	325.7	0.0443
	478.8	0.1012	496.1	0.0819	493.8	0.0730	522.7	0.0684
	665.6	0.1317	673.8	0.1146	672.5	0.1020	710.3	0.0881
	857.6	0.1731	880.1	0.1489	865.8	0.1315	921.4	0.1214
2.7+0.3	105.5	0.0202	105.6	0.0183	112.9	0.0164	117.8	0.0145
	306.7	0.0596	309.6	0.0562	326.2	0.0511	338.3	0.0437
	486.1	0.1049	495.6	0.0875	520.9	0.0796	537.0	0.0690
	665.4	0.1328	678.3	0.1152	714.3	0.1065	735.7	0.0945
	854.8	0.1785	875.6	0.1500	919.0	0.1452	946.4	0.1249
2.5+0.5	101.8	0.0197	108.6	0.0191	116.1	0.0152	121.3	0.0146
	302.2	0.0620	319.9	0.0584	334.7	0.0501	346.3	0.0493
	481.6	0.1010	509.3	0.0909	532.2	0.0850	554.6	0.0718
	656.3	0.1424	694.6	0.1221	723.6	0.1134	748.2	0.0979
	841.6	0.1703	888.3	0.1569	928.2	0.1436	958.6	0.1241
2.3+0.7	99.3	0.0210	104.0	0.0184	108.6	0.0162	115.5	0.0157
	301.5	0.0633	312.8	0.0552	323.4	0.0536	339.3	0.0458
	477.6	0.1009	500.7	0.0916	521.1	0.0816	542.0	0.0734
	653.4	0.1366	680.0	0.1221	710.2	0.1107	736.0	0.1011
	843.8	0.1779	882.7	0.1603	912.6	0.1489	948.0	0.1259

[a]The standard uncertainties *u* are $u(T)$ = 0.3 K, $u(P)$ = 0.01 MPa, $u(c)$=0.001 kmol.m^{-3}.

Table A1.10 Estimated diffusivity (D_{CO2} . 10^9 / ($m^2.s^{-1}$) in aq. (i) (TAEA), (ii) aq. (MDEA + TAEA) and (iii) aq. (AMP + TAEA) using the N_2O analogy

Concentration / ($kmol.m^{-3}$)	*T* / K				
	293.15	303.15	313.15	323.15	333.15
	(i) aq. (TAEA)				
0.1	1.724	2.096	2.564	3.150	4.102
0.3	1.556	1.852	2.271	2.708	3.376
0.5	1.420	1.713	2.026	2.427	2.946
0.7	1.299	1.542	1.833	2.151	2.620
0.9	1.185	1.381	1.644	1.949	2.363
	(ii) aq. (MDEA + TAEA)				
2.9 + 0.1	0.386	0.574	0.852	1.204	1.500
2.7 + 0.3	0.372	0.550	0.796	1.113	1.447
2.5 + 0.5	0.349	0.507	0.722	1.057	1.347
2.3 + 0.7	0.343	0.487	0.685	0.976	1.290
2.1 + 0.9	0.380	0.477	0.676	0.950	1.266
	(iii) aq. (AMP + TAEA)				
2.9 + 0.1	0.432	0.627	0.990	1.336	1.839
2.7 + 0.3	0.384	0.583	0.906	1.279	1.720
2.5 + 0.5	0.367	0.551	0.832	1.159	1.547
2.3 + 0.7	0.349	0.527	0.783	1.072	1.399
2.1 + 0.9	0.336	0.489	0.720	1.030	1.374

Appendix 2

A2.1 Calculation of Uncertainty in the Experimental Measurements

Any physical quantity (Y) such as density, viscosity, solubility, and diffusivity depends on many factors such as temperature(X_1), concentration(X_2), pressure(X_3), etc. So, we can write as shown below:

$Y = f(X_1, X_2, X_3, ..., X_N)$

If an experimental measurement is repeated in independent and unbiased ways, the measurement's result will be slightly different every time. So, it is difficult to get the "best." value. Therefore, the uncertainty term in the experimental measurement is considered in this work.

So how to calculate uncertainty

Step 1: It has taken the mean value of all independent variables (X_1, X_2, X_3,….., X_N) and dependent variable (Y).

Ex: Let's assume 'p' times experiment is repeated

$$Mean\ of\ \ X_1\ (\bar{X}_1) = \frac{(X_{11} + X_{12} + X_{13} + ...X_{1P})}{P}$$

Step 2: Now calculate standard deviation from the mean of all the independent and dependent variables.

Ex: Standard deviation of X1 $$(u_{X_i}) = \left\{ \frac{\sum_{i=0}^{P} \left(\bar{X}_1 - X_{1i}\right)^2}{P(P-1)} \right\}^{0.5}$$

Step 3: After that, calculate combined standard uncertainty (u_c^2).

$$Ex:\ u_c^2 = \sum_{i=1}^{N}\left(\frac{\partial f}{\partial X_i}\right)^2 u_{X_i}^2$$

Step 4: Finally calculate expanded uncertainty (U), taking the level of confidence 95% by multiplying combined uncertainty with 2.

Ex: $U_c = 2*u_c$

Example: (TAEA+H_2O) density (ρ) data from Chapter-3 (Table 3.2) at a given temperatures and concentrations are given below:

Concentration (mol.kg^{-1})	ρ / kg.m^{-3}				
	T / K				
	293.15	303.15	313.15	323.15	333.15
	aq. TAEA (1)				
0.102	1000.9	996.9	993.5	989.3	985.6
0.307	1002.4	998.9	994.9	990.9	986.5
0.512	1004.7	1000.4	996.7	992.3	987.3
0.717	1007.3	1002.7	998.8	994.3	989.2
0.922	1009.7	1004.9	1000.9	996.5	991.3

During the experiment, the temperature is fluctuated 0.3 K. Let's assume that the experiment performed at 313.15 K. So the temperature of the experiment may be 313.45, 313.15, or 312.85 K.

So mean temperature is 313.15 K.

Standard deviation (U_T) = 0.2 K.

Uncertainty in concentration (U_{conc}) = 0.001 mol/kg.

Uncertainty due to sample impurity is also considered. Assume sample purity is 98% and the difference between the density of pure sample and impurity is 10 %.

So, relative uncertainty due to impurity is Ur = 0.1*(1-0.98) = 0.002

So uncertainty due to impurity present in pure compound U_I = Ur * ρ = 1.99 kg/m^3

Now calculate the temperature gradient $\left(\frac{\partial \rho}{\partial T}\right)$. We will find the different slopes at different points to take the average.

$\left(\frac{\partial \rho}{\partial T}\right)$ = 0.425 kg/m^3. K

Similarly we take concentration gradient $\left(\frac{\partial \rho}{\partial con}\right)$ = 9.0524 kg/kmol

Now calculate combined uncertainty (u_c) =

$$\left[\left(U_T\left(\frac{\partial \rho}{\partial T}\right)\right)^2+\left(U_{conc}\left(\frac{\partial \rho}{\partial con}\right)\right)^2+U_I^{\,2}\right] = 1.99 \text{ kg/m}^3$$

Finally expended combined uncertainty Uc = 2* u_c = 3.99 kg/m^3

Appendix 3

A3.1 Brief calculations for solubility measurements of CO_2 in water (Appendix-1, Table A1.2)

All the temperatures, pressures, and volumes are calibrated, and the values are reported here are the calibrated ones.

Cell volume = 875.56 cc

Charge volume = 60.96 cc

Mass of solution = 298.293 gms

Volume of solution = 292.42 cc

Temperature of the cell = 301.18 K

Saturation pressure of the solution, P^{sat} = 0.07 bar

Initial charge pressure (P_{charge}) = 7.0167 bar

Temperature of the Charge section (T_{charge})= 300.55 K

Density of the gas @ P_{charge} and T_{charge} = 0.2908 mmol/cc (Taken from the NIST site)

Total moles in the Charge section = 60.96 × 0.2908 = 17.73 mmol

After isolation of the gas to the Charge to cell section,

Final charge pressure (P_{Final}) = 0.75 bar

Temperature of the Charge section (T_{charge})= 301.57 K

Density of the gas @ P_{Final} and T_{charge} = 0.03 mmol/cc (Taken from the NIST site)

Final moles in the Charge section = 60.96 × 0.03 = 1.83 mmol

Gas transferred to the cell section = 17.73-1.83 = 15.9 mmol

After attaining equilibrium,

pressure in the cell (P_{cell}) = 0.545 bar

Final gas pressure inside the cell ($P_{final\text{-}cell}$)= P_{cell} - P^{sat} = 0.545-0.07 = 0.476 bar

The temperature of the cell section (T_{cell})= 301.18 K

Density of the gas @ $P_{final\text{-}cell}$ and T_{cell} = 0.019 mmol/cc (Taken from the NIST site)

Vapour space in the cell section = 875.56-292.42 = 576.14 cc

Final moles in the cell section = 576.14 × 0.019 = 11.0 mmol

Gas absorbed in the liquid = Gas transferred to the cell section - Final moles in the cell section = 15.9 – 11.0 = 4.9 mmol

Absorbed gas, mmol/gm = Gas absorbed in the liquid / (Mass of solution × (1-% solvent in vapour)/100)

= 4.9 / (298.293 × (1-0.0073)/100)

= 0.0164 mmol /gm

The same procedure is repeated for the subsequent iterations, and the values are given in the below table

P_{CO2} / kPa	**Solubility/ mol.kg^{-1}**	**Henry's constant H, mol.kg^{-1}. kPa^{-1}**
	T = 301.15 K	
47.6	0.0164	
105	0.0346	**3.15 · 10^{-4}-This work**
212.8	0.0674	
411.2	0.1287	

Appendix-4

Typical M-File and Program output:

A4.1 Determining excess molar volume and binary interaction parameters using Redlich-Kister equation for aq. (TAEA+H_2O) system.

```
clc
clear
format long e

% %calculation of densities of pure components
 rho=[976.23 964.1 953.2 943.6 934.2
     998.2 995.7 992.2 988.2 983.2];
%TAEA% Water]
T=[293.15 303.15 313.15       323.15 333.15];
 % 1 is for TAEA and 2 is for water
M=[146.23;18];  %M is molecular weights
%rhom is experimental densities of mixtures in kg/m3
 %row indicates coposition and column indicates temperature

rhom=[1000.98 996.98 993.5 989.3 985.63
    1002.35 998.85 994.98 990.85 986.54
    1004.65 1000.41 996.71 992.32 987.31
    1007.25 1002.68 998.82 994.27 989.19
    1009.65 1004.87 1000.86 996.47 991.32];

%-------------------------------------------------------------
%calculation of pure component volume at set of experimental temperatures from density above
```

```
for j=1:5
   V01(j)=M(1)/rho(1,j);
    V02(j)=M(2)/rho(2,j);
     V0=[ V01; V02] ; %V0 is in m3/kgmol
end
x1=[1.46463384 4.385 7.31426857 10.23948803 13.16]; % wt% of TAEA
x2=[98.53536616 95.615 92.68573143 89.76051197 86.84]; % wt% of water

%-----------------------------------------------------------------
% mole fractions are found using mass percentages

for ii=1:5
   xf1(ii)=(x1(ii)/M(1))/((x1(ii)/M(1))+(x2(ii)/M(2)));    %mole fraction of TAEA
   xf2(ii)=(x2(ii)/M(1))/((x1(ii)/M(1))+(x2(ii)/M(1)));     %mole fraction of water
   xm(ii)=xf1(ii)*M(1)+xf2(ii)*M(2);%xm is the average molecular weight of components
summation(sigma)of (mole fraction *molecular mass)
xf1
xf2
xm;
   for j=1:5
s1(ii,j)=xf1(ii)*V0(1,j)+xf2(ii)*V0(2,j);
% s1 is summation(sigma) of (mole fractions *pure component volume)
%excess volume of liquid mixtures VE=Vm- sigma(x*Vio) %s1 indicates this sigma(x*Vio)
%Vm is the molar volume of the liquid mixture and Vi0 is the molar volume
%of the pure fluids at the system temperature
end
end
s1;
xm;

%-------------------------------------------------------------
%------------ CALCULATION OF EXPERIMENTAL MOLAR VOLUMES
```

```
for jj=1:5 %Vm is molar volume calculate using mole fractions and density
  VM1(jj)=xm(1)/rhom(1,jj); %jj is because of no of compositions taken
  VM2(jj)=xm(2)/rhom(2,jj);
  VM3(jj)=xm(3)/rhom(3,jj);
  VM4(jj)=xm(4)/rhom(4,jj);
  VM5(jj)=xm(5)/rhom(5,jj);
 end
VM=[VM1;VM2;VM3;VM4;VM5];
    VE=VM-s1
% VE IS EXPERIMENTAL EXCESS MOLAR VOLUMES----------------------

%-------------CALCULATION OF Ai ( pair temperature dependent parameter---------
%--------------V12,V23,V31 are excess volumes of pairs of TAEA, MDEA and water
respectively



for ii=1:5
        p1(ii)=xf1(ii)*xf2(ii);
        p2(ii)=p1(ii)*(xf1(ii)-xf2(ii));
        p3(ii)=p1(ii)*(xf1(ii)-xf2(ii))^2;
end
     v12=[p1; p2; p3]';
     r=pinv(v12);
    A=r*VE;
    A1=A';


for j=1:5
       t(j)=T(j);
       t2(j)=T(j)^2;
         end
t1=t;
t12=t2;
```

```
T2=[ones(1,5); t1; t12];
T3=T2';
B=pinv(T3);
coef=B*A1

%  coef =
%           Ao          A1         A2
%     a=  -49.017       -105.9      -57.271
%     b=  0.30875       0.6671      0.36061
%   c= -0.00050389   -0.0010899  -0.00058978

%calculation of densities of mixtures using the calculated coefitients
a=coef(1,:);
b=coef(2,:);
c=coef(3,:);

for kk=1:5
   for nn=1:3
bb(nn,kk)=b(nn)*T(kk);
cc(nn,kk)=c(nn)*(T(kk))^2;
   end
end

for mm=1:5
   Ai1(mm)=a(1)+bb(1,mm)+cc(1,mm);
   Ai2(mm)=a(2)+bb(2,mm)+cc(2,mm);
   Ai3(mm)=a(3)+bb(3,mm)+cc(3,mm);
   Ai=[Ai1;Ai2;Ai3];
end

for rr=1:5
   ve1(rr)=p1(1,1)*Ai(1,rr)+p2(1,1)*Ai(2,rr)+p3(1,1)*Ai(3,rr);
```

```
    ve2(rr)=p1(1,2)*Ai(1,rr)+p2(1,2)*Ai(2,rr)+p3(1,2)*Ai(3,rr);
     ve3(rr)=p1(1,3)*Ai(1,rr)+p2(1,3)*Ai(2,rr)+p3(1,3)*Ai(3,rr);
      ve4(rr)=p1(1,4)*Ai(1,rr)+p2(1,4)*Ai(2,rr)+p3(1,4)*Ai(3,rr);
       ve5(rr)=p1(1,5)*Ai(1,rr)+p2(1,5)*Ai(2,rr)+p3(1,5)*Ai(3,rr);
    end
ve=[ve1;ve2;ve3;ve4;ve5];
Vm=ve+s1;

for zz=1:5
    Rhom1(zz)=xm(1,1)/Vm(1,zz);
    Rhom2(zz)=xm(1,2)/Vm(2,zz);
    Rhom3(zz)=xm(1,3)/Vm(3,zz);
    Rhom4(zz)=xm(1,4)/Vm(4,zz);
    Rhom5(zz)=xm(1,5)/Vm(5,zz);

    Rhom=[Rhom1;Rhom2;Rhom3;Rhom4;Rhom5]
end
 %rhom is experimental densities of mixtures
 rhom;
 %Rhom is ecalculated densities of mixtures
 Rhom;
 Rhom(:,1);
 Rhom(:,3);
 Rhom(:,4);
 Rhom(:,5);

%standard deviation calculation
x=Rhom-rhom;
x1=x.^2;
x2=sum(x1);
x3=sum(x2');
sd=sqrt(x3/24)
```

```
%average absolute absolute deviation calculation
b=abs(x);
P=b./rhom;
P1=sum(P);
P2=sum(P1');
aad=(P2*100)/25
```

Program output:

```
VE =
   -5.611179885446974e-05   -3.200529405199618e-05   -3.475555526001595e-05
  -3.303072458156128e-05   -5.939180548526421e-05
   -9.329698563444872e-05   -8.413179215093283e-05   -8.462624722016879e-05
 -8.806283716578794e-05   -1.058813121826499e-04
   -1.480683942742603e-04   -1.318472311123489e-04   -1.405111729695235e-04
 -1.432929305194702e-04   -1.516425366847041e-04
   -2.093087333353942e-04   -1.937735276439194e-04   -2.049540160642752e-04
  -2.091777716605389e-04   -2.200054357846676e-04
   -2.683819823659402e-04   -2.559508087320167e-04   -2.700892265953166e-04
  -2.818472344509951e-04   -2.953888379767372e-04

coef =
   -1.243476675503389e+02   -2.837171462922246e+02   -1.620227935702026e+02
    8.001890219294860e-01    1.825559350603159e+00    1.042315822573528e+00
   -1.288768376412810e-03   -2.939321465109806e-03   -1.677770343554209e-03
sd =
    3.537781554079003e-01
aad =
    2.731718755247563e-02
```

A4.2 Determining binary interaction parameters for viscosity using Grunberg-Nissan Model for aq. (TAEA+H_2O) system

```
% viscosity regression using Nissan-Grunberg corelation
clc
clear
format long e
%1 is for TAEA, 2 for Water

T=[293.15 303.15 313.15 323.15 333.15]
M=[146.23;18]
x1=[1.46463384 4.385 7.31426857 10.23948803 13.16]; % wt% of TAEA
x2=[98.53536616 95.615 92.68573143 89.76051197 86.84]; % wt% of water
 % mole fractions are found using mass percentages
for i=1:5
    xf1(i)=(x1(i)/M(1))/((x1(i)/M(1))+(x2(i)/M(2)))
    xf2(i)=(x2(i)/M(2))/((x1(i)/M(1))+(x2(i)/M(2)))

end
% eta1 and  eta2  are the viscosities of the pure components
% viscosities are in m Pa sec
    eta1=[12.475 7.8291 5.3559 3.7774 3.1368];
    eta2=[1.002 0.7978 0.6531 0.5471 0.4658];

    %     etam is the experimental viscosities

etam=[0.99 0.83 0.70 0.59 0.46
    1.12 0.97 0.82 0.71 0.59
    1.26 1.07 0.94 0.82 0.70
    1.41 1.22 1.07 0.95 0.81
    1.58 1.40 1.22 1.08 0.92];

       % Viscosities of pure component
      for j=1:5
          lneta1(j)=log(eta1(j));
          lneta2(j)=log(eta2(j));
      end

       %-----------Viscosities of measured viscosities-------
     for ii=1:5 %ii indicates composition
         for n=1:5 %n indicates temperature
             lnetam(ii,n)=log(etam(ii,n));
         end
     end

      %-------------------------------------------------------------------
---
  %ln etam=sigma(xlnetai)  + doublesigma (xixjiGij)
  %A=sigma(xlnetai)
  %B=doublesigma (xixjiGij)
     lnetam1=lnetam
     for m=1:5
         for k=1:5
             A(m,k)=(xf1(m))*(lneta1(k))+(xf2(m))*(lneta2(k));
         end
     end
     B=lnetam1-A
     for kk=1:5
     x12(kk)=xf1(kk)*xf2(kk);% calculation of coefficient attached to G
```

```
     end

     C=x12
     B1=B'
     D=pinv(C)
     G12=B1*D
      %-------------------------------------------------------------------
----
  %------------Gij=a+bT+cT2-----------------------------------------------
     for j=1:5
          t(j)=T(j);
          t2(j)=T(j)^2;
      end
      t1=t;
      t12=t2;
      T2=[ones(1,5); t1; t12];
      T3=T2';
      B=pinv(T3);
      coef=B*G12
%------------------------calculation of viscosity using the coefficients
    a=coef(1,1);
    b=coef(2,1);
    c=coef(3,1);
    for ii=1:5

        bb(ii)=b*T(ii);
        cc(ii)=c*T(ii)^2;

    end
G12=a*ones(5,1)+bb(:,1)+cc(:,1);

for mm=1:5
    for nn=1:5

Lnetam(mm,nn)=xf1(mm)*lneta1(nn)+xf2(mm)*lneta2(nn)+x12(mm)*G12(nn);
    end
end
 % Etam is the calculated viscosity
 % etam is the experimental viscosity
Etam=exp(Lnetam)
Etam(:,1)
Etam(:,2)
Etam(:,3)
Etam(:,4)
Etam(:,5)
%calculation of standard deviation
error=Etam-etam
m=error.^2
m1=sum(m)
m2=sum(m1)'
sd=sqrt(m2/25)
%calculation of average absolute deviation
b=abs(error)
P=b./etam
P1=sum(P)
P2=sum(P1')
aad=(P2*100)/26
```

Program Output:

```
coef =

   -1.174381763370208e+03
    7.324796214166682e+00
   -1.106598130715793e-02
a =

   -1.174381763370208e+03

b =

7.324796214166682e+00
c =

   -1.106598130715793e-02


aad =

    9.602193973944999e+00
```

A4.3 Solubility using Arrhenius type equation Model for aq. (MDEA+TAEA+H_2O) system

```
function Arrhenious_equation

format short g

E0=[38529

   1.2355e+05

       -20617

        717.62];

options=optimset('Display','iter','MaxIter',5000,'MaxFunEvals',5000,'TolFun
',1e-10);

[E,resnorm,residual,exitflag,output] = lsqnonlin(@myfun,E0,[],[],options)

function f2=myfun(E)

H= [5961    6511  7161  7732

    6300    7101  7509  8127

    6652    7306  7880  8470

    6921    7628  8285  8779];

x=(H);

T=[293.15

    303.15

    313.15

    323.15];

Cm1=[0.1 0.3 0.5 0.7];

Cm2=[2.9 2.7 2.5 2.3];

for i=1:4

Y1(i)=(E(1)+(E(2)*Cm1(1))+(E(3)*Cm2(1)))*(exp(-E(4)/T(i)));

Y2(i)=(E(1)+(E(2)*Cm1(2))+(E(3)*Cm2(2)))*(exp(-E(4)/T(i)));

Y3(i)=(E(1)+(E(2)*Cm1(3))+(E(3)*Cm2(3)))*(exp(-E(4)/T(i)));

Y4(i)=(E(1)+(E(2)*Cm1(4))+(E(3)*Cm2(4)))*(exp(-E(4)/T(i)));

%Y5(i)=(E(1)+(E(2)*Cm1(5))+(E(3)*(Cm1(5)^2))+(E(4)*Cm2(5))+(E(5)*(Cm2(5)^2)
)+(E(6)*Cm1(5)*Cm2(5)))*(exp(-E(7)/T(i)));

%Y6(i)=(E(1)+(E(2)*Cm1(6))+(E(3)*(Cm1(6)^2))+(E(4)*Cm2(6))+(E(5)*(Cm2(6)^2)
)+(E(6)*Cm1(6)*Cm2(6)))*(exp(-E(7)/T(i)));

%Y7(i)=(E(1)+(E(2)*Cm1(7))+(E(3)*(Cm1(7)^2))+(E(4)*Cm2(7))+(E(5)*(Cm2(7)^2)
)+(E(6)*Cm1(7)*Cm2(7)))*(exp(-E(7)/T(i)));

end

y1=(x(1,:)-Y1);
```

```
y2=(x(2,:)-Y2);
y3=(x(3,:)-Y3);
y4=(x(4,:)-Y4);
%y5=(x(5,:)-Y5);
%y6=(x(6,:)-Y6);
%y7=(x(7,:)-Y7);
% s=std(y1)
plot(T,x(1,:),T,Y1,T,x(2,:),T,Y2,T,x(3,:),T,Y3,T,x(4,:))
Y=[Y1;Y2;Y3;Y4]
ans=Y';
%standard deviation calculation
err=x-Y;
err1=err.^2;
err2=sum(err1);
err3=sum(err2');
sd=sqrt(err3/15)
%average absolute deviation calculation
b=abs(err);
P=b./x;
P1=sum(P);
P2=sum(P1');
aad=(P2*100)/16
tt=E
f2=[y1
y2
y3
y4]
%y5
%y6
%y7
```

Program output:

aad = 0.65372

E =

-1.8617e+05

```
   1.1074e+05
        89402
       772.26


resnorm =
        67555
residual =


      -79.533      -77.931       13.662       17.867
      -46.792       178.01    -0.71238       21.756
      -1.0507       48.943       7.9132      -26.355
      -38.309        36.88       50.539      -108.47


exitflag =
     3
output =


    firstorderopt: 7.783e-05
       iterations: 63
        funcCount: 320
     cgiterations: 0
        algorithm: 'trust-region-reflective'
          message: 'Local minimum possible.

lsqnonlin stopped because the final change in the sum of squares relative to
its initial v...'
```